M68-2

RADAR-OPTICS IMAGING
A FEASIBILITY STUDY - INTERIM REPORT

K.R. Johnson
J.F.A. Ormsby
N.M. Tomljanovich

JANUARY 1968

THE MITRE CORPORATION
BOX 208
BEDFORD, MASSACHUSETTS

This is a formal report prepared by MITRE as part of its effort under the cited project and contract. It has not been reviewed by the Directorate of Security Review, Department of Defense, and is not for public release.

This research was supported by the Advanced Research Projects Agency, Project DEFENDER (ARPA Order No. 596), and was monitored by the Electronics Systems Division AFSC under Air Force Contract No. AF19(628)-5165, MITRE Project No. 8051.

M68-2

RADAR-OPTICS IMAGING
A FEASIBILITY STUDY - INTERIM REPORT

K. R. Johnson
J. F. A. Ormsby
N. M. Tomljanovich

JANUARY 1968

THE MITRE
BOX 208
BEDFORD, MASSACHUSETTS

This research was supported by the Advanced Research Projects Agency, Project DEFENDER (ARPA Order No. 596), and was monitored by the Electronics Systems Division AFSC under Air Force Contract No. AF19(628)-5165, MITRE Project No. 8051.

ABSTRACT

An investigation and evaluation is given on the possible application of radar-optics imaging methods. The discussion concentrates largely on microwave holography. Problem areas and alternatives are treated, including a brief discussion on thinned array techniques.

The analytical work centers on array imaging, sampled reconstruction, and sensitivity-noise effects. In addition to other system considerations, an example is given comparing microwave and optical setups. Finally, an examination is made of experimental back-up in terms of requirements, advantages, frequency selection, and appropriate optical simulation.

BLANK PAGE

TABLE OF CONTENTS

TABLE OF CONTENTS (CONCLUDED)

SECTION I

BACKGROUND INFORMATION

HISTORICAL BACKGROUND

Studies were initiated under this project very early in 1967 to consider radar-optics methods using large filled apertures as well as scattering center map processing from thinned array configurations. Emphasis was also given to wideband imaging which in particular corresponded well with the point of view adopted by the IDA subpanel on radar imaging. This early work on the use of radar-optics analogs in image formation included a preliminary investigation of phase degradation due to atmosphere inhomogeneities on maintaining coherence across the array in addition to an establishment of the problem areas requiring study and resolution to allow radar-optics imaging.

Last year, imaging methods using both thinned simple arrays and especially large filled arrays were established and suggested having potential application to a full range of target sources. In this context the possibility of obtaining direct real-time images using radar-optics on large arrays was to be dealt with initially as a feasibility study. The present report represents the first formal account of the studies accomplished to date together with an indication of the advances made along with difficulties and possibilities remaining.

PROBLEM AREA AND IMAGING ALTERNATIVES

The target environment can include both the target source and other background sources of widely varying characteristics. It is then essential that high resolution be combined with a real-time capability to produce images

which can allow identification and discrimination in the shortest possible time. Such a requirement dictates the use of large filled arrays.

Alternatives using thinned array techniques or pure optical methods could be considered.

Using relatively simple arrays including monostatic, interferometer and trilateration measurements, a number of wideband and narrowband inverse methods have been developed recently under this program which create maps of the target as returns from prominent scattering centers. These maps are possible in one, two, or three dimensions and allow estimates to be made on size, shape and motion information. The methods vary in their use of data with certain ones depending on amplitude or amplitude and phase, others relying on polarization or frequency diversity and some requiring a priori motion information. However, the ability to perform real time imaging so necessary in the present applications is severely restricted or impossible with such techniques due to the processing time requirements for obtaining the various single dimension of resolution and the need for synthesizing a composite multi-dimensional map.

Use of filled-in large apertures constitute the basis for obtaining images in real-time. The possibility for obtaining such structured three dimensional images using radar-optics analogs directly to allow immediate recognition and interpretation establishes the necessity of such an approach in the realm of differentiation and identification among classes of target sources. Of course, such a capability can also provide the various processing alternatives for inverse methods already mentioned as possible with thinned arrays.

Further, the use of microwave methods as opposed to purely optical methods has the advantages of no cloud cover and greater signal to noise sensitivity.

FEASIBILITY STUDY

The present report is intended to provide a perspective on the possible application of radar-optics imaging methods. The emphasis will be on those topics which have been treated in depth to date. The work will be discussed in relation to the major aspects which justify and facilitate the application of such methods. The various problem areas will be enumerated and related, alternative procedures together with their advantages and disadvantages will be discussed, and the findings in particular study areas will be presented in sufficient detail to establish present conclusions and future efforts.

SECTION II

PRELIMINARIES

BASIC SYSTEM CONSIDERATIONS

To be successful microwave imaging must provide a display which allows visual recognition and interpretation of the scattering source in at least near real-time. It is useful to consider target sources of maximum characteristic linear dimensions of about 10 meters and to provide, for example, a possible 10:1 resolution in each dimension. The object to be viewed can be undergoing translational and rotational motion either alone or in the presence of other scatterers. The ranges in question are in the order of a few hundred kilometers.

As is known, for such ranges, target dimensions, and resolution requirements, the ground array overall linear dimensions must be a few tens of kilometers and the array stations must be separated by no more than a few kilometers. In particular, the individual array stations must be spaced sufficiently close so as to sample the spatial frequencies in the field received from the target and at the same time provide a sufficiently large overall array size to obtain the desired target resolution.

Of course array thinning can occur if one effects resolution by a synthetic aperture approach using, for example, doppler processing at the loss of real-time operations. It is the desire to maintain a real time capability to which the present study of a large real aperatures system is directed. Some rearrangement such as a periodic station placement may be useful but for the present report only uniform spacing will be considered.

The scattering at microwave frequencies expected from the targets can to a large extent be adequately represented by the geometric theory of diffraction. As such, the target is basically equivalent to a collection of scattering centers. Ideally, and assuming a sufficiently large dynamic signal range, the number of centers can be made to cover the body by means of greater diffusion of illumination and produce an image approaching that expected at optical frequencies at least to the extent that major discontinuities on the body will appear. To what extent this enhancement of image quality can be attained will be considered as part of the continuing investigation. In any case the different bistatic returns obtained by each array station from a single illuminating source can cause, for example, the smearing of the point scatterer along an edge and so provide additional visual verification of an edge geometry.

The application of holographic methods allows the possibility of direct three dimensional visual displays as images scaled from microwave to optical frequencies without the need for explicit processing to account for phase information. This requires the use of a reference field in addition to that from the target. Such a reference source can be either from a real or a synthetic separate source or possibly one derived from the target itself. The former approach treated in the present report establishes strict requirements on the knowledge of array station locations to small fractions of the microwave wavelength as well as the need for a fully coherent array. However, it appears that the state of the art in laser ranging, for example, can cope with the station location requirement. The advantage of relaxing knowledge of station location accuracy and a non-coherent array derive from use of the target as reference source. A practical scheme to accomplish this is still lacking.

In order to create a visual image from the collected microwave field, there must be, as noted, a conversion from microwave to optical frequencies. Consideration of the effects of using sampled data to create a continuous viewable image is to be given large emphasis in the present report. Questions on magnification, resolution, focus, field of view, and image displacement are of concern here.

In order to practically assess the various system considerations, an experimental facility capable of simulating such a system is a definite requirement and preliminary investigations on such a capability are included in the study.

MAJOR STUDY AREAS

It appears that a practical system to realize the desired goal of obtaining improved three dimensional images in real time can be approached. This possibility is based partially on reasonable estimates on array size and station spacing as well as the possibility of realizing the required accuracy in determining station location.

To appreciate these aspects as well as the overall investigation more fully, the various problem areas and their relationships which must be considered in answering questions on desirability and feasibility, a run down of the major study areas and their status is useful. The problem areas are grouped generally under four major study areas: justification, feasibility, implementation, and interpretation.

Justification

A large portion of the desirability of such an imaging method hinges on the question of image quality. If by using a large array a recognizable

visual image can be achieved in addition to having a real-time capability, then such an approach is clearly justified. The question of real-time capability is basically established by the large array arrangement. Any processing times associated with conversion of microwave data to optical frequencies should not appreciably alter this. Actual times would have to be established after the details of processing schemes are finalized.

The basic question of image quality can only be fully considered by combining experimental with analytical studies which must be in part approximate. The need for establishing an experimental capability is thus paramount. In fact, the lack of such a facility to date has prevented a fuller treatment on the question of quality in the present report.

Problem areas include:

(a) Scattering range work (microwave and/or optical)

range design,
experiment design,
simulation.

(b) Image interpretation

recognition and discrimination of shapes.

The choice of microwave or optical simulation experiments is not clear-cut and will be discussed in the section of the present report titled Experimental Work.

Feasibility

The use of radar-optics methods, as noted, involves the use of a large array operating at microwave frequencies. The process of forming an image after conversion to optical frequencies can be accomplished as

either a one-step or two-step process. The one-step process treats the array as a lens while the two-step process is the holographic method. Consideration of both methods has been made in relation to questions of accuracy of station location and image formation and resolution.

The present report considers a number of items concerned with feasibility such as the various aspects of one-or two-step array imaging methods and a comparison of these, requirements on and achievement of station location accuracy and phase coherency across the array, signal sensitivity in particular with respect to thermal noise, and off-zenith behavior. Additional work on atmospheric degradation is also in progress but will be detailed in a later report. The question of a practical method for using the target as a reference source is also being considered.

Problem areas include:

(a) Array Imaging
    one-step (lens),
    two-step (holography).

(b) Station Location (array geometry)
    requirements,
    feasible methods.

(c) Coherent Array
    requirements,
    feasible methods,
    reference signal.

(d) Atmospheric Degradation

(e) Sensitivities

S/N - outputs,

system parameter needs,

coherent integration.

Implementation

It is clear that a number of items must bear on questions of feasibility and implementation. These include, for example, sensitivity and station location. A large area also in this category is that of sampled holography. The present report denotes considerable attention to sampled holography, giving a number of alternatives, while some discussion is given to the other items in the list below.

Problem areas include:

(a) Sampled holography

method implementation,

image effects.

(b) Sensitivity

system parameters.

(c) Other Items

aperiodic array,

reference sources,

illumination diffusing,

array thinning.

Interpretation

The question of output usage in the present context demands that proper interpretation be made on the final visual image. Work presently

being carried on* could lead to an approximate analytic basis for judging the effect of image formation accounting for polarization. Possible results on these matters will be given in a later report. Needless to say, discrimination studies given under Justification also bear on the present topic of interpretation. However, this and the other items on the list below will be dealt with in future efforts.

Problem areas include:

(a) Polarization
    image enhancement.

(b) Optical processing
    spatial filtering,
    display distortion.

(c) Computer Processing
    filtering,
    reconstruction quality,
    simulation.

(d) Techniques for improving recognizability
    smear and fill-in effects.

PLANS FOR FUTURE WORK

There are a number of areas which are to be treated in the continuing work. In view of the completed investigations and present status our first emphasis will be to undertake the investigation of image quality and the areas of investigation associated with setting up experimental efforts under Justification in addition to work in the other categories. This will include questions

*By R. P. Porter

on work in station locations: non-planar arrays, generation and placement of reference sources, array thinning and aperiodic spacing, coherent integration, chaff effects, diffuse illumination, polarization, recognition, and discrimination processing effects on real-time capability.

In addition to answering questions in these areas, a decision on one-step or two-step processing will also be reached.

REPORT OUTLINE

The remainder of the report will discuss the results of analytical studies and experimental considerations as separate items. The analytical work will center around three main topics: array imaging, sampled reconstruction, and sensitivity and S/N effects. These are discussed in summary fashion in the body of the report followed by corresponding detailed analysis in the Appendices. Other system considerations are given, followed by a system example which brings together all of the analytical work and provides a set of system parameters.

The next discussion in the body of the report concentrates on experimental work and considers requirements, advantages, choice of frequencies as well as an appropriate optical simulation facility. The main part of the report ends with conclusions based on completed investigations highlighting prospects, deficiencies and future directions of effort.

SECTION III

SUMMARY OF ANALYTIC STUDY

RADAR-OPTICS IMAGING*

Introduction

The imaging schemes involve a basic microwave environment consisting of an array surface, S_A, situated over a plane, S_H, and a complex disturbance located in a finite region removed from S_A and caused by the interaction of a scattering source with incident quasi-monochromatic radiation, say, of wave number $k = 2\pi/\lambda$. If a plane, S_o, is taken parallel to S_H at a distance ℓ above S_H and intersecting the region of complex disturbance, then on S_o the complex distrubance is denoted by $D(\bar{\xi})$. Each point on S_o is given by vector $\bar{\xi} = (\xi_1, \xi_2)$ and on S_H by vector $\bar{x} = (x_1, x_2)$. If $\bar{r}'$ is a vector defining a position on the surface S_A, then the disturbance on S_o causes a field on S_A which can be given by

$$\psi_o(\bar{r}') = \frac{-1}{2\pi} \int_{S_o} D(\bar{\xi}) \frac{e^{ikr}}{r} \left(ik - \frac{1}{r}\right) \frac{\hat{i}_z \cdot \bar{r}}{r} \, d\bar{\xi} \qquad (1)$$

where,

$\hat{i}_z$ is a unit vector in the z direction and

$\bar{r}$, $\bar{r}'$, S_A, and S_o etc. are shown in the cross section that follows:

*Further details are found in Appendix 1.

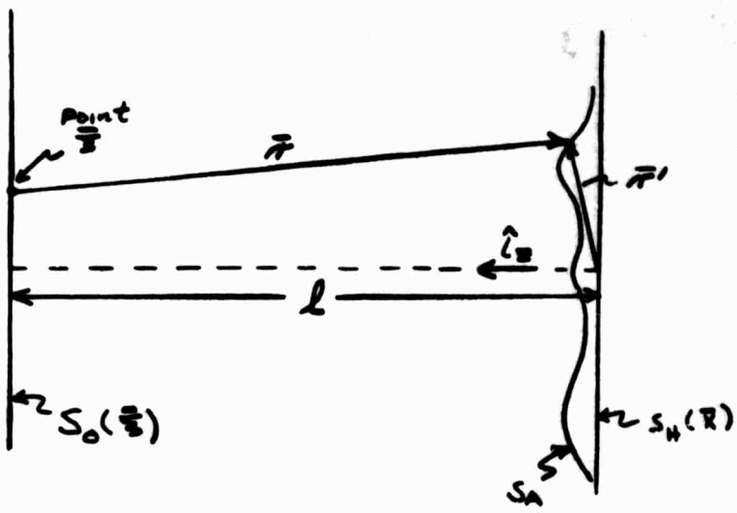

The effect of the disturbance not on the plane S_o can be treated by considering the disturbance on a sequence of such planes taken at different distances from S_H given by $\ell + \xi_3$. In general $\Psi_o(\bar{r}'(\bar{x})) = \Psi_o(\bar{x})$ and for S_A planar, $\Psi_o(\bar{r}') = \Psi_o(\bar{x})$. The equation for Ψ_o reduces to

$$\psi_o(\bar{r}') = -\frac{ik}{2\pi} \int_{S_o} D(\bar{\xi}) \frac{e^{ikr}}{r} d\bar{\xi} \qquad (2)$$

for $k \gg 1/r$ and $\frac{\hat{i}_z \cdot \bar{r}}{r} \cong 1$

This equation is the basic equation which is the starting point for either a one-step (lens) treatment or a two-step (holographic) analysis. A brief indication of the one-step approach to illustrate this relationship will now be given. Since, however, the bulk of the study in this reporting period has been concerned with the two-step process, the major portion of this summary will be devoted to results from the holographic analysis.

One-Step Process

Taking $D(\bar{\xi}) = 0$ for $\bar{\xi}$ outside the object together with conditions on the array aperture size given by

$$\frac{|\bar{x} - \bar{\xi}|^2}{\ell^2} \ll 1 \qquad \text{(implied by } \frac{\hat{\imath}_+ \cdot \bar{r}}{r} \cong 1\text{)} \tag{3}$$

and on the object given by

$$\frac{k|\bar{\xi}|^2}{2\ell} \ll 1 \qquad \text{(Fraunhofer condition for the object)} \tag{4}$$

then for a planar array

$$\psi_o(\bar{x}) = \frac{-ik}{2\pi} \int_{S_o} D(\bar{\xi}) \frac{e^{ikr}}{r} d\bar{\xi} \cong \frac{-ik}{2\pi\ell} e^{+ik\ell(1+|\bar{x}|^2/2\ell^2)} \int_{-\infty}^{\infty} D(\bar{\xi}) e^{-ik\frac{\bar{x}\cdot\bar{\xi}}{\ell}} d\bar{\xi} \tag{5}$$

or

$$\psi_o'(\bar{x}) = \left[\frac{i2\pi\ell}{k} e^{-ik\ell(1+|\bar{x}|^2/2\ell^2)}\right] \psi_o(\bar{x}) = \int_{-\infty}^{\infty} D(\bar{\xi}) e^{-ik\frac{\bar{x}\cdot\bar{\xi}}{\ell}} d\bar{\xi} \tag{6}$$

so that

$$D(\bar{\xi}) = \frac{k^2}{4\pi^2\ell^2} \int_{-\infty}^{\infty} \psi_o'(\bar{x}) e^{ik\frac{\bar{x}\cdot\bar{\xi}}{\ell}} d\bar{x} \tag{7}$$

Thus a simple Fourier pair relationship exists between $\Psi_o'(\bar{x})$ and $D(\bar{\xi})$ if the phase term $\frac{i2\pi\ell}{k} e^{-ik\ell\left(1+(\bar{x})^2/2\ell^2\right)}$ can be accurately generated. This requirement in turn demands accurate position location knowledge in $\bar{x}$ on the aperture plane to a fraction of a wavelength. When the Fourier relationship holds, we have the array acting as a simple lens equivalent. Retrieval of $D(\bar{\xi})$ visually is then possible by simple lens imaging of the field $\Psi_o(\bar{x})$ converted to optical frequencies. Such a process, as briefly described, is the one-step or lens imaging approach in radar-optics.

Two-Step Process: Hologram Formation

Returning to the equation for $\Psi_o(\bar{r}')$ and introducing a second target as a point source reference the total field becomes

$$\psi_T(\bar{r}') = \psi_o(\bar{r}') + \psi_R(\bar{r}') = \psi_o(\bar{r}') + B\frac{e^{ikr_R}}{r_R} \qquad (8)$$

where B is a complex constant and r_R is the distance from the reference source to S_A.

The reference is located at $(\bar{\xi}_R, \xi_{3R})$ and is at a distance $\ell + \xi_{3R}$ from S_H.

Then without imposing the Fraunhofer condition but assuming ℓ large in comparison to the array and object extensions in the phase terms and using ℓ for r and $\ell + \xi_{3R}$ for r_R in the denominators of Ψ_o and Ψ_R respectively the formation of the hologram is given by

$$I(\bar{r}') = \psi_T(\bar{r}')\,\psi_T^*(\bar{r}') = \sum_{i=1}^{4} I_i \tag{9}$$

where, using $\bar{r}' = \bar{r}'(\bar{x})$ and denoting I as $I(\bar{x})$,

$$I_1(\bar{x}) = A_1 \int_{S_0}\int_{S_0} D(\bar{\xi}) D^*(\bar{\xi}') e^{-ik\frac{\bar{x}\cdot(\bar{\xi}-\bar{\xi}')}{l} + ik\frac{(|\bar{\xi}|^2 - |\bar{\xi}'|^2)}{2l}} d\bar{\xi}\, d\bar{\xi}'$$

$$I_2(\bar{x}) = A_2 \int_{S_0} \left[D(\bar{\xi}) e^{ik|\bar{\xi}|^2/2l}\right] e^{-ik\frac{\bar{x}\cdot\bar{\xi}}{l}} d\bar{\xi}$$

$$I_3(\bar{x}) = A_2^* \int_{S_0} \left[D^*(\bar{\xi}) e^{-ik|\bar{\xi}|^2/2l}\right] e^{ik\frac{\bar{x}\cdot\bar{\xi}}{l}} d\bar{\xi}$$

$$I_4(\bar{x}) = A_4 \tag{10}$$

and

$$A_1 = \frac{k^2}{4\pi^2 l^2}$$

$$A_2 = \frac{-ikB^*}{2\pi l(l+\Xi_{3R})} e^{-ik\left[\Xi_{3R} - \frac{|\bar{x}|^2 \Xi_{3R}}{2l(l+\Xi_{3R})} + \frac{\bar{x}\cdot\bar{\Xi}_R}{l+\Xi_{3R}} + \frac{|\bar{\Xi}_R|^2 + X_3^2}{2(l+\Xi_{3R})} - \frac{X_3^2}{2l}\right]}$$

$$A_4 = \frac{BB^*}{(l+\Xi_{3R})^2} \tag{11}$$

This step of constructing the hologram together with a second step of reconstructing an image constitutes the two-step or holographic imaging approach in radar-optics.

Notice that with the Fraunhofer condition imposed the usual Fourier pair relationship exists between $I_2(\bar{x})$ or $I_3(\bar{x})$ and $D(\bar{\xi})$ if compensation is made for the respective phase factors A_2 or $A_3 = A_2^*$.

Two-Step Process: Reconstruction

In the reconstruction from the hologram, it is the satisfying of the focusing condition which eliminates the effect of quadratic phase terms and provides effectively a Fourier pair relationship and a resulting image of the scattering source. In dealing with a synthesized reference source, the location of receivers in the aperture must still be known to accuracies of a small part of a wavelength.

The reconstruction will take place at optical frequencies so that a scaled version of the hologram $I(\bar{x})$ is used in say a $\bar{u}$ plane as $I'(\bar{u})$ with

$$\bar{x} = m(\bar{u} + \bar{u}_d - \bar{\Delta}) \tag{12}$$

where

m is the scale factor, $\bar{u}_d$ a bias term, and

$\bar{\Delta}(\bar{x})$ a distortion term.

The reconstruction is effected by passing a spherical coherent wavefront say of wave number k' through the scaled hologram $I'(\bar{u})$ and focusing by means of a lens (with focal length f). This leads to a distribution $\Psi(\bar{\alpha})$ in an image

plane, S_I, with z_1 the distance from the lens focal point to the scaled hologram plane, S_{Hd}, and z_2 the distance from the scaled hologram plane to the image plane. Using range approximations with respect to hologram and image extent similar to those in the microwave situation, the image field becomes

$$\psi_I(\bar{\alpha}) = T \int_{S_{Hd}} I\left[m(\bar{u} + \bar{u}_d - \bar{\Delta})\right] Q e^{-ik' \frac{\bar{\alpha}\cdot\bar{u}}{z_2}} d\bar{u} \qquad (13)$$

where

$$Q = e^{ik'\left[\frac{|\bar{u}|^2}{2}\left(\frac{1}{z_1} + \frac{1}{z_2}\right)\right]}$$

$$T = \frac{-ik'ACf}{2\pi z_2 z_1} e^{ik'\left(z_1 + z_2 + f + \frac{|\bar{\alpha}|^2}{2z_2}\right)}$$

A = transmittance ratio from hologram (scaled)

C = intensity of reconstruction light source

$\frac{Cf}{z_1}$ = intensity of light impinging on hologram (scaled)

The image field can be rewritten for the separate terms I_i in I as

$$\psi_{I_i}(\bar{\alpha}) = T \int_{S_{Hd}} I_i Q e^{-ik' \frac{\bar{\alpha}\cdot\bar{u}}{z_2}} d\bar{u} \qquad (14)$$

With i = 2 for example,

$$\psi_{I_2}(\bar{\alpha}) = T \int_{S_{Hol}} \int_{S_o} Q(\bar{u}) A_2(\bar{u}) \left(D(\bar{\xi}) e^{ikW(\bar{\xi})/2\ell}\right) e^{-ik\bar{\alpha}\cdot\bar{u}/z_2} e^{-ik(\bar{u}+\bar{u}_d-\bar{\Delta})\cdot\bar{\xi}/\ell m} d\bar{u}\, d\bar{\xi} \quad (15)$$

Under the following conditions,

$k\frac{|\bar{\xi}|^2}{\ell} << 1$ Fraunhofer condition for object

$\frac{k|x_3|L^2}{\ell^2}\left(\frac{\xi_{3R}}{\ell} + \frac{2L_D}{L}\right) << 1$ conditions on array planarity.

$k'\left(\frac{1}{z_1}+\frac{1}{z_2}\right) + \frac{k m^2 \xi_{3R}}{\ell(\ell+\xi_{3R})} = 0$ optical focusing condition

then with $\bar{\Delta} = 0$

$$\psi_{I_2}(\bar{\alpha}) = F_2' D\left(-\frac{\ell k'\bar{\alpha}}{m k z_2} + \frac{\ell \bar{\xi}_2 + m \xi_{3R} \bar{u}_d}{\ell + \xi_{3R}}\right) \quad (16)$$

where F_2' is a complex coefficient in which $\bar{\alpha}$ only appears as a phase factor so that $\Psi_{I_2}(\bar{\alpha})$ is magnified by $\left|\frac{\bar{\alpha}}{\bar{\xi}}\right| = \frac{mkz_2}{k'\ell}$ and translated by $\frac{\ell\,\bar{\xi}_R + m\xi_{3R}\bar{u}_d}{\ell + \xi_{3R}}$ (on the object plane) image of the original object distribution $D(\bar{\xi})$. The image is real for $z_2>0$ and virtual (viewable image) for $z_2<0$.

The above result assumed also that the planes S_o and S_{H_f} (and so S_{Hd}) are infinite in extent, which in fact violates the condition $\frac{z\cdot\bar{r}}{r} \cong 1$. Taking $D(\bar{\xi}) = 0$ outside the target extent causes no difficulty but since the aperture in S_H (and S_{Hd}) is of finite extent, the actual value for I should be modified by a truncation function in the $\bar{x}$ plane, say Rect $(\bar{x})$ which results in a convolution with a sinc $(\bar{\alpha})$ function in $\psi_{I_1}(\bar{\alpha})$ and thus a "smear out" of the image. Resolution thus improves as the size of the aperture increases.

Effects, of course, from Ψ_{Ii}, i = 1, 3, 4 are also obtained. For i = 1,

$$\psi_{I_1}(\bar{\alpha}) = F_1' \int_{\bar{y}} D^*(\bar{y})\, D\left(\bar{y} - \frac{k'\ell\,\bar{\alpha}}{mkz_2}\right) d\bar{y} \qquad (17)$$

which is a convolution smearing of $D(\bar{\xi})$ in the image plane. By shifting $\psi_{I_2}(\bar{\alpha})$ off axis by means of the translational term $\frac{\ell\,\bar{\xi}_R + m\xi_{3R}\bar{u}_d}{\ell + \xi_{3R}}$ (that is by $\bar{\xi}_R$ or $\bar{u}_d$ control) then a non overlap between ψ_{I_2} and ψ_{I_1} is accomplished.

For $i = 4$,

$$\psi_{I_4}(\bar{\alpha}) = F_4' \, s\left(\frac{k'\bar{\alpha}}{z_2}\right) \tag{18}$$

a delta function (ideally) on axis in the image plane. Finally for $i = 3$,

$$\psi_{I_3}(\bar{\alpha}) = F_3' D^*\left(\frac{\ell k'\bar{\alpha}}{m k z_2} + \frac{\ell \bar{\xi}_R}{\ell + \xi_{3R}} + \frac{m \xi_{3R} \bar{u}_d}{\ell + \xi_{3R}}\right) \tag{19}$$

where with $\psi_{I_2}(\bar{\alpha})$ in focus, $\psi_{I_3}(\bar{\alpha})$ is not (unless $\xi_{3R} = 0$) and ψ_{I_2} and ψ_{I_3} appear on opposite sides of the optical axis to prevent overlap.

Image Characteristics

The various conditions for the selection of reference placement, station accuracy, and system parameters to establish an image in terms of the microwave receiving aperture array and the optical reconstruction are illustrated in detail in the section on a Illustrative System Example.

Using the basic equations and conditions noted above, various parameters describing the imaging process can be derived. Since details for some of these are given in Appendix 1, it suffices here to state the results. If 2L is the overall linear dimension extent of the array and with the Fraunhofer condition for the object holding, the resolution in the target plane is given by

$$L_d = \frac{\lambda \ell}{2L} = \frac{\pi \ell}{kL} \tag{20}$$

and in the z (longitundinal direction) by

$$\ell_{\parallel} = \frac{\lambda \ell^2}{L^2} = 2\frac{\ell L_d}{L} \tag{21}$$

which is much poorer than L_d.

Values for the parallel (to the object plane) and the perpendicular (in the z direction) magnification factors, which are ratios of distances in the image plane over respective distances in the object plane, can be given as

$$m_{\parallel} = \frac{m k z_2}{k' \ell}$$

and

$$m_{\perp} = \frac{k m^2 z_2^2}{k' \ell^2} = \frac{m z_2}{\ell} m_{\parallel} \tag{22}$$

SAMPLED PROCESSING AND HOLOGRAPHY*

To obtain microwave information by an array aperture for eventual conversion to an optical image, a sampling of the received field is required. In order to account properly for the spatial frequencies corresponding to a target source of approximately 10 meters in extent, a minimum spacing

*Further details are found in Appendix 2

distance, (2b), is needed, and should be approximately a few kilometers. The spatial extent of each receiving aperture, usually less than a few meters, for example, must be small compared to the minimum spatial period caused by any increase in effective source extent resulting from a combination of target and reference source. Finally, the number of receivers is determined by the overall extent of the array. For resolution cells in the order of 1 meter, this requires array dimensions of a few tens of kilometers or approximately 100 sampling stations over the array surface.

Once the field is accurately measured in amplitude and phase, various possibilities can be used to apply this sampled data to form a continuous visual image. The first and simplest method so far considered and discussed in detail, converts in a straightforward manner from a sampled microwave hologram to a sampled hologram scaled to optical frequencies. Over each sampling cell in two dimensions, the hologram amplitude-only function, I, is fixed at its center value. Reconstruction takes place directly from the sampled hologram.

Two alternatives have also been analyzed, and constitute the second and third methods. The second method is more complicated than the first since it converts the sampled hologram mentioned above into a continuous hologram as an intermediate step, prior to reconstruction. The third approach (suggested by R. Roig) first converts the sampled field in amplitude and phase into a continuous field prior to any processing for a visual image. This method has the major disadvantage that control of both the amplitude and phase of the very small reconstructing light sources must be maintained over the scaled aperture. More particularly, extremely severe requirements are placed on the location of these light sources as scaled down from the

microwave location requirements. However sampling amplitude and phase of the field rather than the intensity used in holography has the advantage of requiring the minimum number of samples without introducing error.

An Approach to Sampled Holography

To begin, the first method converts the hologram $I(\bar{x})$ sampled at positions (x_{1j}, x_{2n}) in $\bar{x}$ on S_H into the scaled version (scaling factor m), with sampling cells centered at (u_{1j}, u_{2n}) in $\bar{u}$ on S_{Hd} where, with p, $\bar{u}_d$ and $\bar{\Delta} = 0$, $x_{1j} = m\,u_{1j}$ and $x_{2n} = m\,u_{2n}$.

The sampling takes place uniformly at distance 2b in each dimension of $\bar{x}$, and I is taken constant over each sampling cell so that for all j, n within the cell defined by:

$$|x_1 - x_{1j}| < b', \quad |x_2 - x_{2n}| < b' \tag{23}$$

where b' may be less than or equal to b,

$$I(\bar{x}) = I(x_{1j}, x_{2n}),$$

with

$$x_{1j} = j(2b), \quad x_{2n} = n(2b).$$

Thus, in the S_H plane, the sampled version of I_2 results in

$$I_{S_2}(\bar{x}) = \sum_{j,n} Rect\left(\frac{x_1 - x_{1j}}{b'}\right) Rect\left(\frac{x_2 - x_{2n}}{b'}\right) I_2(x_{1j}, x_{2n}) \tag{24}$$

and, in the S_{Hd} plane,

$$I'_{S_2}(\bar{u}) = I_{S_2}(m\bar{u}) = I_{S_2}(\bar{x}) \tag{25}$$

The reconstructed field then becomes, in the S_I plane,

$$\psi_{I_{S_2}}(\bar{\alpha}) = \frac{-ik'AC f}{2\pi z_1 z_2} e^{ik'(z_1+z_2+f+\frac{|\bar{\alpha}|^2}{2z_2})} \int \sum_{S_{uv}} \sum_{j,m} \mathrm{Rect}\left[\frac{m u_1 - u_{1j}}{b'}\right] \mathrm{Rect}\left[\frac{m(u_2 - u_{2n})}{b'}\right] \times I_2(m u_{1j}, m u_{2n}) e^{ik'[\,]} d\bar{u} \qquad (26)$$

where

$$[\,] = \frac{|\bar{u}|^2}{2}\left(\frac{1}{z_1} + \frac{1}{z_2}\right) - \frac{\bar{\alpha}\cdot\bar{u}}{z_2}$$

Together with $|u_1 - u_{1j}| < \frac{b'}{m}$, $|u_2 - u_{2n}| < \frac{b'}{m}$, to permit focusing, the following conditions must be satisfied.

$$\frac{k'|u_1^2 - u_{1j}^2|}{2} q \ll 1$$
$$b'|u_2^2 - u_{2n}^2| q \ll 1 \qquad (27)$$

where

$$q = \frac{1}{z_1} + \frac{1}{z_2}$$

Taking

$$\bar{\alpha} = \alpha_1 \hat{u}_1 + \alpha_2 \hat{u}_2 \quad \text{and} \quad \bar{u}_{jn} = u_{1j}\hat{u}_1 + u_{2n}\hat{u}_2, \qquad (28)$$

then the reconstructed image becomes

$$\psi_{I_{s_2}}(\bar{\alpha}) = -\frac{2ik'ACfb^2}{\pi z_1 z_2 m^2} \frac{\sin\frac{k'\alpha_1 b'}{mz_2}}{\frac{k'\alpha_1 b'}{mz_2}} \frac{\sin\frac{k'\alpha_2 b'}{mz_2}}{\frac{k'\alpha_2 b'}{mz_2}} e^{ik'(z_1+z_2+f+\frac{|\bar{\alpha}|^2}{2z_2})}$$

$$\times \sum_{j,m} e^{ik'g\frac{|\bar{u}_{jm}|^2}{2} - ik'\frac{\bar{\alpha}\cdot\bar{u}_{jm}}{z_2}} I_2(mu_{1j}, mu_{2m}). \tag{29}$$

If the conditions

$$\frac{k|\bar{\xi}|^2}{2\ell} \ll 1, \qquad \frac{k|x_3|L^2}{\ell^2}\left(\frac{z_{3R}}{\ell} + \frac{2L_D}{L}\right) \ll 1 \tag{30}$$

are assumed, and $D(\bar{\xi})$ is taken to be zero for $|\xi_i| > L_D$, $i = 1, 2$, where $2L_D$ is the maximum linear extent of the target in each dimension of the of the S_o plane, then in the region $|\xi_i| < L_D$,

$$D(\bar{\xi}) = \sum_{j,m}^{\infty} a_{j,m} e^{\frac{i\pi}{L_D}(j\xi_1 + m\xi_2)} \tag{31}$$

with

$$a_{j,m} = \frac{\pi}{2L_D^2} \tilde{D}\left(\frac{\pi j}{L_D}, \frac{\pi m}{L_D}\right) \tag{32}$$

where $\tilde{D}$ is the Fourier transform of D.

On inserting the appropriate focusing condition, and taking b to give

$$2b = \frac{\lambda \ell}{2 L_D} = \frac{\pi \ell}{k L_D} \tag{33}$$

then

$$\psi_{I_{S_2}}(\bar{\alpha}) = -\frac{k' B^* A C \ell}{z_1 z_2 (\ell + \xi_{3R}) k m^2} \frac{\sin \frac{k' \alpha_1 b'}{m z_2}}{\frac{k' \alpha_1 b'}{m z_2}} \frac{\sin \frac{k' \alpha_2 b'}{m z_2}}{\frac{k' \alpha_2 b'}{m z_2}}$$

$$\times e^{ik'(z_1 + z_2 + f + \frac{|\bar{\alpha}|^2}{2 z_2}) + i k \xi_{R3} - \frac{i k |\bar{\xi}_R|^2}{2(\ell + \xi_{3R})}} D\left(-\frac{\ell k' \bar{\alpha}}{k m z_2} + \frac{\ell \bar{\xi}_R}{\ell + \xi_{3R}}\right) \tag{34}$$

which, with the various assumptions and restrictions, such as on b, demonstrates the possibility of forming a magnified and translated image of $D(\bar{\xi})$. The modulation intensity due to the use of a sampling cell hologram is clearly indicated in the sinc functions. To reduce degradation, the image must be contained between zeroes of these functions in the $\bar{\alpha}$ plane. Of course, the always-present smearing effect of the finite array size will cause additional degradation, as was pointed out in the previous subsection on radar-optics imaging.

The transition to the above expression for $\psi_{I_{S2}}(\bar{\alpha})$ from the preceeding expression for that quantity is presented in detail in Appendix 2; however, it is appropriate to point out here that, although it is not apparent from the above, the fields in the image plane resulting from the various terms of the hologram are periodic, so that fields from the different terms interfere with each other. This interference can be reduced by focusing.

The question of degradation of the image represented by the above expression will be dealt with at greater length in Appendix 2 .

In addition to the sampling requirement stated above, the conditions on $|u_1^2 - u_{1j}^2|$ and $|u_2^2 - u_{2n}^2|$ previously given imply restrictions on $|\xi_{3R}|$ for a given value of b. This restriction may be stated approximately (assuming $|\xi_{3R}| \ll \ell$), as $|\xi_{3R}| \ll \frac{2L_D \ell}{\pi b}$.

It is assumed in the foregoing that the scattered field from the target (and from the reference source, if an actual reference is used) is sampled at a point. This requires that the dimensions of the receiving antenna be small compared to the reciprocal of the highest spatial frequency appearing in the measured field (i.e., small compared to $\lambda \ell / L_T$, where L_T is the maximum linear dimension of the complex of target and reference, if there is an actual reference.) This is not a severe restriction.

Additional considerations on the significance of the various approximations is required, for example, in any comparison of the various sampling methods. Some discussion on the requirements of power levels, coherent integration, noise levels, target and reference source constraints, and image size, is given in the sections on Sensitivity, Further System Considerations, and Illustrative System Example.

Alternative Approaches

In order to avoid the sinc modulation and the periodicity in the image plane caused by the finite sampling cell size, the second reconstruction method first converts the sampled hologram to a continuous hologram. This is done by first taking the Fourier transform with an "f to f" lens for each sampled hologram cell. The new field is then given by

$$\psi_T'(\bar{w}) = \sum_{jm} \psi'_{jm}(\bar{w}) = \frac{-2ik'b^2}{\pi f m} e^{i2k'f} \sum_{jm} I(\bar{u}_{j,m}) \frac{\sin \frac{k'b(w_1-u_{ij})}{fm}}{\frac{k'b}{fm}(w_1-u_{ij})} \frac{\sin \frac{k'b(w_2-u_{2m})}{fm}}{\frac{k'b}{fm}(w_2-u_{2m})} \tag{35}$$

If the focal plane of these processing lenses is such as to let zeroes of sinc function occur at $\bar{w}_{j,n} = \bar{u}_{j,n}$, then

$$f = \frac{2b^2k'}{4m^2} \tag{36}$$

and by the sampling theorem

$$\sum_{j,m} = I(\bar{w}) \tag{37}$$

that is, a field having magnitude proportional to the original continuous hologram (scaled down) is produced;

$$\psi_T'(\bar{w}) = -i e^{i2k'f} I(\bar{w}). \tag{38}$$

Use of this field permits reproduction of a continuous hologram from which an image of the original distribution, $D(\bar{\xi})$ may be obtained.

The third method seeks to reproduce the (scaled down) original scattered field, ψ', directly. This leads to using the set of values $\psi(\bar{x}_{j,n})$ as weights for the interpolation with the effect of a multi-hole pierced lens to generate sinc interpolation functions, as were used in the second method, to reproduce now $\psi(\bar{x})$. The complication of implementing and locating a complex light modulation at the holes with values $\psi(\bar{x}_{j,n})$ is most severe.

This approach involves smearing effects from finite cell size and depth of focus difficulty. An implementation to facilitate obtaining a viewable image has been suggested. Details on such matters will not be presented in the present report.

SENSITIVITY AND THERMAL NOISE*

Of particular concern in studying signal degradation is the effect of receiver thermal noise on the image reconstructed from sampled data. This can be measured in terms of a signal-to-noise ratio (SNR) between image and noise intensity. It appears likely that this ratio should be largely unaffected by the particular method used for image reconstruction. The effective SNR depends in a complex manner on the nature of the scattering source for given array and receiver noise characteristics. This ratio of image intensity to background receiver thermal noise intensity is strongly influenced by the nonlinearities of the holographic process.

In order to expedite obtaining an appreciation of the importance of SNR and its influence on system parameters, a number of approximations are made. The method used is generally applicable and gives results in terms of such system parameters as transmitter power, transmitter and receiver antenna gains, array dimensions, and coherent integration times.

In an attempt to investigate the effects over a range of targets, approximate expressions for the SNR are given for an unresolved point target and a resolved plate target. A function of the reference signal level, this ratio asymptotically approaches a maximum as the reference level

---

* Further detail found in Appendix 3.

increases. For the unresolved target, the ratio depends on the scattering cross section, while for the resolved plate, the asymptotic value is independent of plate size.

The Noise Model

The analysis begins with a number of assumptions. All antennae in the array receive the same polarization under matched load conditions. The effective received voltage comes from N coherently added pulses. The resultant noise is essentially unvarying in time intervals less than $\tau_p \cong 1/\Delta f$, where the receiver bandwidth, Δf, is small compared to center frequency f, and τ_p is single pulse duration.

This leads to received voltage V_N given by

$$V_N = \sum_{j=1}^{N} V_j = \sum_{j=1}^{N} (V_{r_j} + n_j) = NV_r + \sum_{j=1}^{N} n_j \qquad (39)$$

where j refers to the particular pulse, V_r (= V_{r_j} for all j, assuming appropriate phase shifts to permit coherent integration) is the received pulse complex voltage without thermal noise and the received complex noise voltage for the jth pulse is $n_j = |n_j| e^{i(2\pi ft + \phi_{nj})}$, with $|n_j|$ and and ϕ_{nj} essentially constant during the jth pulse.

The ensemble average on $|V_N|^2$ gives

$$\overline{|V_N|^2} = N^2 |V_r|^2 + N\overline{|n|^2}, \qquad (40)$$

where

$$\overline{|n|^2} = \overline{n_j n_j^*} \quad \text{(independent of j)}.$$

The voltage, NV_r, would be produced by a single pulse incident electric field of magnitude

$$|E_{i_I}| = N|V_r|\sqrt{\frac{\pi\eta}{G_R\lambda^2 R_a}}, \tag{41}$$

where R_a is the radiation resistance of the antenna, G_R the gain of the receiving antenna, and η the impedance of free space.

Also, the incident electric field E_N corresponding, in the same sense, to the noise voltage, $\sum_{j=1}^{N} n_j$, has mean square magnitude of

$$\overline{|E_N|^2} = \frac{8\pi\eta N\tilde{k}T\Delta f}{G_R\lambda^2}, \tag{42}$$

where $\tilde{k}$ is the Boltzmann constant and T is the total noise temperature.

Thus the voltage, $\sum_{j=1}^{N} n_j$, present after coherent integration of N pulses, can be represented for narrowband thermal noise by

$$|E_N|e^{i\phi}$$

where the amplitude, $|E_N|$, is Rayleigh distributed, with $\overline{|E_N|^2}$ given above, and the phase, ϕ, is uniformly distributed over $(0, 2\pi)$, with $|E_N|$ and ϕ independent at different stations and independent of each other at a given station for thermal background noise.

The effective total field at the array plane is

$$E_T(\bar{x}) = \underset{\text{(object)}}{E_D(\bar{x})} + \underset{\text{(reference)}}{E_R(\bar{x})} + \underset{\text{(noise)}}{E_N(\bar{x})}, \tag{43}$$

and the power flux is $|E_T|^2/2n$, with $|E_T|^2$ a measure of the hologram intensity, I. By proper adjustment to separate the terms of the hologram $|E_D|^2$, $|E_R|^2$, $E_R E_D^*$, the reconstructed image can be obtained from the term $E_D E_R^*$. Now, however, the following degradation terms caused by the noises appear in the hologram.

$$I_N(\bar{x}) = |E_N|^2 + E_D E_N^* + E_R E_N^* + E_N E_D^* + E_N E_R^* \tag{44}$$

Noise Effect on Reconstructed Image

In the analysis of the reconstruction process from sampled data, the expression for $\psi_{I_{S2}}(\bar{\alpha})$ contained a sum, S, which has a mean squared magnitude of

$$\overline{SS^*} = \sum_{j,n}\sum_{j',n'} e^{ik'z_{i/2}(|\bar{u}_{j,n}|^2 - |\bar{u}_{j',n'}|^2) - ik'\frac{\bar{\alpha}}{z_2}\cdot(\bar{u}_{j,n} - \bar{u}_{j',n'})} I_N(n\bar{u}_{j,n}) I_N(n\bar{u}_{j',n'}) \tag{45}$$

With assumptions of homogenity and independence, an evaluation results in

$$\overline{SS^*} = M\left(\overline{|E_N|^2}\right)^2 + 2\,\overline{|E_N|^2} \sum_{j,m} |a_{j,m}|^2 + \left(\overline{|E_N|^2}\right)^2 P \qquad (46)$$

where

$$\alpha_{j,n} = E_{Dj,n} + E_{Rj,n} \qquad (47)$$

M = total number of stations

$$P = \left| \sum_{j,m} e^{ik' g/2 |\overline{u}_{j,m}|^2 - ik' \frac{\overline{\alpha} \cdot \overline{u}_{j,m}}{R_0}} \right|^2.$$

Considering P as a random walk near the edges gives P on the order of M. Thus,

$$P \sim M \qquad (48)$$

Assuming additional reduction in $\sum_{j,n} |\alpha_{j,n}|^2$ due to phase variation over j, n gives

$$\overline{SS^*} = M\overline{|E_N|^2}\left[2\overline{|E_N|^2} + 2\left(E_{DA}^2 + E_{RA}^2\right)\right] \qquad (49)$$

where

$$E_{DA}^2 = \frac{1}{M} \sum_{j,m} |E_{Dj,m}|^2 ,$$

$$E_{RA}^2 = \frac{1}{M} \sum_{j,m} |E_{Rj,m}|^2 . \qquad (50)$$

With no thermal noise of course, $\overline{S\,S^*} = 0$.

Application to Two Target Sources

Two specific targets are now considered: (1) Point target unresolved, and (2) flat plate resolved target.

Point Target Unresolved

It is assumed that the target is located at $\bar{\xi}_S$ with $D(\bar{\xi}) = A' \delta(\bar{\xi} - \bar{\xi}_S)$, A' = constant and the array surface planar with $x_3 = 0$. The target field $\psi_0(\bar{r}') = E_0(\bar{r}')$, and target cross section is σ. A' is evaluated from energy flow considerations as

$$A' = \frac{(P_T G_T \sigma \eta)^{1/2}}{\sqrt{2}\, k\, \ell_T} \qquad (51)$$

where

P_T = transmitted power during each pulse,

G_T = transmitter gain,

ℓ_T = range from target to transmitter.

After N coherent returns,

$$E_D(\bar{X}) = -i \frac{(P_T G_T \sigma \eta)^{1/2}}{2\sqrt{2}\,\pi \ell \ell_T} N e^{ik\left(\ell + \frac{|\bar{X}|^2}{2\ell} - \frac{\bar{X}\cdot\bar{\xi}_S}{\ell} + \frac{|\bar{\xi}_S|^2}{2\ell}\right)} \qquad (52)$$

The reference field at the array $\psi_R(\bar{r}') = E_R(\bar{r}')$ is given by

$$E_R(\bar{x}) = \frac{B}{\ell + \bar{s}_{3R}} e^{ik\left[\ell + \bar{s}_{3R} + \frac{|\bar{x}|^2}{2(\ell+\bar{s}_{3R})} - \frac{\bar{x}\cdot\bar{s}_R}{\ell+\bar{s}_{3R}} + \frac{|\bar{s}_R|^2}{2(\ell+\bar{s}_{3R})}\right]} \tag{53}$$

with B constant.

With $|E_{Dj,n}|^2$ and $|E_{Rj,n}|^2$ assumed constant over the array (i.e. over j , n), giving

$$E_{DA}^2 = \frac{P_T G_T \sigma h N^2}{8\pi^3 \ell^2 \ell_T^2}, \quad E_{RA}^2 = \frac{|B|^2}{(\ell+\bar{s}_{3R})^2}, \tag{54}$$

the mean squared magnitude of the contribution to the reconstructed field, $\psi_{I_{S_2}}(\bar{\alpha})$, from the contribution in S due to the noise term I_N in the hologram I, is given by

$$\overline{|E_{\substack{Rec \\ Noise}}|^2} = \frac{4k^2A^2C^2f^2b^4}{\pi^2 z_1^2 z_2^2 m^4}\ \overline{SS^*} = K\overline{SS^*} \tag{55}$$

where the sinc terms in $\psi_{I_{S2}}$ are neglected since in any SNR calculation they would not appear.

To obtain a SNR a comparison is made, after reconstruction, between the squared field magnitude of the center of the diffraction pattern of the holographic aperture (which is actually obtained in reconstruction rather than a point image) with the mean squared magnitude of the noise field. Using, for a large number of stations, the continuous hologram in place of the sampled hologram to reconstruct, E_{Rec} becomes

$$E_{REC} = 4 \frac{F_2 L^2}{m^2} \operatorname{sinc} \nu \operatorname{sinc} \gamma \tag{56}$$

where

$$|F_2|^2 = \frac{(A')^2}{16} \frac{k^2 |B|^2 (k')^2 A^2 C^2 f^2}{+ z_1^2 z_2^2 l^2 (l + \xi_{3R})^2}$$

$$\nu = \frac{L}{m} \left(\frac{k' \alpha_1}{z_2} - \frac{k m \xi_{R1}}{l + \xi_{3R}} \right) \tag{57}$$

$$\gamma = \frac{L}{m} \left(\frac{k' \alpha_1}{z_2} - \frac{k m \xi_{R2}}{l + \xi_{3R}} \right)$$

The squared reconstructed field at the point where the image of the point target should appear, after N coherent pulses, is

$$|E_{\substack{REC \\ POINT}}|^2 = \frac{L^4 |B|^2 (k')^2 A^2 C^2 f^2 N^2 P_T G_T \sigma \eta}{2 \pi^4 l_T^2 m^4 z_1^2 z_2^2 l^2 (l + \xi_{3R})^2} \tag{58}$$

The SNR is then

$$R_o^2 \triangleq \frac{|E_{REC_{POINT}}|^2}{|E_{REC_{NOISE}}|^2} = \frac{L^4 |B|^2 N P_T G_T \sigma G_R}{16 \pi k^2 l^2 l_T^2 (l + \xi_{3R})^2 b^4 M \tilde{k} T \Delta f} \left[\frac{16 \pi \eta N \tilde{k} T \Delta f}{G_R \lambda^2} + 2 \left(\frac{P G_T \sigma \eta N^2}{8 \pi l^2 l_T^2} + \frac{|B|^2}{(l + \xi_{3R})^2} \right) \right]^{-1} \tag{59}$$

Flat Plate Resolved Target

It is assumed that $D(\bar{\xi}) = B'$ Rect. $(\bar{\xi}/a)$ and the perfectly-conducting plate has sides of length $2a \gg \lambda$ so that the broadside cross section is

$$\sigma_p = \frac{64\pi a^4}{\lambda^2} .$$

From power flow considerations,

$$B' = \left(\frac{P_T G_T h}{2\pi \ell_T^2} \right)^{1/2} \tag{60}$$

and after N coherent returns with a Fraunhofer conditon on the target,

$$E_b(\bar{\gamma}) = \frac{-2ik a^2 N}{\pi \ell \ell_T} \left(\frac{P_T G_T h}{2\pi} \right)^{1/2} e^{ik\left(\ell + \frac{|\bar{\gamma}|^2}{2\ell}\right)} \frac{\ell^2}{k^2 a^2 x_1 x_2} \sin\frac{kax_1}{\ell} \sin\frac{kax_2}{\ell} \tag{61}$$

The array average, E_{DA}^2, can be approximated by a continuous average over the area of the array to yield $E_{DA}^2 \sim N^2 P_T G_T h a^2 / 2\pi \ell \ell_T L^2$ over the array, then neglecting the effects of sinc terms, as with the noise.

$$|E_{REC_{PLATE}}|^2 = \frac{(k')^2 |B|^2 A^2 C^2 f^2 \ell^2 P_T G_T h N^2}{2\pi z_1^2 z_2^2 (\ell + \xi_{3R})^2 k^2 m^4 \ell_T^2} \tag{62}$$

so that the SNR is given by

$$R_L^2 \triangleq \frac{|E_{REC_{PLATE}}|^2}{|E_{REC_{NOISE}}|^2} = \frac{\pi |B|^2 \ell^2 P_T G_T G_R N}{16 (\ell + \xi_{3R})^2 k^4 \ell_T^2 b^4 M \tilde{k} T_{sf}} \left[\frac{8\pi h N \tilde{k} T_{sf}}{G_R \lambda^2} + 2\left(\frac{P_T G_T a^2 h N^2}{2\pi \ell \ell_T L^2} + \frac{|B|^2}{(\ell + \xi_{3R})^2} \right) \right]^{-1} \tag{63}$$

As $|B|^2 \to \infty$,

$$R_\sigma^2 \to R_{\sigma MAX}^2 = \frac{L^4 \lambda^2 \sigma F_R}{\pi \ell_T^2 \ell^2 b^4 M} \qquad \text{(depends on } \sigma\text{)} \qquad (64)$$

$$R_L^2 \to R_{LMAX}^2 = \frac{\lambda^4 \ell^2 F_R}{32 \ell_T^2 b^4 M} \qquad \text{(independent of a)} \qquad (65)$$

where

$$F_R = \frac{P_T G_T G_R N}{(4\pi)^2 \tilde{R} T_A f} \qquad (66)$$

Note that the magnitude of the reconstructed field at the center of the diffraction spot for a point target equals the magnitude of the reconstructed field in the interior of the image for a plate, if the point target has cross section

$$\sigma_1 = \frac{\pi \lambda^2 \ell^4}{4 L^4} \qquad (67)$$

This also gives $R^2_{0MAX} = R^2_{LMAX}$. Of course, these values can in general differ widely as the numerical example in Appendix 3 clearly indicates. For example, if N = 100

$$R_{\sigma MAX}^2 = 15 \text{ db} \qquad \text{and} \qquad R_{LMAX}^2 = 66 \text{ db}$$

with $\sigma = 10^{-2}$ m^2 for the point target and the result being independent of the plate cross-section, provided that the plate is large enough to be resolved. Such a spread in SNR suggests the need for some type of amplitude compression. Additional computation also indicates compatibility between

total transmit time for N = 100 pulses and the time to restrict relative movement between major target scattering points to be less than 1/10 of the operating wavelength.

SECTION IV

FURTHER SYSTEM CONSIDERATIONS

STATION LOCATION REQUIREMENT FOR LARGE APERTURE RADAR ARRAYS

The analysis of radar-optics imaging, as summarized in Section III and detailed for holographic images in Appendix 1, indicates that in obtaining the image, unless an actual reference source is used, one of the most crucial requirements imposed on the system for one- or two-step imaging is the need of knowing the location of each station to within a small fraction of the operating wavelength.

Once the location of all stations is known to such accuracy, it is then possible to synthesize a reference near the target by tracking the target and calculating the appropriate complex reference field that each station would have observed if the reference point source were actually so located.

Although the above requirement seems quite stringent, it is nevertheless possible with the present technological means to obtain the location of each station within the desired accuracy. This report will briefly review long-baseline measuring techniques[1], the station location accuracy requirement and then, to establish feasibility, will indicate a systematic method of measuring the accurate location of a large number of stations.

Accurate Distance Measuring Techniques

There are two types of long-baseline measuring techniques: those using the "time of arrival" approach and those using the "phase difference" approach; furthermore, both of the above types can be subdivided into two broad classes: optical and microwave measuring schemes.

The "time of arrival" technique at optical or microwave frequencies measures distances by sending a short pulse signal to a planar reflector, located at one end of the path to be measured, and recording the transit time back to the transmitting or a separate receiver, located at the other end of the path.

The geometrical path D between the above two points is

$$D = \frac{\tau}{2} \bar{V}_g \tag{68}$$

where τ is the two-way transit time and $\bar{V}_g$ is the average group velocity of the transmitted short pulse over the path. The range accuracy depends on the accuracy of measuring the transit time and the average group velocity $\bar{V}_g$.

Although the accuracy in transit time gets better as the pulse length gets smaller, a too short pulse will be broadened by a dispersive medium such as the atmosphere and hence there is a limit on how much can be gained in accuracy by going to a smaller pulse length.

The accuracy of optical range measurements by means of pulsed lasers is better than that of microwave measurements because of reduced atmospheric effects due to a lesser water vapor contribution.

Before discussing atmospheric effects and other systematic errors in general, let us indicate the other approach which is used to measure precisely long distances.

The "phase difference" or "interferometry" technique was first investigated by Bergstrand in the early 1950's[2], and it laid the foundation of modern optical distance measurements. The approach can briefly be summarized as follows: a light beam is amplitude-modulated at a frequency f and sent out to an optical reflector at the end of the path to be measured.

The returned light's phase is compared to that of the transmitted light.

If the measured phase difference is $\Delta\theta$, the two-way path length to the end reflector is $2L = \left(n + \frac{\Delta\theta}{2\pi}\right)\lambda$ and it is ambiguous because of the unknown quantity "n".

The ambiguity can be removed by performing the same measurement at various frequencies.

A similar scheme can be implemented for the microwave system.

Very precise geometrical path distances between two points can only be obtained if all forms of errors are properly accounted for. The factors affecting the accuracy of measurements for both optical and microwave systems are:

(a) Stability of transmitting source,

(b) atmospheric effects due to the changing index of refraction,

(c) accuracy of the phase measuring system, and

(d) uncertainty from lunar and solar tides in the solid earth.

For long distance measurements, the atmospheric effect is the biggest problem.

Taking, as an example, the "phase difference" approach, the path L that is obtained is the optical path which is the sum of two terms: the geometrical path D plus the additional path difference Q due to the atmosphere.

$$L = D + Q$$

$$L = \int_{P_1}^{P_2} n' \, ds = \int_{P_1}^{P_2} ds + \int_{P_1}^{P_2} (n' - 1) \, ds \qquad (69)$$

where n' the group index of refraction defined as

$$n'(s) = \frac{c}{V_g(s)} \tag{70}$$

is a varying function along the path. To obtain the desired geometric path, it is necessary to calculate the optical correction

$$Q = \int_{P_1}^{P_2} (n' - 1)\, ds \tag{71}$$

which can only be done if the group index of refraction is known at many points along the path. However, since the atmospheric contribution to the index of refraction is about 300 parts per million, the air density must be known to one part in 300 in order to permit an overall distance accuracy of a part per million. Thus the atmospheric pressure and temperature for many points along the path must be known to one part in 300, a rather difficult task. To avoid making temperature and pressure measurements at many points along the measured path in calculating Q (the optical correction) a scheme has been recently proposed for the optical case[3, 4].

It uses measurements obtained at two largely different wavelengths (one in the red and the other in the blue part of the visible spectrum); the approach takes the difference

$$\Delta Q = Q_B - Q_R \tag{72}$$

of the two optical path corrections (equal to the optical path difference ΔL) and finds that the ratio of ΔQ to Q_R is a constant which is essentially independent of the atmospheric density along the path and is known from

laboratory measurements[5, 6]. Thus an accurate measured value of ΔQ can be used to find the desired path correction Q_R to approximately the same fractional accuracy.

As an example, for a path of 15-km ΔQ is about 40 cm, and this would have to be measured to 0.4 cm to give 3 part-in-10^7 accuracy in L

$$\frac{\Delta L}{L} = \frac{\Delta(\Delta Q)}{\Delta Q} \cdot \frac{\Delta Q}{L} = \frac{40 \times 10^{-2}}{15 \times 10^{5}} \approx 3 \times 10^{-7}$$

A similar scheme could be devised for the microwave system. However, because of the necessity of using two greatly different wavelengths and therefore two transmitting and receiving systems, its practicability is greatly reduced.

In addition to the above drawbacks the microwave distance measuring systems seem to be less accurate than the optical systems because of their greater sensitivity to atmospheric water vapor.

The overall accuracy of present optical long-baseline distance measuring systems, correcting for the atmospheric effects, is one part-in-10^6.

If the scheme using two greatly different wavelengths is used, then it is hoped that an overall accuracy of a few parts in 10^7 can be achieved.

Station Location Accuracy Requirements

When a large radar array is used to do optical imaging, there are two modes in which such array can be operated: either as a lens, or as a holographic recording medium. In both cases, however, the requirement on station location can be obtained from the following simple analysis.

Given an object field distribution $D(\bar{\xi})$ a distance ℓ away from the recording non-planar array and assuming for the time being a continuous array (see diagram below), the complex field produced at point P is (See Section III and Appendix 1)

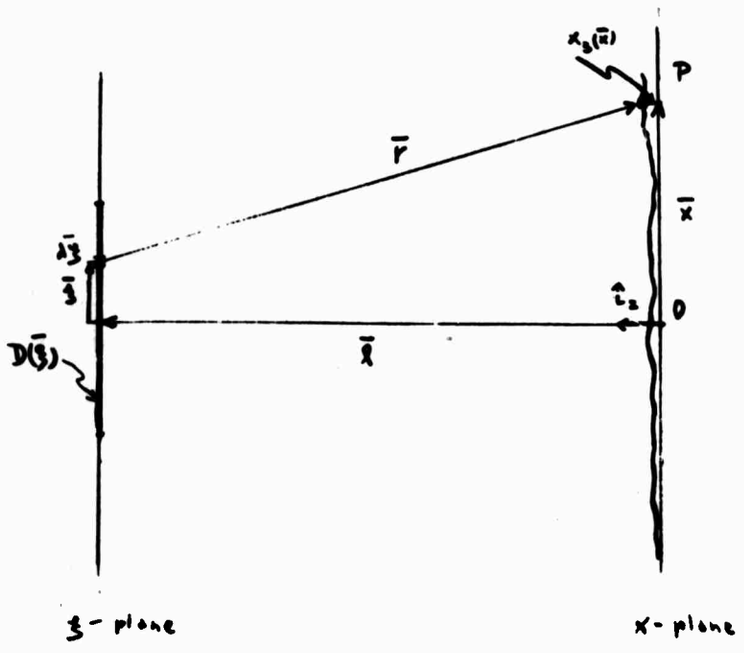

$$\Psi_0(\bar{x}) = -\frac{ik}{2\pi}\int D(\bar{\xi})\,\frac{e^{ikr}}{r}\,d\bar{\xi} \qquad (73)$$

for $$k \gg \frac{1}{r} \quad \text{and} \quad \frac{\hat{i}_3\cdot\bar{r}}{r} \simeq 1$$

where

$$r = \sqrt{(\ell - x_3)^2 + |\bar{x} - \bar{\xi}|^2} = (\ell - x_3)\left[1 + \frac{|\bar{x} - \bar{\xi}|^2}{2(\ell - x_3)^2} + \cdots\right] \qquad (74)$$

Assuming $\frac{|\bar{x}-\bar{\xi}|^2}{(\ell - x_3)^2} \ll 1$ and $\frac{x_3}{\ell} \ll 1$

$$r = (\ell - x_3) + \frac{1}{2}\frac{|\bar{x}-\bar{\xi}|^2}{\ell} + \frac{1}{2}\frac{x_3|\bar{x}-\bar{\xi}|^2}{\ell^2} = \tag{75}$$

$$= (\ell - x_3) + \frac{1}{2}\frac{|\bar{x}|^2}{\ell}\left[1 + \frac{x_3}{\ell}\right] - \left[\frac{\bar{x}\cdot\bar{\xi}}{\ell} - \frac{|\bar{\xi}|^2}{2\ell}\right]\left[1 + \frac{x_3}{\ell}\right]$$

Using the above approximation in the exponent and the approximation $r \simeq \ell$ in the denominator, the integral becomes

$$\psi_0(\bar{x}) = -\frac{ik}{2\pi\ell}\, e^{ik\left[(\ell - x_3) + \frac{|\bar{x}|^2}{2\ell}\left(1 + \frac{x_3}{\ell}\right)\right]} \int D(\bar{\xi})\, e^{-i\frac{k}{\ell}\left[\bar{x}\cdot\bar{\xi} - \frac{|\bar{\xi}|^2}{2}\right]\left(1 + \frac{x_3}{\ell}\right)} d\bar{\xi} \tag{76}$$

If a proper phase compensation is introduced across the array such that the new complex field amplitude over the array is

$$\psi_0'(\bar{x}) = i\frac{2\pi\ell}{k}\, e^{-ik\left[(\ell - x_3) + \frac{|\bar{x}|^2}{2\ell}\left(1 + \frac{x_3(\bar{x})}{\ell}\right)\right]} \psi_0(\bar{x}) \tag{77}$$

then

$$\psi_0'(\bar{x}) = \int D(\bar{\xi})\, e^{-i\frac{k}{\ell}\left[\bar{x}\cdot\bar{\xi} - \frac{|\bar{\xi}|^2}{2}\right]\left(1 + \frac{x_3(\bar{x})}{\ell}\right)} d\bar{\xi} \tag{78}$$

and if the Fraunhofer condition is applied $\frac{|\bar{\xi}|^2}{2\ell} \ll 1$, together with the array planarity condition : $\frac{x_3(\bar{x}\cdot\bar{\xi})}{\ell^2} \ll 1$

then

$$\psi_o'(\bar{x}) = \int D(\bar{\xi})\, e^{-ik\frac{\bar{x}\cdot\bar{\xi}}{\ell}}\, d\bar{\xi} \qquad (79)$$

and a Fourier transform condition exists between the complex field ψ_0 and the object field distribution $D(\bar{\xi})$.

In effect, however, because of station location inaccuracy, the phase term over the array will deviate from the desired one and will add a random phase contribution to the useful complex field ψ' .

Such random phase distribution will degrade the quality of the Fourier transform of ψ' and thus will decrease the resolution of the image.

A criterion must then be imposed on the accuracy of measuring the location of all stations which clearly depend on how much phase variations one can tolerate over the array.

Looking at the phase term

$$e^{i\phi} = e^{ik\left[(\ell - x_3) + \frac{|\bar{x}|^2}{2\ell}\left(1 + \frac{x_3}{\ell}\right)\right]} \qquad (80)$$

the phase error is clearly related to the errors in the measurements of ℓ, $\bar{x}$ and x_3

$$\Delta\phi = k\left[\Delta\ell - \Delta x_3 + \frac{|\bar{x}|\Delta|\bar{x}|}{\ell^2}\left(1 + \frac{x_3}{\ell}\right) + \frac{|\bar{x}|^2}{2\ell^2}\left[\Delta x_3 - \left(1 + \frac{2x_3}{\ell}\right)\Delta\ell\right]\right] \qquad (81)$$

The maximum phase error is obtained when x is maximum: $x_{max} = L$ (where $2L$ is the array size) and when all errors are arranged so as to give such a maximum,

$$\Delta\phi_{max} = k\left[\Delta\ell + \Delta x_3 + \frac{L}{\ell}\Delta|\bar{x}|\left(1+\frac{x_3}{\ell}\right) + \frac{L^2}{2\rho^2}\left[\Delta x_3 + \left(1+\frac{2x_3}{\rho}\right)\Delta\ell\right]\right] =$$

$$\simeq k\left[\Delta\ell + \Delta x_3 + \frac{L}{\ell}\Delta|\bar{x}|\left(1+\frac{x_3}{\rho}\right)\right] \qquad (82)$$

since $\frac{L}{\ell} \simeq .1$

$$\Delta\phi_{max} \simeq k\left[\Delta\ell + .1\,\Delta|\bar{x}| + \Delta x_3\right]$$

However, in determining L, one needs the vertical position of all M stations of the array and therefore $\Delta\ell \approx \frac{\Delta x_3}{M}$. For $M \simeq 100$, the $\Delta\ell$ term can be neglected and

$$\Delta\phi_{max} = k\left(\Delta x_3 + .1\,\Delta|\bar{x}|\right) \qquad (83)$$

From the above relation one sees that distance errors in the x_3-direction are ten times more critical than those in the $\bar{x}$-direction and contribute mostly to the phase errors.

Assuming that one can measure Δx_3 and $\Delta|\bar{x}|$ with the same accuracy, then

$$\Delta|\bar{x}| \simeq \Delta x_3 = \frac{\Delta\phi_{max}}{k} = \frac{\Delta\phi_{max}}{2\pi}\ \lambda \qquad (84)$$

In the following analysis we assume that a maximum phase error of 20^0 will not affect the quality of the reconstructed image. In the future, a more detailed investigation, considering the random phase errors over the array, will be carried out to determine exactly what maximum phase error one can tolerate in order to be able to successfully reconstruct the image. For the moment, however, taking $\Delta\phi_{max} \simeq 20^0$, the maximum tolerated error in distance is

$$\Delta x_3 = \frac{20}{360}\ \lambda = \frac{1}{18}\ \lambda \simeq .5 \text{ cm} \quad \text{for} \quad \lambda = 10 \text{ cm}$$

Actually, the distance error in the planar direction needs to be about ten times less critical

$$\Delta|\bar{x}| \simeq 10\ \Delta x_3 \simeq 5 \text{ cm}$$

The fractional accuracy in the planar direction, if $L \approx 15$ km, is then

$$\frac{\Delta|\bar{x}|}{L} = \frac{5}{1.5 \times 10^6} = \frac{3}{10^6}$$

an accuracy which, using the optical distance measuring system outlined above, can presently be achieved.

A Systematic Approach for Locating Large Number of Stations in a Radar Array

This approach will briefly outline a method, using the accurate distance measuring instruments discussed previously, to measure the location of all stations of the radar array to within the desired accuracy.

For a radar array of 100 stations or more, the task of precisely locating in three dimensions all stations is a long and involved process.

It is desirable to keep the number of optical distance measuring instruments to a minimum and to set up the experiment so that the errors in the planar direction are about as equal as those in the vertical direction.

Bouncing laser beams from station to station will give a good accuracy in the planar direction but not in the non-planar or vertical direction.

On the other hand, bouncing laser beams off satellites will decrease the accuracy in both dimensions because of the long paths measured.

A compromise which is proposed here is to bounce laser beams between stations themselves as well as between stations and non-planarly located targets (such as tall towers, balloons or helicopters); this approach will maintain the accuracy desired and in addition will equalize the errors in the different dimensions.

Furthermore, to keep the number of optical instruments to a minimum, it is useful to locate a minimum number of stations at a time. First, the whole array can be divided in several subgroups, each made up of such a minimum number. After each station of a subgroup is located relative to a "common" station of that subgroup for all subgroups, the next step would be

to locate in position and orientation each subgroup relative to a "common" subgroup.

Let us then determine the minimum number of stations which are sufficient to permit determination of their locations relative to one another.

Each station has an optical distance measuring instrument bouncing a laser beam off reflectors fixed on the other stations and off reflectors fixed on a non-planarly located target (balloon, tower, helicopter, etc.).

The independent unknowns are the 3-dimensional locations of all N stations relative to one of them, i.e., a "common" station, and the 3-dimensional location of the non-planarly located reflector on the target.

$$\mathcal{N}_u = 3(N-1) + 3 = 3N \tag{85}$$

The number of different measurements that can be obtained bouncing laser beams off reflectors fixed on the other stations and the non-planarly located target is

$$\mathcal{N}_m = \frac{N!}{N-2!\,2!} + N =$$

$$= \frac{N(N-1)}{2} + N = \frac{N(N+1)}{2} \tag{86}$$

To be able to solve for the unknowns, the following inequality must be imposed between the number of unknowns and the number of measurements.

$$N_m \geq N_u$$

or

$$\frac{N(N+1)}{2} \geq 3N \tag{87}$$

or

$$N \geq 5$$

Thus, using one measurement per station and a non-planarly located target, at least 5 stations are required to completely determine their position. For a large array of M stations, using the above approach and using five laser distance measuring instruments $\frac{M}{5}$ times, all stations on each of the $\frac{M}{5}$ subgroups will be located relative to one "common" station of each subgroup.

The next step is to locate in position and orientation all subgroups relative to a "common" subgroup. This can be done first by locating in position any orientation sets of subgroups relative to a "common" subgroup of each set, and then all of the sets relative to a "common" set.

Since we are locating in orientation, as well as in position, three points of each subgroup must be located each time relative to a station of the "common" subgroup.

Conclusions

This report has considered, in some detail, station location accuracy requirements for optical imaging, the various distance measuring techniques

one could use to achieve such requirements, and finally has outlined a systematic approach of getting accurate three-dimensional locations of a large number of stations using a minimum number of optical distance measuring instruments. There is further work to be done in investigating how the random phase errors, introduced over the array, decrease the resolution of the reconstructed image and how the maximum station location accuracy. affecting the resolution, limits the maximum resolution of the radar array for coherent optical imaging, and puts a limit on the use of the array, beyond which no gain in resolution is attainable.

OTHER SYSTEM CONSIDERATIONS

There are many other system considerations, which although quite important, have not as yet been investigated in detail.

Nevertheless, it is felt that some of these considerations, which will contribute additional areas of research, should be discussed here to indicate possibilities of simplifying or improving the imaging ability of the discussed large radar array.

The four main considerations which will be described briefly here are:

(a) Coherence Requirements and Possibility of Achievement

(b) Reference Source Used: Synthetic or Actual

(c) Diffuse Illumination

(d) Off-Zenith Behavior of the System

Coherence Requirement and Possibility of Achievement

As shown in Section III, if a large radar array is used as a lens to do optical imaging, the basic requirements imposed on the system are a precise knowledge of station location and a fully phase-coherent array.

The theoretical analysis developed in the subsection dealing with station location accuracy has shown that any inaccuracy in the determination of station location will add a random phase variation over the array which will degrade the reconstructed image. Similarly, any inaccuracy in obtaining a fully coherent array will also add a random phase over the array and thus will also affect the resolution of the reconstructed image. The total random phase variation over the array $\phi_R(\bar{x})$ can then be considered as a sum of the two above contributions:

$$\phi_R(\bar{x}) = \phi_R^{(s)}(\bar{x}) + \phi_R^{(c)}(\bar{x}) \qquad (88)$$

Assuming that the maximum allowable rms total phase error at each station is 20^o, and if the phase error due to station location inaccuracy is 10^o, all stations must be phase-coherent to within 10^o. Again, for a large number of stations, this is a quite stringent requirement which nevertheless can be achieved in several different ways.

One approach, which is customarily used to provide a phase reference for multistatic radar systems, is the use of phase stable microwave links. For distances greater than a few kilometers, fluctuations in the transmitting medium necessitate multipath procedures to correct for such fluctuations.

A better approach of obtaining a coherent phase reference is by utilizing the frequency stability of atomic clocks. These are accurate to 1 part in 10^{14}. If, for each station of the radar array, an atomic clock is provided and all clocks are calibrated in phase by observation of an astronomic source, a coherent phase reference would be established over the array.

An interferometer using atomic clocks to provide coherent local oscillator signals has been operated for astronomical purposes with a base-

line of 461,000 λ at 610 MHz [7] yielding resolution only slightly inferior to that attainable with optical systems [8].

One proposal considers the construction of a 3000-mile baseline interferometer, using atomic clocks to provide a phase reference. At the suggested operating frequency of 1000 MHz, phase recalibration would be required about once a day. With the same clock stability, operation at 3000 MHz (S-band), recalibration would be required about three times as often. The clock accuracy is more than adequate for our purpose and when using such an approach the total phase error will mostly be due to station location inaccuracy.

A third approach would be a combination of the two previously discussed methods. It would consist of maintaining phase coherence of several subgroups of stations by microwave links and phase coherence between each subgroup of the array by atomic clocks. All the different approaches will be investigated more thoroughly in future work.

Reference Source Used: Synthetic or Actual

When the radar array is used as holographic recording system, the requirements of station location accuracy and coherence accuracy depend on whether an actual or a synthesized reference point source is used.

If an actual reference point source is used near the target and is moving with the target, each station directly measures the amplitude and phase difference needed for obtaining the hologram and thus a coherent phase reference is not required over the array. Each station must still be capable of measuring the phase and amplitude of the complex field. However, the system needed to preserve coherence throughout the array is eliminated. Furthermore, since each station now measures only the relative phase

between the object and the reference point and not the absolute phase of the object scattered field, and since such relative phase depends to a lesser extent on station location if the reference is close to the target, the requirement of station location is also relaxed. To investigate how much this requirement is relaxed, let us consider the complex object field expression over the radar array obtained, when the Fraunhofer condition and the array planarity condition are obeyed.

$$\psi_0(\bar{x}) = -\frac{ik}{2\pi\ell}\, e^{ik\left[\ell - x_3 + \left(1+\frac{x_3}{\ell}\right)\frac{|\bar{x}|^2}{2\ell}\right]} \int D(\bar{\xi})\, e^{-ik\frac{\bar{x}\cdot\bar{\xi}}{\ell}}\, d\bar{\xi} \tag{89}$$

If a reference point is present at the origin of ξ-plane, the complex field of that reference is

$$\psi_R(\bar{x}) = B\,\frac{e^{ikr_R}}{r_R} \simeq B\,\frac{e^{ik\left[\ell - x_3 + \frac{|\bar{x}|^2}{2\ell}\left(1+\frac{x_3}{\ell}\right)\right]}}{\ell} \tag{90}$$

The virtual image term (see Section III and Appendix I) can be written as

$$\psi_0(\bar{x})\,\psi_R^*(\bar{x}) = -\frac{ikB^*}{2\pi\ell^2}\int D(\bar{\xi})\, e^{-ik\frac{\bar{x}\cdot\bar{\xi}}{\ell}}\, d\bar{\xi} \tag{91}$$

and it is directly related to the Fourier transform of the object field distribution $D(\bar{\xi})$. Required station location accuracy depends now only on the variation of the above term and not on an additional phase term in front of the integral (Equation 89). The maximum variation of the above equation or the smallest fringe over the array occurs for the largest target dimension ξ max.

For the one-dimensional case and assuming $D(\bar{\xi}) = \text{const} = K$ over the target, the above integral becomes

$$\psi_o(\bar{x})\,\psi_k^*(\bar{x}) = -\frac{ikB^*K}{2\pi\ell^2}\int_{-\frac{\xi_{max}}{2}}^{\frac{\xi_{max}}{2}} e^{-ik\frac{\bar{x}\cdot\bar{\xi}}{\ell}}\,d\bar{\xi} = -\frac{ikB^*K}{4\pi\ell^2}\,\text{sinc}\,\frac{k\xi_{max}}{2\ell}\times \tag{92}$$

The lobe width Δx_ξ of which is obtained by setting

$$\frac{k\xi_{max}}{2\ell}\Delta x_\xi = \pi \tag{93}$$

or

$$\Delta x_\xi = \frac{\ell\lambda}{\xi_{max}} \tag{94}$$

For

$$\ell = 300\text{ km} = 3\times10^7\text{ cm} \quad \xi_{max} = 10^3\text{ cm} \quad \lambda = 10\text{ cm}$$

$$\Delta x_\xi = \frac{3\times10^7\times10}{10^3} = 3\times10^5\text{ cm} = 3\text{ km} \tag{95}$$

Choosing one one hundredth of such width as the criterion for station location tolerance, one still sees that the requirement becomes

$$\Delta x = \frac{\Delta x_\xi}{100} = 30\text{ meters} \tag{96}$$

clearly a much more relaxed requirement than if an actual reference was not near the target. The actual reference from a target could be a prominent scattering center or a specular point on the target. However, in most cases, an actual reference is hard to find because a specular point might not be present for that view and a prominent scattering center might not be visible at all stations of the array.

If a synthesized reference is used to obtain a hologram (or for that matter, if the array is used as a lens) then it must be possible to calculate the phase variation over the array due to a point source located near the target. The phase variation, given by Equation (90) is

$$e^{ik\left[\rho - x_3 + \left(1 + \frac{x_3}{\rho}\right)\frac{|\bar{x}|^2}{2\rho}\right]} \tag{97}$$

and it changes the field values function $\psi_o(\bar{x})$ at the array to a new field value function $\psi_o'(\bar{x})$, which is the Fourier transform of the object source distribution $D(\bar{\xi})$. (See Equation 78).

$$\psi_o'(x) = \int D(\bar{\xi})\, e^{-ik\frac{\bar{x}\cdot\bar{\xi}}{\rho}}\, d\bar{\xi} \tag{98}$$

To be able to calculate such a phase variation over the array, the stringent station location and coherence requirements of the one-step processing must be imposed on the system.

Diffuse Illumination

When optical-type imaging is done for general targets by means of large aperture radar arrays operating at microwave frequencies, the image obtained resembles that which would be obtained from very smooth objects; more specifically, only a few highlights (such as specular points, edge scatttering centers) show up on the object, while the remaining features remain hidden.

The reason for such peculiar behavior of microwave imaging versus optical imaging for the same target is that the microwave wavelength used is much larger than the optical one, and thus most information is obtained from regions, aside from specular points, which have discontinuities or roughness larger than the microwave wavelength used.

For one transmitter and a particular receiver, the number, position and type of scattering centers on a general target, which contribute mostly to the electromagnetic scattering, and thus those points which will image, are given by Keller's geometrical theory of diffraction [9].

Using an array of receivers, but still only one transmitter, each receiver, seeing the target from a slightly different direction, will measure the scattering due mostly to slightly different points on the target. Hence, the image obtained will be a more filled one than for monostatic systems, since each scattering center will be smeared along the edges or discontinuities on the target, and thus will add to the recognizability of the target.

In order for the microwave image to resemble the optical image of an object, it is necessary to simulate the diffuse scattering at optical wavelengths.

One approach toward that objective consists of illuminating the target from different directions, so that although for each illuminator the target does not scatter diffusively, the combined scattering for all illuminators appears diffuse to the extent that returns from the target come from the large fraction of the extent of each region of discontinuity, and not only from a few scattering centers.

If an image is then processed using the array data, the image will look like an outlined sketch of the target, resembling the target more closely than would a three-dimensional structure of scattering centers.

There are several ways of implementing such "diffuse" target illumination. Using about a dozen transmitters placed at different locations (some of which will be outside the array) one could illuminate the target simultaneously or in sequence.

The simultaneous illumination requires that the different transmitters produce a combined incident wavefront at the target, which is diffuse but coherent at the same time in order to be able to do coherent imaging using the radar array.

This requirement imposes, in turn, stringent station location accuracy as well as coherency requirements, so that appropriate phase delays may be used between transmitters to permit the construction of the incident coherent wavefront. Furthermore, since the targets dealt with by the array are moving, an extremely precise tracking of the target is required in order to vary the phase delays between transmitters in order to always be able to construct a coherent incident wavefront. One of the many difficulties of generating such diffuse illumination, using the simultaneous approach, is the additional phase change introduced by atmospheric inhomogeneities along the different paths for each illuminating beam, degrading the combined coherent wavefront. A quantitive analysis of the degradation of the coherent wavefront generated by several transmitters due to atmospheric inhomogeneities, together with other considerations involved in producing a coherent diffuse illumination, will be conducted in the future.

The sequential illumination approach, not having to generate a combined coherent incident wavefront, does not suffer from the station location and coherency requirements, but on the other hand does involve the fact that since each transmitter illuminates in sequence the moving target, it will be viewed at different times.

The question of maximum coherent integration times, pulse duration, dealt with in Appendix 3, must enter in the discussion of the sequential approach to simulate diffuse illumination.

For target velocity V = 7000 m/sec, the pulse duration time, τ, necessary for the target not to have moved more than 1/10 λ (λ = 10 cm) in that time interval, was found to be

$$\tau \approx 10^{-6} \text{ sec.} \tag{99}$$

The maximum coherent integration time T_{max}, to allow for as high a S/N ratio as possible without blurring the hologram, was found to be

$$T_{max} = 10^{-3} \text{ sec.} \tag{100}$$

based on estimates of maximum target size and rotation rate. The signal-to-noise analysis indicated the desirability of coherently integrating at least 100 pulses.

Using the sequential approach to diffuse illumination without having to maintain phase coherence between stations, the most convenient way to proceed might be to transmit from each transmitting station, for example, one hundred 1 μ-second pulses, coherently integrate them at the receivers, process them to obtain the hologram and reconstruct an image, then superimpose 10 of these separate images to obtain the "combined" final image which will be a more detailed sketch of the target than would each of the individual images.

A blurring, due to the motion of the target, might be present. To reduce the blurring, one might obtain each separate image with less coherent integration time.

All of the above approaches to simulate diffuse illumination will be investigated in greater detail in the future.

Off-Zenith Behavior of the System

The results obtained in the technical analysis developed so far consider the target to be located at the zenith of the radar array.

In most cases, however, the target will not be at the zenith of the array's center and a brief analysis is needed to indicate the differences that do arise.

Consider the same diagram as included at the beginning of this section, but with a target placed off-zenith and assume for simplicity a planar array. (See diagram below).

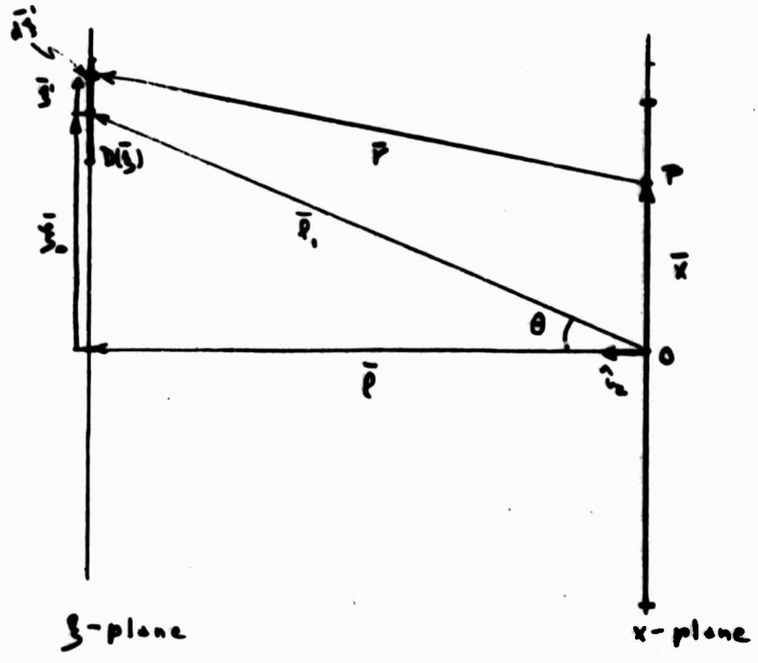

The complex field $\psi_0(\bar{x})$ at any point P of the array due to a complex object source distribution $D(\bar{\xi})$ located in the vicinity of $\bar{\xi}_0$ is given by the usual expression

$$\psi_0(\bar{x}) = -\frac{ikb}{2\pi}\int D(\bar{\xi})\frac{e^{ikr}}{r}\,d\bar{\xi} \tag{101}$$

where $b = \frac{\hat{\xi}_0\cdot\bar{p}}{p} = \text{const.}$

$$r = \sqrt{l^2 + |\bar{x}-\bar{\xi}|^2} = \sqrt{l^2 + \xi_0^2 + |\bar{x}-\bar{\xi}|^2 - \xi_0^2} \tag{102}$$

Assuming that $\frac{|\bar{x}-\bar{\xi}|^2 - \xi_0^2}{l_1^2} \ll 1$ where $l^2 + \xi_0^2 = l_1^2$

the above expression for r, after a change of variable, $\bar{\xi} = \bar{\xi}_0 + \bar{\xi}'$,

becomes

$$r = l_1 + \frac{|\bar{x}|^2}{2l_1} - \frac{\bar{x}\cdot(\bar{\xi}_0+\bar{\xi}')}{l_1} + \frac{\bar{\xi}_0\cdot\bar{\xi}'}{l_1} + \frac{|\bar{\xi}'|^2}{2l_1} \tag{103}$$

Using such an expression for r in the exponent of the integral, but only the approximation $r \simeq l_1$ in the denominator, the complex field amplitude at point P becomes

$$\psi_0(\bar{x}) = -\frac{ikb}{2\pi l_1}e^{ik\left[l_1 + \frac{|\bar{x}|^2}{2l_1} - \frac{\bar{x}\cdot\bar{\xi}_0}{l_1}\right]}\int D(\bar{\xi}_0+\bar{\xi}')\,e^{-\frac{ik}{l_1}\left[\bar{x}\cdot\bar{\xi}' - \bar{\xi}_0\cdot\bar{\xi}' - \frac{|\bar{\xi}'|^2}{2}\right]}d\bar{\xi}' \tag{104}$$

Assuming the Fraunhofer condition, $\frac{|\bar{\xi}'|^2}{2\ell_1} \ll 1$,

and introducing the proper phase modulation over the array, one can obtain the new complex field $\psi_o'(\bar{x})$:

$$\Psi_o'(\bar{x}) = i\frac{2\pi\ell_1}{kb}\, e^{-ik\left[\ell_1 + \frac{|\bar{x}|^2}{2\ell_1} - \frac{\bar{x}\cdot\bar{\xi}_o}{\ell_1}\right]} \Psi_o(\bar{x}) \qquad (105)$$

which is

$$\Psi_o'(\bar{x}) = \int D(\bar{\xi}_o + \bar{\xi}')\, e^{-i\frac{k}{\ell_1}\left[\bar{x}\cdot\bar{\xi}' - \bar{\xi}_o\cdot\bar{\xi}'\right]} d\bar{\xi}' \qquad (106)$$

The Fourier Transform of $\psi_o'(\bar{x})$ over an infinite planar array will then be:

$$T_F\left\{\Psi_o'(\bar{x})\right\} = \frac{k^2}{4\pi^2\ell_1^2}\int \Psi_o'(\bar{x})\, e^{+ik\frac{\bar{x}\cdot\bar{\alpha}}{\ell_1}} d\bar{x} =$$

$$= \frac{k^2}{4\pi^2\ell_1^2}\int D(\bar{\xi}_o + \bar{\xi}')\int e^{-i\frac{k}{\ell_1}\bar{x}\cdot(\bar{\xi}'-\bar{\alpha})} d\bar{x}\, e^{ik\frac{\bar{\xi}_o\cdot\bar{\xi}'}{\ell_1}} d\bar{\xi}' =$$

(107)

$$= \int D(\bar{\xi}_0 + \bar{\xi}') \, \delta^{(2)}(\bar{\xi}' - \bar{\alpha}) \, e^{i k \frac{\bar{\xi}_0 \cdot \bar{\xi}'}{\ell_1}} \, d\bar{\xi}' =$$

$$= D(\bar{\xi}_0 + \bar{\alpha}) \, e^{i k \frac{\bar{\xi}_0 \cdot \bar{\alpha}}{\ell_1}}$$

which is the complex source distribution, $D(\bar{\xi}_0 + \bar{\alpha})$, apart from a linear phase term. Since one is interested only in the magnitude square of the image and not in the complex quantity, the phase terms will not effect the quality of the image.

If the planar array is of finite extent, $2L$, in one of the two planar directors, according to the above equation, the complex source distribution $D(\bar{\xi})$ is then convolved with the function

$$\operatorname{sinc} \frac{k \bar{L} \cdot (\bar{\xi}' - \bar{\alpha})}{\ell_1} \tag{108}$$

The transverse resolution, L_{d_θ}, in the α-plane for a point source in the ξ-plane is then obtained by setting

$$\frac{kL}{\ell_1} \cdot L_{d_\theta} = \pi \tag{109}$$

or

$$L_{d_\theta} = \frac{\lambda \ell_1}{2L} = \frac{\lambda \ell}{2L \cos\theta} = \frac{L_d|_{\theta=0}}{\cos\theta} \tag{110}$$

The above expression indicates the the off-zenith transverse resolution is poorer than the zenith transverse resolution by a factor $\cos\theta$, where θ is the angular orientation of the viewed target relative to the zenith of the array. This result is consistent with the optical resolution formula, which equates the resolution to λ/α, where α is the angle subtended by the optical viewing system. Similarly, the longitudinal resolution ℓ_d, and the parallel and perpendicular magnifications given in Section III and in Appendix 1, will change and will be poorer when the target is in an off-zenith position. A complete investigation of such off-zenith behavior will be carried out in the near future.

An additional result will be affected by the off-zenith behavior; for a target located at an angle θ relative to the normal to the array, the sampling interval, established for the $\theta = 0$ direction, will be able to measure higher spatial frequencies because the sampling interval will appear smaller by a fraction $\cos\theta$ in the θ-direction and thus targets of larger spatial extent can be dealt with. In summary, the off-zenith behavior of the system will permit imaging larger regions of space with poorer resolution and magnification at low elevation angles, and imaging smaller regions with better resolution and magnification at higher elevation angles.

SECTION V

AN ILLUSTRATIVE SYSTEM EXAMPLE

In order to allow greater appreciation of the various constraints and requirements associated with microwave imaging, calculations for appropriate parameters are given that are applicable to a two-step process with sampled data and optical reconstruction.

To begin we choose the following operating data:

microwave wavelength, $\lambda = 0.1\text{m}$ ($k = \frac{2\pi}{\lambda} = 62.8\text{m}^{-1}$);

optical wavelength, $\lambda' = 0.5 \times 10^{-6}\text{m}$ ($k' = \frac{2\pi}{\lambda'} = 1.26 \times 10^{7}\text{m}^{-1}$);

frequency ratio, $k'/k = \lambda/\lambda' = 2 \times 10^{5}$;

$\ell = 3 \times 10^{5}\text{m}$;

$L_D = 5\text{m}$ (half linear target extent);

$L_d = 1\text{m}$ (linear resolution size).

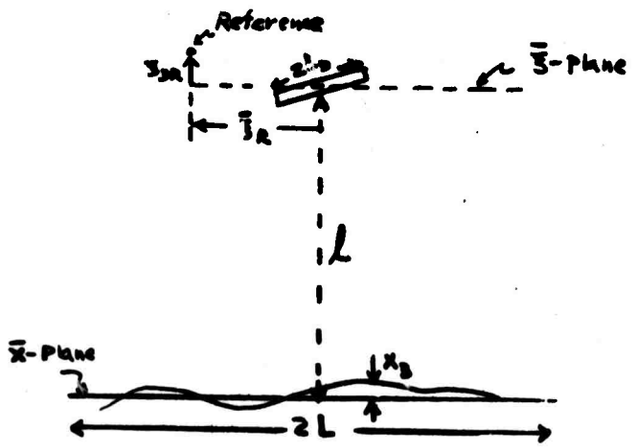

MICROWAVE SET-UP

Array Size (2L):

$$\text{From } L_d = \frac{\lambda \ell}{2L}, \tag{111}$$

$$2L = \frac{\lambda \ell}{L_d} = 30 \text{ km.} \tag{112}$$

Microwave Station Spacing (2b):

$$2b \leq \frac{\lambda \ell}{2 L_D} = 3 \text{ km.} \tag{113}$$

Number of Stations in Square Array (M):

$$M = \left(\frac{2L}{2b} + 1\right)^2 = 121 \tag{114}$$

Obliquity Condition (Microwave):

$$\frac{|\bar{x} - \bar{s}|^2}{(\ell - x_s)^2} \approx \frac{(L + L_D)^2}{\ell^2} \approx \left(\frac{L}{\ell}\right)^2 \approx .003 \ll 1 \tag{115}$$

Fraunhofer Condition (Microwave):

$$\frac{k|\bar{s}|^2}{2\ell} \leq \frac{2kL_D^2}{\ell} \approx .01 \ll 1 \tag{116}$$

Tolerance on Array Planarity:

Using $\ell \sim \ell + \xi_{3R}$, and assuming $|\xi_{3R}| < 1$ km.

$$\frac{k|x_s|L^2}{\ell^2}\left(\frac{\xi_{3R}}{\ell} + \frac{2L_p}{L}\right) << 1 \tag{117}$$

requires

$$|x_s| << 2 \text{ km.} \tag{118}$$

OPTICAL SET-UP

Quadratic Phase Variation Requirements for Sampled Holography

For u_1 satisfying $|u_1 - u_{1j}| < \frac{b'}{m}$, it is necessary that

$$\frac{k'|u_1^2 - u_{1j}^2|g}{2} << 1 \tag{119}$$

that is,

$$\frac{k'b'Lg}{m^2} << 1 \tag{120}$$

From the focusing condition (see below)

$$k'g = -\frac{km^2\xi_{3R}}{\ell(\ell+\xi_{3R})} \tag{121}$$

so it is required that

$$b' \ll \frac{\lambda \ell^2}{2\pi L |\xi_{3R}|} \tag{122}$$

in which $|\xi_{3R}|/\ell \ll 1$ has been used. Hence, if $\xi_{3R} = -500\text{m}$,

$$b' \ll 200\,\text{m} \tag{123}$$

or

$$\frac{2b'}{m} \ll 66\ \text{microns} \tag{124}$$

where m is the scale factor, here set equal to 0.6×10^7, because, as will be seen, such a value leads to convenient optical parameters. A value of b' of ~ 20m would be reasonable. A condition similar to the above pertains to $|u_2^2 - u_{2n}^2|$, resulting in the same requirement on b'.

Optical Focusing Condition

The focusing condition for $\psi_{I_{S2}}$ is

$$k'\left(\frac{1}{z_1} + \frac{1}{z_2}\right) + \frac{k m^2 \xi_{3R}}{\ell(\ell + \xi_{3R})} = 0, \tag{125}$$

in which, it will be recalled, z_1 and z_2 are, respectively, the distances from the focal point of the spherical wave used in the reconstruction to the hologram and the distance from the hologram to the image. A negative value of z_2 corresponds to a virtual image. Using $\xi_{3R} = -500m$,

$$z_2 = \frac{-z_1}{1 - z_1} \tag{126}$$

If $z_1 = 0.9m$,

$$z_2 = -9m \tag{127}$$

Image Magnification from Reconstruction and Viewing

$$m_T = \text{Overall Magnification} = \frac{\beta_e}{\beta_o} = \frac{\text{1/2 angle on eye (aided or not) from image}}{\text{1/2 angle on eye from original object}}$$

Let $\beta_e = 1/12$ radian $\approx 5^o$

$$m_T = \frac{\beta_e}{\beta_o} = \frac{\beta_e}{L_o/\ell} = 5 \times 10^3 \tag{128}$$

But m_T may be written as $(Mag_1)(Mag_2) = \left(\frac{mk}{k'}\right)\left(\frac{i_I}{f_e}\right)$, where Mag_1 and Mag_2 the angular magnifications due to the reconstruction process and due to viewing the reconstructed virtual image with a telescope, respectively. A convenient set of optical parameters results from a choice of $Mag_1 = 30$ and $Mag_2 = 5 \times 10^3/30 = 166.4$.

Reconstruction:

From $m\frac{k}{k'} = 30$, $m = 0.6 \times 10^7$ (scaling factor), so that

$$2L_{H_3} = \frac{2L_H}{m} = 5\,mm \tag{129}$$

The expression $m\frac{k}{k'}$ for Mag_1 comes from

$$\psi(\bar{\alpha}) \sim D\left(-\frac{\ell k'\bar{\alpha}}{kmz_2} + \frac{\ell\bar{\xi}_R}{\ell + z_{3R}}\right) = D(\bar{s}) \tag{130}$$

since for 1 unit change in $\bar{\alpha}$, image plane, there results $\frac{\ell k'}{kmz_2}$ units change in $\bar{\xi}$, object plane.

Thus,

$$\frac{L_2}{L_{D_I}} = \frac{\ell k'}{kmz_2} = \frac{1}{m_H} \tag{131}$$

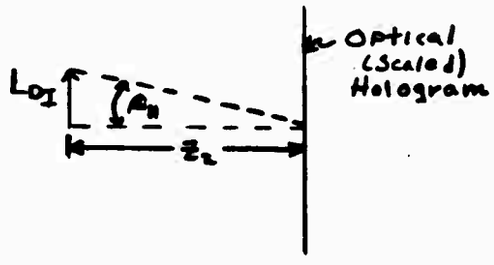

where $m_{||}$, the parallel magnification, is discussed in Appendix 1. The angular magnification, Mag_1, is then obtained as follows. Let

$$\beta_H = \frac{L_{DI}}{|z_2|}, \text{ and } \beta_o = \frac{L_D}{\ell} \tag{132}$$

Then

$$Mag_1 = \frac{\beta_H}{\beta_o} = \frac{L_{DI}}{L_D}\frac{\ell}{|z_2|} = \frac{km}{k'} \tag{133}$$

Viewing:

Telescope viewing: objective lens: $$\frac{1}{|z_2|} + \frac{1}{i_I} = \frac{1}{f_o} \tag{134}$$

eyepiece lens: $$\frac{1}{i_{e_o}} + \frac{1}{i_{e_I}} = \frac{1}{f_e} \tag{135}$$

With telescope, $i_{e_I} = -\infty$, so that $i_{e_o} = f_e$,

$$Mag_2 = \frac{i_I}{i_{e_o}} = \frac{i_I}{f_e} \tag{136}$$

A Mag_2 of 166.4 may be achieved with $z_2 = -9m$, $f_o = 1m$, and $f_e = 6.8mm$.

Non-Overlap of Images:

For non-overlap of I_1 and I_2 we consider the following:

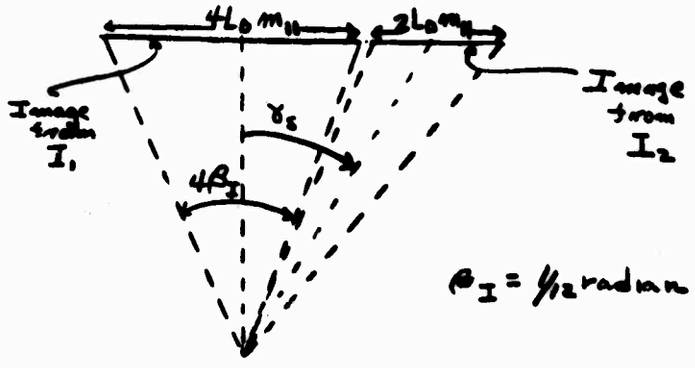

Separating the I_1 and I_2 images will automatically separate the I_2 image from the I_3 and I_4 images. The effective length of the image from I_1 is $4L_D m_{||}$, since it is the autocorrelation of $D(\bar{\xi})$.

If we let γ_S be the angular displacement of the center of the image due to I_2 from the zero axis, then from the sketch it is required that

$$\gamma_s > 3\beta_I = \frac{3}{12} \text{ radian} \approx 15^\circ \tag{137}$$

From the form of $\psi_{I_{S2}}$, the origin of coordinates in the object plane is mapped into the point $\bar{\alpha}_{o2}$ in the image plane (considering only the image resulting from I_2) where

$$-\frac{l k' \bar{\kappa}_{o2}}{k m z_2} + \frac{l \bar{\gamma}_R}{l + \gamma_{3R}} = 0 \tag{138}$$

so that

$$\frac{|\bar{\alpha}_{02}|}{|z_2|} = \frac{k m |\bar{\xi}_R|}{\ell k'} \tag{139}$$

assuming, as before that $|\xi_{3R}| \ll \ell$. Accounting for the viewing telescope, we want an angular shift such that

$$\frac{|\bar{\alpha}_{02}|}{|z_2|} \frac{i_I}{f_c} = \frac{km}{k'} \frac{|\bar{\xi}_R|}{\ell} \frac{i_I}{f_c} = m_T \frac{|\bar{\xi}_R|}{\ell} \geq 3\beta_I, \tag{140}$$

or

$$|\bar{\xi}_R| \geq \frac{\ell}{m_T} 3\beta_I = 15m. \tag{141}$$

Image Placement with Respect to Zeroes of Sinx/x Intensity Modulation

It is shown in Appendix 2, Method 1, that the reconstructed image is modulated in intensity by a two-dimensional sinx/x function. The zeros of this function are separated by

$$|\Delta\alpha| = \frac{m|z_2|\pi}{k' b'} \tag{142}$$

or, in angle by,

$$\frac{|\Delta\alpha|}{|z_2|} = \frac{m\pi}{k'b} \frac{b}{b'} = \frac{mk}{k'} \frac{2L_D}{\ell} \frac{b}{b'} \tag{143}$$

in which the sampling condition $2b = \ell\pi/L_D k$ has been used. It will be recalled that mk/k' is just the angular magnification resulting from the reconstruction process, and $2L_D/\ell = 2\beta_o$, the angle subtended by the target as seen by an observer's unaided eye. Thus

$$\frac{|\Delta x|}{|z_i|} = 2\beta_H \frac{b}{b'} \tag{144}$$

where $2\beta_H$ is the angle subtended by the virtual image of the target as seen by an observer in the plane of the scaled down hologram. Thus, if $b/b' \geq 1$, the image fits between zeros of the intensity modulation. In this example b' was chosen previously to be $\approx$ 20m, and b was chosen as 1.5×10^3m. Hence, $b/b' \approx 75$, and the variation of intensity modulation across the image is small.

SECTION VI

EXPERIMENTAL WORK

REQUIREMENTS AND ADVANTAGES

Experimental measurements are required in order to investigate and establish actual results at microwave frequencies that are independent of any analyses which rely on approximations. This need is most critical to supplement the analysis that provides data to process an image, judge its quality, and evaluate recognition capability. In addition of course, study and verification of other areas associated with one- or two-step processing can be carried out. Illustrative of the wide range of application for experiment are type of illumination, type of reference and placement effects, station location accuracy, array thinning, array non-planarity, sampling, image reconstruction, and, generally, evaluation of error effects.

Areas that could be investigated concerning image quality include the kind of image possible, image realism, filled-in view of target discontinuities, monostatic and multistatic illumination with simple or multiple transmission, and the benefit of polarization diversity. In addition, methods of carrying out coherent processing for image improvement within time constraints compatible with target movement and real-time outputs are of concern. Chaff effects, image distortion and discrimination, and the use of spatial filtering, for example, are also important in determining image quality.

Once accurate and appropriate microwave data is available, the task of synthesizing such data and evaluating the results of the many experiments

possible can be handled by computer processing. However, even though obtaining experimental data is fundamental, questions on range versatility, feasibility, and applicability are important.

The degree to which optical simulation is used will depend on (1) whether or not range data is taken initially at optical frequencies, and (2) whether one- or two-step image processing is being considered. The use of direct optical processing for constructing an image with the one-step approach is not as obvious as in two-step processing, and will be dealt with in future study, particularly since, as noted in the conclusions, the one-step processing might be favored over the two-step processing, when all factors have been considered.

CHOICE OF RANGE FREQUENCY

The desired goal is to perform range measurements that simulate the actual target-array microwave environment as closely as possible. Thus, it is desirable that the array be in the target far field, that is, that the Fraunhofer condition hold.

If one chooses an operating range frequency in the microwave spectrum under such conditions, the target-to-array distance and array size become large and impractical. Alternatively, for reasonably sized arrays and distances, operation in the microwave region actually requires Fresnel scattering rather than Fraunhofer scattering.

On the other hand, operating in the optical frequency range, for which a wealth of technical and experimental data exist, permits a proper Fraunhofer simulation together with reasonable and, in fact, very convenient target-to-array distance and array size. A possible difficulty occurs in the scaled-target size which can be in the order of hundredths of a millimeter. Even

here, a large variety of target specimens are available to represent actual targets ranging from smooth ones to those with many discontinuities.

Considering the factors of overall convenience and proper simulation, it appears that experimental data on the target can be taken conveniently at optical frequencies.

OPTICAL SIMULATION

Once the data is obtained, processing can take place by means of a computer or by actual optical systems. For two-step (holographic) processing, optical means offer a natural and most effective approach. Even with one-step processing, it seems that forming an image might be carried out by optical processing and display.

The use of optical experimentation, both in simulating target return and processing to reproduce an image, requires establishment of an experimental facility, comprising, at least, an optical bench, an associated laser, and photographic equipment. Also, an experienced experimentalist should be obtained to operate the equipment.

A survey was made of appropriate benches with associated mounts, lenses, spatial filters, alignment sets, together with gas lasers (which, in fact, are quite adequate for the present purposes). Such a system with sufficient versatility and accuracy would cost about $10,000.00.

In addition, microdensitometer readouts for a scanned analysis of the hologram or image patterns can be obtained on a rental basis for about $40.00 per run.

Considering the importance and usefulness of the experimental aspects of this study, the adequacy and convenience of the optical mode, and the particular low cost of implementing an optical set up, it is strongly recommended that this activity be initiated and supported.

SECTION VII

CONCLUSIONS

MAIN RESULTS

The purpose of the present study is to assess the feasibility of using large microwave apertures for obtaining real-time, three-dimensional target images.

Two basic approaches are considered: (1) one-step processing, which treats the array as a lens, and, (2) two-step processing, in which a hologram is constructed from the microwave data prior to forming an image. This study, whose preliminary conclusions are summarized below, provides information on feasibility, with detailed analytical support.

In using two-step processing, a separate reference signal is required. This can be either synthesized or obtained from an actual reference source. Very accurate knowledge of array station location and a fully coherent array are required for both one-step and two-step processing, except in the latter case when the target itself can provide the reference signal. However, establishment of coherency by microwave links and/or atomic clocks and determination of station location by laser ranging appear possible.

When a station spacing based on the spatial frequency content of the field from the target only is used in the two-step processing, some fold-over of replicas of images from terms of the hologram on the desired virtual image of the target is caused. The fold-over effect can be dealt with without altering the station spacing by defocusing the undesired images. Two-step process would be dealing with at least a hundred stations located over an array surface of about a thousand square kilometers.

A variety of approaches are available to reproduce an image from the sampled microwave data. Three approaches have been noted, with particular emphasis being given to image reconstruction from a sampled scaled optical hologram. A calculation of the effects of thermal noise is given for the sampled holographic process and SNR is determined in terms of scatterer properties and microwave system parameters.

Although the lateral resolution can be under a meter in both processes, the longitudinal resolution is much poorer, by approximately a factory of forty, due to the fact that the range to the target is at least about ten times the maximum linear extent of the array.

To date, approaches considered for using the target as a microwave reference source appear impractical. However, use of the target as a reference would be advantageous, because it would remove the strict requirement on accuracy of the knowledge of station location. Such accuracy requirements, together with the large minimum number of stations and the poor longitudinal resolution, weigh against the adoption of the two-step holographic method without the use of the target as a reference source.

In either method the effects of off-zenith target position do not appear to be a serious problem.

Inasmuch as the two-step processing, requiring a filled array, does not yield a good three-dimensional virtual image because of the poor longitudinal resolution, it may be advisable to explore relaxing the three-dimensional image requirement, thus permitting the use of thinner arrays, such as a Mills cross, for the formation of a two-dimensional image

possessing similar transverse resolution capability as the filled array considered for use in the two-step processing.

Application of such arrays together with possible greater diffusivity of illumination can produce the advantages of improved image quality and real-time viewing at microwave frequencies. To fully explore such advantages in image quality and usefulness, the need for optical range data remains an important requirement.

FUTURE EFFORTS

Now that the various major advantages and disadvantages are understood, analysis and experimentation in future work can concentrate on particular areas. Optimum array layouts to reduce the number of stations and maintain the required resolutions will be considered. The enhancement of image quality from illumination diffusivity needs further work. Direct optical methods for constructing an image using the one-step process will also be considered. Details of carrying out methods of obtaining accurate station location determination and a fully coherent array can be established.

In addition, methods for obtaining a reference source from the target will be investigated, since having an actual reference relaxes the coherence and station location requirements.

The decision as to the superiority of the one-or the two-step process can only be reached after both approaches have been fully explored.

Recognizability of the image in various target environments, together with the use of focusing, reference placement, and spatial filtering, need further study. The formation of a simulated image using range data is of prime importance here, and detailed specifications on range design and experimentation will proceed.

APPENDIX 1

CONTINUOUS HOLOGRAPHY

The purpose of the following analysis is severalfold. First, it is intended to provide an example of the conventional scalar wave equation treatment of the formation of a hologram and of image reproduction therefrom. Second, it is intended to provide a framework for the study of tolerances that must be observed in order to keep within acceptable limits the effects on the reproduced image of such factors as a rough hologram recording surface, distortion of the hologram between recording and reproduction, and phase errors in the reference signal used in forming the hologram. In addition, the analysis furnishes the basic relations that are required for the study of the effect of the location of the source of the reference signal on positions of the reproduced images and on depth of focus, for the study of the magnification that may be achieved by the system as a function of various system parameters, and for the study of the reproduction of an image from a "discrete" hologram synthesized from sampled values of a continuous hologram. No attempt is made in the following to improve on the conventional scalar wave equation treatment, except for the simple provision for the inclusion of various error terms that are usually omitted.

FORMATION OF THE HOLOGRAM

In Figure 1, let S_H be an infinite plane tangent to the earth's surface at some point P_T. Let a coordinate system (x_1, x_2) be established on S_H with P_T as origin, and define the unit vectors $\hat{i}_1$ and $\hat{i}_2$ along the x_1- and x_2 - axes, respectively. Erect an x_3 axis perpendicular to S_H with the direction of positive x_3 being to the left in the figure. At a distance ℓ from S_H consider a plane S_o having defined on it coordinates (ξ_1, ξ_2),

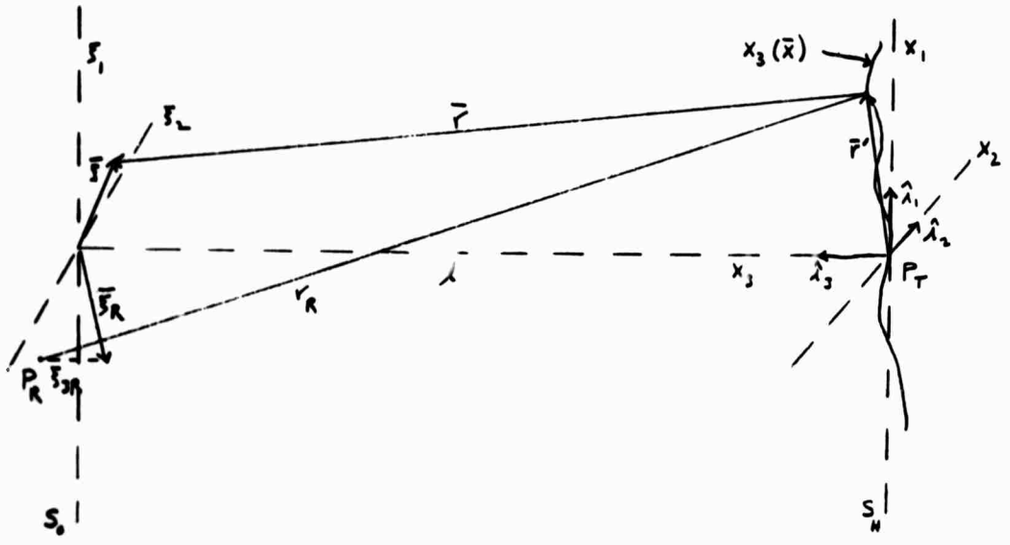

Figure 1. Hologram Recording Geometry

with the origin of coordinates at the point at which the previously defined x_3 - axis pierces S_o. The ξ_1 - and ξ_2 - axes are parallel to the x_1 - and x_2 - axes, respectively. The unit vector $\hat{i}_3$ is normal to S_H and directed to the left in the figure. On the plane S_o, let there be defined a complex function $D(\bar{\xi})$, which will be taken as the value on S_o of a disturbance propagating in space in accordance with the scalar wave equation. Harmonic time dependence of the form $e^{-i\omega t}$ is assumed.

Define the following vectors for arbitrary x_1, x_2, x_3, ξ_1, and ξ_2.

$$\bar{x} = \hat{\lambda}_1 x_1 + \hat{\lambda}_2 x_2$$

$$\bar{r}' = \bar{x} + \hat{\lambda}_3 x_3$$

$$\bar{\xi} = \hat{\lambda}_1 \xi_1 + \hat{\lambda}_2 \xi_2$$

$$\bar{r} = \bar{\xi} + \hat{\lambda}_3 l - \bar{r}'$$

It is assumed that the hologram is to be recorded on a surface

$$x_3 \equiv x_3(\bar{x}).$$

The reference wave used in forming the hologram is assumed to be a spherical wave emitted from a point source at the point P_R located at $\bar{\xi}_R + \hat{i}_3 \xi_{3R}$, where

$$\bar{\xi}_R = \hat{\lambda}_1 \xi_{1R} + \hat{\lambda}_2 \xi_{2R}.$$

If a quasi-monochromatic[10] propagating disturbance ψ, of wave number k, takes on the values $D(\bar{\xi})$ on S_o, the value of the disturbance on the surface $x_3(\bar{x})$ may be approximated by[11]

$$\psi_0(\bar{r}') = -\frac{1}{2\pi} \int_{S_o} D(\bar{\xi}) \frac{e^{ikr}}{r} \left(ik - \frac{1}{r}\right) \frac{\hat{\lambda}_3 \cdot \bar{r}}{r} d\bar{\xi}, \qquad (1)$$

where $r = |\bar{r}|$. If it is assumed that

$$k \gg \frac{1}{r},$$

and

$$\frac{\hat{\lambda}_2 \cdot \bar{r}}{r} \approx 1$$

over the region of S_o for which $D(\bar{\xi}) \neq 0$, and over some region of interest of S_H, Equation (1) may be simplified to

$$\psi_o(\bar{r}') = -\frac{ik}{2\pi} \int_{S_o} D(\bar{\xi}) \frac{e^{ikr}}{r} d\bar{\xi}. \tag{2}$$

Now introduce an approximation for r.

$$r^2 = (l - x_3)^2 + (x_1 - \xi_1)^2 + (x_2 - \xi_2)^2$$

$$= (l - x_3)^2 \left[1 + \frac{(x_1 - \xi_1)^2 + (x_2 - \xi_2)^2}{2(l - x_3)^2} \right].$$

If all the terms except the first in the above bracket are small compared to unity, the binomial expansion theorem yields the following approximation for r.

$$r = l - x_3 + \frac{(x_1 - \xi_1)^2 + (x_2 - \xi_2)^2}{2(l - x_3)}$$

or, if $|x_3|/l << 1$,

$$r = l - x_3 + \frac{(x_1 - \xi_1)^2 + (x_2 - \xi_2)^2}{2l}\left(1 + \frac{x_3}{l}\right). \tag{3}$$

Assume the reference signal received at $\bar{r}'$ is

$$\psi_R(\bar{r}') = \frac{B e^{ikr_R}}{r_R}, \tag{4}$$

where B is a constant. Making that approximation for r_R that corresponds to the approximation of Equation (3) for r,

$$r_R = \ell - x_3 + r_{3R} + \frac{(x_1 - r_{1R})^2 + (x_2 - r_{2R})^2}{2(\ell + r_{3R})} \left(1 + \frac{x_3}{\ell + r_{3R}}\right). \tag{5}$$

The total disturbance $\psi_T(\bar{r}')$ reaching the point $\bar{r}'$ is the sum of that due to the distribution $D(\bar{\xi})$ on S_o and the reference signal. Thus

$$\Psi_T(\bar{r}') = \Psi_o(\bar{r}') + \Psi_R(\bar{r}'). \tag{6}$$

Now in the phase factors in Equations (2) and (4), substitute the approximations for r and r_R; however, in the denominators of those equations, which are slowly varying, substitute the more crude approximations ℓ and $\ell + \xi_{3R}$ for r and r_R, respectively. Also, in the phase factor of the reference signal, incorporate a term $ik\delta$, where $\delta \equiv \delta(\bar{x})$, which may be used later to represent an error in the synthesis of an artificial reference signal. Substituting the resulting expressions for $\psi_o(\bar{r}')$ into Equation (6) there is obtained

$$\Psi_T(\bar{r}') = -\frac{ik}{2\pi\ell}\int_{S_o} D(\bar{\xi})\, e^{ik\left[\ell + \frac{|\bar{x}|^2}{2\ell} - \frac{\bar{x}\cdot\bar{\xi}}{\ell} - x_3 + \frac{|\bar{\xi}|^2}{2\ell} + \frac{x_3}{2\ell^2}|\bar{x}-\bar{\xi}|^2\right]} d\bar{\xi}$$

$$+ \frac{R}{\ell + r_{3R}}\, e^{ik\left[\delta + \ell + r_{3R} + \frac{|\bar{x}|^2}{2(\ell + r_{3R})} - \frac{\bar{x}\cdot\bar{r}_R}{\ell + r_{3R}} - x_3 + \frac{|\bar{r}_R|^2}{2(\ell + r_{3R})} + \frac{x_3|\bar{x}-\bar{r}_R|^2}{2(\ell + r_{3R})^2}\right]} \tag{7}$$

The power flux incident at $\bar{r}'$ is proportional to

$$I(\bar{r}') = \Psi_T(\bar{r}')\,\Psi_T^*(\bar{r}'), \tag{8}$$

in which the asterisk indicates the complex conjugate. Substituting Equation (7) into Equation (8) yields

$$
\begin{aligned}
I(\bar{r}') = \frac{k^2}{4\pi^2 \ell^2} \int_{S_0} \int_{S_1} D(\bar{r}) D^*(\bar{r}')\, e^{ik\left(\ell + \frac{|\bar{x}|^2}{2\ell} - \frac{\bar{x}\cdot\bar{r}}{\ell} - x_3 + \frac{|\bar{r}|^2}{2\ell} + \frac{x_3|\bar{x}-\bar{r}|^2}{2\ell^2}\right)} \\
\times e^{-ik\left(\ell + \frac{|\bar{x}|^2}{2\ell} - \frac{\bar{x}\cdot\bar{r}'}{\ell} - x_3 + \frac{|\bar{r}'|^2}{2\ell} + \frac{x_3|\bar{x}-\bar{r}'|^2}{2\ell^2}\right)} d\bar{r}\, d\bar{r}' \\
- \frac{ikB^*}{2\pi\ell(\ell + r_{3R})} e^{-ik\left[s + \ell + r_{3R} + \frac{|\bar{x}|^2}{2(\ell + r_{3R})} - \frac{\bar{x}\cdot\bar{r}_R}{\ell + r_{3R}} - x_3 + \frac{|\bar{r}_R|^2}{2(\ell + r_{3R})} + \frac{x_3|\bar{x}-\bar{r}_R|^2}{2(\ell + r_{3R})^2}\right]} \\
\times \int_{S_0} D(\bar{r})\, e^{ik\left(\ell + \frac{|\bar{x}|^2}{2\ell} - \frac{\bar{x}\cdot\bar{r}}{\ell} - x_3 + \frac{|\bar{r}|^2}{2\ell} + \frac{x_3|\bar{x}-\bar{r}|^2}{2\ell^2}\right)} d\bar{r} \\
+ \frac{ikB}{2\pi\ell(\ell + r_{3R})} e^{ik\left[s + \ell + r_{3R} + \frac{|\bar{x}|^2}{2(\ell + r_{3R})} - \frac{\bar{x}\cdot\bar{r}_R}{\ell + r_{3R}} - x_3 + \frac{|\bar{r}_R|^2}{2(\ell + r_{3R})} + \frac{x_3|\bar{x}-\bar{r}_R|^2}{2(\ell + r_{3R})^2}\right]} \\
\times \int_{S_0} D^*(\bar{r})\, e^{-ik\left(\ell + \frac{|\bar{x}|^2}{2\ell} - \frac{\bar{x}\cdot\bar{r}}{\ell} - x_3 + \frac{|\bar{r}|^2}{2\ell} + \frac{x_3|\bar{x}-\bar{r}|^2}{2\ell^2}\right)} d\bar{r} \\
+ \frac{BB^*}{(\ell + r_{3R})^2}
\end{aligned}
\tag{9}
$$

The quantity $I(\bar{r}')$ is proportional to the power flux density on the hologram plane. In the optical case, if this power flux density distribution had fallen on a piece of film, the film could be processed so that the film density would be proportional to the logarithm of the flux density. The result would be an optical hologram.

Having obtained the hologram corresponding to Equation (9), the task is to reconstruct an image of the original "object" - in the present case to reconstruct the disturbance $D(\bar{\xi})$. For ease in discussing the

reconstruction, let Equation (9) be written

$$I(\bar{r}') = I_1 + I_2 + I_3 + I_4, \tag{10}$$

in which I_1 through I_4 represent the four terms of Equation (9). That is, making obvious simplifications, and using $\bar{r}' \equiv \bar{r}'(\bar{x})$ to permit replacing $\bar{r}'$ in the argument of I by $\bar{x}$,

$$I_1(\bar{x}) = \frac{k^2}{4\pi^2 l^2} \iint_{S_0} D(\bar{r}) D^*(\bar{r}) e^{-ik\frac{\bar{x}\cdot(\bar{r}-\bar{r}')}{l} + ik\frac{|\bar{r}|^2 - |\bar{r}'|^2}{2l}} \times e^{-ik\frac{x_3}{2l^2}\left[2\bar{x}\cdot(\bar{r}-\bar{r}') + |\bar{r}|^2 - |\bar{r}'|^2\right]} d\bar{r}\, d\bar{r}', \tag{11}$$

$$I_2(\bar{x}) = -\frac{ikB^*}{2\pi l(l+r_{3R})} e^{-ik\left[s + r_{3R} - \frac{|\bar{x}|^2 r_{3R}}{2l(l+r_{3R})} - \frac{\bar{x}\cdot\bar{r}_R}{l+r_{3R}} + \frac{|\bar{r}_R|^2}{2(l+r_{3R})} + \frac{x_3|\bar{x}-\bar{r}_R|^2}{2(l+r_{3R})^2}\right]} \times \int_{S_0} D(\bar{r}) e^{-ik\frac{\bar{x}\cdot\bar{r}}{l} + ik\frac{|\bar{r}|^2}{2l} + ik\frac{x_3|\bar{x}-\bar{r}|^2}{2l^2}} d\bar{r}, \tag{12}$$

$$I_3(\bar{x}) = \frac{ikB}{2\pi l(l+r_{3R})} e^{ik\left[s + r_{3R} - \frac{|\bar{x}|^2 r_{3R}}{2l(l+r_{3R})} - \frac{\bar{x}\cdot\bar{r}_R}{l+r_{3R}} + \frac{|\bar{r}_R|^2}{2(l+r_{3R})} + \frac{x_3|\bar{x}-\bar{r}_R|^2}{2(l+r_{3R})^2}\right]} \times \int_{S_0} D^*(\bar{r}) e^{ik\frac{\bar{x}\cdot\bar{r}}{l} - ik\frac{|\bar{r}|^2}{2l} - ik\frac{x_3|\bar{x}-\bar{r}|^2}{2l^2}} d\bar{r} = I_2^*, \tag{13}$$

$$I_4(\bar{x}) = \frac{BB^*}{(l+r_{3R})^2}. \tag{14}$$

RECONSTRUCTION OF THE IMAGE

An image may be reconstructed by passing coherent light through the hologram. For generality, it will be assumed that a spherical coherent wavefront is used for reconstruction, as shown in Figure 2.

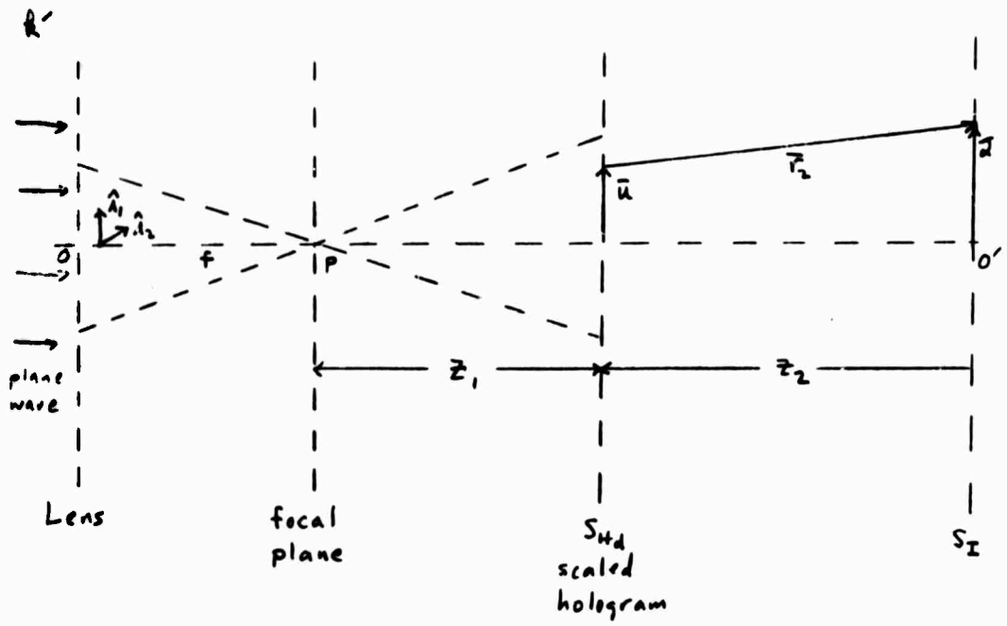

Figure 2. Reconstruction Geometry

Let the illuminating radiation be of wavenumber k'. The hologram will be assumed scaled down in size, so that one unit of distance in the S_{Hd} plane corresponds to m units in the S_H plane. The point at $\bar{x} = 0$ in the S_H plane will be assumed to lie at $\bar{u} = -\bar{u}_d$ in the S_{Hd} plane, and it will be

assumed that the hologram has been distorted somewhat, so that the point that was at $\bar{x}$ on the S_H plane maps into the point

$$\bar{u} \equiv \bar{u}(\bar{x}) \equiv \frac{\bar{x}}{m} - \bar{u}_d + \bar{\Delta} \qquad (15)$$

in the S_{Hd} plane. Here $\bar{\Delta} = \bar{\Delta}(\bar{u})$, and $\bar{\Delta}(-\bar{u}_d) = 0$.

As a reference, take as zero the phase of a ray that has just passed through the center of the lens in Figure 2. The phase of that ray at the focal point, P, of the lens will then be k'f, where f is the focal length of the lens. Now consider that ray through the focal point that pierces the hologram at point P_H located at $\bar{u}$. Then the distance from P to P_H is

$$\left[z_1^2 + |\bar{u}|^2\right]^{\frac{1}{2}},$$

or, retaining the quadratic term in $|\bar{u}|$ in a binomial expansion,

$$z_1 + \frac{|\bar{u}|^2}{2z_1}.$$

The phase of the disturbance propagating along the abovementioned ray is then, at the hologram surface,

$$k'f + k'z_1 + k'\frac{|\bar{u}|^2}{2z_1} .$$

Now let $\bar{r}_2$ be a vector from a point on the plane S_I to the point P_H. Then

$$r_2^2 = |\bar{r}_2|^2 = |\bar{\alpha} - \bar{u}|^2 + z_2^2$$
$$= z_2^2 \left[1 + \frac{|\bar{\alpha} - \bar{u}|^2}{z_2^2} \right],$$

and, retaining quadratic terms in $|\bar{\alpha} - \bar{u}|$ in a binomial expansion,

$$r_2 = z_2 + \frac{|\bar{\alpha} - \bar{u}|^2}{2z_2} .$$

Using Equation (2), the disturbance at the point $\bar{\alpha}$ on the plane S_I may be calculated as an integral over the hologram. At the right hand side of the hologram, the disturbance ψ is

$$\frac{ACf}{z_1} e^{ik'f + ik'z_1 + ik'\frac{|\bar{u}|^2}{2z_1}} I\left[m(\bar{u} + \bar{u}_d - \bar{\alpha})\right],$$

where A is the constant of proportionality relating the power flux density I to the fraction of the incident field intensity* transmitted by the hologram in

* In this work, intensity refers to electric field strength.

the reconstruction process, Cf/z_1 is the intensity of the coherent illumination incident on the hologram, and C is the intensity of the plane wave incident on the lens. In the MKS system, the units of A are meter^2/volts^2. Now, the disturbance at $\bar{\alpha}$ is, using Equation 2,

$$\psi_I(\bar{\imath}) = \frac{-A i k' C f}{2\pi z_1} \int_{S_{Hd}} \frac{e^{ik' r_2}}{r_2} e^{ik' f + ik' z_1 + ik' \frac{|\bar{u}|^2}{2z_1}} I[m(\bar{u} + \bar{u}_d - \bar{\alpha})] d\bar{u}.$$

Setting $r_2 \approx z_2$ in the denominator of the above, and using the usual binomial expansion approximation for r_2 in the phase factor, there results

$$\psi_I(\bar{\imath}) = -\frac{A i k' C f}{2\pi z_1 z_2} e^{ik'\left(z_1 + z_1 + f + \frac{|\bar{u}|^2}{2z_1}\right)} \int_{S_{Hd}} I[m(\bar{u} + \bar{u}_d - \bar{\alpha})]$$

$$\times e^{-ik' \frac{|\bar{u}|^2}{2}\left(\frac{1}{z_1} + \frac{1}{z_2}\right) - ik' \frac{\bar{\imath}\cdot\bar{u}}{z_2}} d\bar{u}. \qquad (16)$$

Equation (16) is linear in the terms I_1 through I_4 comprising I. Let us determine the contribution to $\psi_I(\bar{\alpha})$ of each of these four terms.

(a) Contribution from I_1. Let

$$\psi_{x_3}(\bar{x}) = -\frac{A i k' k^2 c_+}{8\pi^3 z_1 z_2 \ell^2} e^{ik'\left(z_1+z_2+f+\frac{|\bar{u}|^2}{2f_2}\right)} \int_{S_H} e^{ik'\frac{|\bar{u}|^2}{2}\left(\frac{1}{f_1}+\frac{1}{f_2}\right)}$$

$$\times e^{-ik'\frac{\bar{x}\cdot\bar{u}}{f_2}} \int_{S_0} D(\bar{\xi}) e^{-ikm(\bar{u}+\bar{u}_d-\bar{a})\cdot\frac{\bar{\xi}}{\ell}} e^{ik\frac{|\bar{\xi}|^2}{2\ell}} e^{-ik\frac{x_3\bar{x}\cdot\bar{\xi}}{\ell^2}} e^{-ik\frac{x_3|\bar{\xi}|^2}{2\ell^2}} d\bar{\xi} \qquad (17)$$

$$\times \int_{S_0} D^*(\bar{\xi}') e^{ikm(\bar{u}+\bar{u}_d-\bar{a})\cdot\frac{\bar{\xi}'}{\ell}} e^{-ik\frac{|\bar{\xi}'|^2}{2\ell}} e^{ik\frac{x_3\bar{x}\cdot\bar{\xi}'}{\ell^2}} e^{ik\frac{x_3|\bar{\xi}'|^2}{2\ell^2}} d\bar{\xi}' d\bar{u}.$$

Now assume that the region of $\bar{\xi}$ in the plane S_0 over which $D(\bar{\xi}) \neq 0$ is sufficiently restricted so that the plane S_H lies in the Fraunhofer region of any radiation arriving at S_H from the distribution $D(\bar{\xi})$. That is, for all $\bar{\xi}$ for which $D(\bar{\xi}) \neq 0$,

$$\frac{k|\bar{\xi}|^2}{2\ell} << 1. \qquad (18)$$

Further, assume $|kx_3\bar{x}\cdot\bar{\xi}/\ell^2| << 1$, $k|x_3||\bar{\xi}|^2/2\ell^2 << 1$.

The restriction that the hologram plane, S_H, lie in the Fraunhofer region of the scattering complex is not essential. If the condition of Equation (18) is not met, the phase factor $\exp(-ik|\bar{\xi}|^2/2\ell)$ may be grouped with the disturbance $D(\bar{\xi})$, and the entire analysis carried through. The reconstructed image will then contain this same phase factor, but, in optical viewing, it is the squared amplitude of the field that is important, and this squared amplitude is unchanged by the phase factor. The entire resulting procedure is termed Fresnel holography.

Define

$$\tilde{D}(\bar{\gamma}) = \frac{1}{2\pi}\int_{S_0} D(\bar{\xi}) e^{-i\bar{\gamma}\cdot\bar{\xi}} d\bar{\xi}. \qquad (19)$$

The plane S_0 is presumed infinite, although $D(\bar{\xi})$ is non-zero over only a finite region of S_0. Letting

$$F_1 = \frac{-A i k' k^2 C f}{8\pi^2 z_1 z_2 d^2} e^{i k' \left(z_1 + z_2 + f + \frac{|\bar{w}|^2}{2 z_2} \right)} \qquad (20)$$

and using the Fraunhofer condition, Equation (18), Equation (17) becomes

$$\Psi_{I_{S1}}(\bar{\rho}) = 4\pi^2 F_1 \int_{S_{Hd}} e^{i k' \frac{|\bar{w}|^2}{2}\left(\frac{1}{z_1} + \frac{1}{z_2}\right) - i k' \frac{\bar{\rho}\cdot\bar{w}}{z_2}} \tilde{D}\left(k m \frac{\bar{u} + \bar{u}_d - \bar{\Delta}}{d}\right) \tilde{D}^*\left(k m \frac{\bar{u} + \bar{u}_d - \bar{\Delta}}{d}\right) d\bar{u}. \qquad (21)$$

Now impose the focusing condition

$$C_1: \qquad \frac{1}{z_1} + \frac{1}{z_2} = 0.$$

Equation (21) becomes

$$\Psi_{I_{S1}}(\bar{\rho}) = 4\pi^2 F_1 \int_{S_{Hd}} e^{-i k' \frac{\bar{\rho}\cdot\bar{w}}{z_2}} \tilde{D}\left(k m \frac{\bar{u} + \bar{u}_d - \bar{\Delta}}{d}\right) \tilde{D}^*\left(k m \frac{\bar{u} + \bar{u}_d - \bar{\Delta}}{d}\right) d\bar{u}. \qquad (22)$$

Assuming $\bar{\Delta} = 0$ (this is convenient but not necessary) the above integral will be expressed as a convolution. Let

$$\bar{w} = k m \frac{\bar{u} + \bar{u}_d}{d}.$$

Then

$$\Psi_{I_{21}}(\bar{\rho}) = 4\pi^2 F_1 \frac{\lambda^2}{k^2 m^2} \int_{\bar{w}} e^{-i \frac{k' \bar{w}}{z_2} \cdot \left(\frac{\lambda \bar{w}}{k m} - \bar{u}_d \right)} \tilde{D}(\bar{w})\, \tilde{D}^*(\bar{w})\, d\bar{w}$$

$$= \frac{4\pi^2 F_1 \lambda^2}{k^2 m^2} e^{i k' \frac{\bar{\rho} \cdot \bar{u}_d}{z_2 k m}} \int_{\bar{v}} D^*(\bar{v})\, D\left(\bar{v} - \frac{k' \bar{\rho} \lambda}{k z_2 m} \right) d\bar{v}. \tag{23}$$

(b) Contribution from I_2. Let

$$\Psi_{I_{22}}(\bar{\rho}) = \frac{-A k_B^* k' C f}{4\pi^2 z_1 z_2 \lambda (\lambda + s_{3R})} e^{i k' \left(z_1 + z_2 + f + \frac{|\bar{\rho}|^2}{2 z_2} \right) - i k \left(s_{3R} + \frac{|\bar{s}_R|^2}{2(\lambda + s_{3R})} \right)}$$

$$\times \int_{S_{u_d}} e^{i k' \frac{|\bar{u}|^2}{2} \left(\frac{1}{z_1} + \frac{1}{z_2} \right) - i k' \frac{\bar{\rho} \cdot \bar{u}}{z_2} - i k \delta + i k \frac{m^2 |\bar{u} + \bar{u}_d - \bar{a}|^2 s_{3R}}{2\lambda(\lambda + s_{3R})}}$$

$$\times e^{i k m \frac{(\bar{u} + \bar{u}_d - \bar{a}) \cdot \bar{s}_R}{\lambda + s_{3R}} - i k \frac{x_2 |\bar{x} - \bar{s}_R|^2}{2(\lambda + s_{3R})^2}} \int_{S_1} D(\bar{s})\, e^{-i k m \frac{\bar{u} + \bar{u}_d - \bar{a}}{\lambda} \cdot \bar{s}}$$

$$\times e^{i k \frac{|\bar{s}|^2}{2\lambda} + i k \frac{x_2 |\bar{x} - \bar{s}|^2}{2\lambda^2}} d\bar{s}\, d\bar{u}. \tag{24}$$

Now, using the Fraunhofer condition

$$\frac{k |\bar{s}|^2}{2\lambda} << 1,$$

and assuming that

$$\frac{k|x_3|\,|\bar{x}-\bar{\xi}|^2}{2\ell^2} << 1 \tag{25}$$

and

$$\frac{k\,|x_3|\,|\bar{x}-\bar{r}_n|^2}{2(\ell+r_{3n})^2} << 1, \tag{26}$$

which impose requirements on $|x_3|$, Equation (24) becomes

$$\psi_{I_{52}}(\bar{x}) = F_2 \int_{S_{nd}} e^{ik'\frac{|\bar{u}|^2}{2}\left(\frac{1}{r_1}+\frac{1}{r_2}\right) - ik'\frac{\bar{u}\cdot\bar{u}}{r_2} - iks + ik\frac{m^2|\bar{u}+\bar{u}_d-\bar{a}|^2 r_{3n}}{2\ell(\ell+r_{3n})}}$$

$$\times e^{ikm\frac{(\bar{u}+\bar{u}_d-\bar{a})\cdot\bar{r}_n}{\ell+r_{3n}}}\; 2\pi\,\tilde{D}\left(km\frac{\bar{u}+\bar{u}_d-\bar{a}}{\ell}\right) d\bar{u}, \tag{27}$$

where F_2 is the factor multiplying the double integral in Equation (24).
Now note that

$$|\bar{u}+\bar{u}_d-\bar{a}|^2 = |\bar{u}|^2+|\bar{u}_d|^2+|\bar{a}|^2+2\bar{u}\cdot\bar{u}_d-2\bar{u}\cdot\bar{a}-2\bar{u}_d\cdot\bar{a}. \tag{28}$$

To obtain the focusing condition for $\psi_{I_{S2}}$, in the exponent equate to zero the coefficient of $i\frac{|u|^2}{2}$.

$$C_2: \qquad k'\left(\frac{1}{z_1}+\frac{1}{z_1}\right)+\frac{km^2 r_{3R}}{l(l+r_{3R})}=0 \tag{29}$$

Using Equations (28) and (29), Equation (27) becomes

$$\psi_{I_{S2}}(\bar{z}) = 2\pi F_2\, e^{ikm^2\frac{|\bar{u}_d|^2 r_{3R}}{2l(l+r_{3R})}} \int_{S_{Hd}} e^{-ik'\frac{\bar{z}\cdot\bar{u}}{z_2}-ik\delta}$$

$$\times e^{ik\frac{m^2 r_{3R}}{2l(l+r_{3R})}\left(|\bar{\Delta}|^2-2\bar{u}_d\cdot\bar{\Delta}\right)+ik\frac{m}{l+r_{3R}}(\bar{u}+\bar{u}_d-\bar{\Delta})\cdot\bar{r}_R}$$

$$\times e^{ikm^2\frac{r_{3R}\bar{u}}{l(l+r_{3R})}\cdot(\bar{u}_d-\bar{\Delta})}\,\tilde{D}\left(km\frac{\bar{u}+\bar{u}_d-\bar{\Delta}}{l}\right)d\bar{u}.$$

In the case in which the errors δ, and $\bar{\Delta}$, are zero, this is

Letting $\bar{w} = km\,\frac{\bar{u}+\bar{u}_d}{d}$, this becomes

$$\psi_{I_{S2}}(\bar{\alpha}) = 2\pi F_2\, e^{\,ik m^2 \frac{|\bar{u}_d|^2 r_{3R}}{2d(d+r_{3R})} + ik\frac{m\bar{u}_d\cdot\bar{r}_R}{d+r_{3R}}}$$

$$\times \frac{d^2}{k^2m^2}\int_{\bar{w}} e^{-i\left(\frac{d\bar{w}}{km}-\bar{u}_d\right)\cdot\left(\frac{k'\bar{\alpha}}{z_2}-\frac{km\bar{r}_R}{d+r_{3R}}-\frac{km^2\bar{u}_d r_{3R}}{d(d+r_{3R})}\right)}\bar{D}(\bar{w})\,d\bar{w},$$

so

$$\psi_{I_{S2}}(\bar{\alpha}) = 4\pi^2 F_2\, e^{\,ik m^2\frac{|\bar{u}_d|^2}{2(d+r_{3R})} + ik\frac{m\bar{u}_d\cdot\bar{r}_R}{d+r_{3R}} + i\bar{u}_d\cdot\left(\frac{k'\bar{\alpha}}{z_2}-\frac{km\bar{r}_R}{d+r_{3R}}-km^2\frac{\bar{u}_d r_{3R}}{d(d+r_{3R})}\right)}$$

$$\times \frac{d^2}{k^2m^2}\,D\left[-\frac{d}{km}\left(\frac{k'\bar{\alpha}}{z_2}-\frac{km\bar{r}_R}{d+r_{3R}}-\frac{km^2\bar{u}_d r_{3R}}{d(d+r_{3R})}\right)\right], \qquad (30)$$

Representing the entire coefficient of D by F_2', the expression for $\psi_{I_{S2}}(\bar{\alpha})$ is

$$\psi_{I_{S2}}(\bar{\alpha}) = F_2'\,D\left(-\frac{dk'\bar{\alpha}}{mkz_2}+\frac{d\bar{r}_R}{d+r_{3R}}+\frac{m r_{3R}\bar{u}_d}{d+r_{3R}}\right). \qquad (31)$$

Equation (31) indicates that at the value of z_2 satisfying Equation (29), there will appear an image of the original distribution on S_o. The image is magnified and translated, and may be a real or virtual image depending on whether z_2 is greater than or less than zero, respectively.

(c) Contribution from I_3. Let

$$\psi_{I_{s_3}}(\bar{\alpha}) = \frac{A k B k' C f}{4\pi^2 z_1 z_2 \ell (\ell + r_{3R})} e^{ik'\left(z_1 + z_2 + f + \frac{|\bar{\alpha}|^2}{2z_2}\right) + ik\left[r_{3R} + \frac{|\bar{r}_R|^2}{2(\ell + r_{3R})}\right]}$$

$$\times \int_{S_{wd}} e^{ik'\frac{|\bar{w}|^2}{2}\left(\frac{1}{z_1} + \frac{1}{z_2}\right) - ik'\frac{\bar{\alpha}\cdot\bar{w}}{z_2} + ikS - ikm^2\frac{|\bar{w}+\bar{w}_d-\bar{n}|^2 r_{3R}}{2\ell(\ell + r_{3R})} - ikm\frac{(\bar{n}+\bar{w}_d-\bar{\alpha})\cdot\bar{h}}{\ell + r_{3R}}}$$

$$\times e^{ik\frac{x_3|\bar{x}-\bar{r}_R|^2}{2(\ell + r_{3R})^2}} \int_{S_o} D^*(\bar{r})\, e^{ikm\frac{\bar{w}+\bar{w}_d-\bar{n}}{\ell}\cdot\bar{r} - ik\frac{|\bar{r}|^2}{2\ell} - ik\frac{x_3|\bar{x}-\bar{r}|^2}{2\ell^2}} d\bar{r}\, d\bar{w}. \tag{32}$$

and let

$$F_3 = \frac{A k B k' C f}{4\pi^2 z_1 z_2 \ell (\ell + r_{3R})} e^{ik'\left(z_1 + z_2 + f + \frac{|\bar{\alpha}|^2}{2z_2}\right) + ik\left[r_{3R} + \frac{|\bar{r}_R|^2}{2(\ell + r_{3R})}\right]} \tag{33}$$

Using the Fraunhofer condition,

$$\frac{k|\bar{r}|^2}{2\ell} << 1,$$

and assuming Equations (25) and (26) are valid, Equation (33) becomes

$$\Psi_{I_{s_2}}(\bar{s}) = F_1 \int_{S_{ud}} e^{-ik' \frac{|\bar{u}|^2}{2} \left(\frac{1}{r_1} + \frac{1}{r_2}\right) - ik' \frac{\bar{s}\cdot\bar{u}}{r_2} + ik\delta - ikm^2 \frac{|\bar{u}+\bar{u}_d-\bar{a}|^2 r_{2R}}{2d(d+r_{2R})}}$$

$$\times e^{-ikm \frac{(\bar{u}+\bar{u}_d-\bar{a})\cdot\bar{r}_R}{d+r_{2R}}} \quad 2\pi \tilde{D}^* \left(km \frac{\bar{u}+\bar{u}_d-\bar{a}}{d}\right) d\bar{u}. \tag{34}$$

Using Equation (28), inserting the focusing condition

$$C_3: \qquad k'\left(\frac{1}{r_1} + \frac{1}{r_2}\right) - km^2 \frac{r_{2R}}{d(d+r_{2R})} = 0, \tag{35}$$

there results

$$\Psi_{I_{s_2}}(\bar{s}) = 2\pi F_1 e^{-ik \frac{m^2 |\bar{u}_d|^2 r_{2R}}{2d(d+r_{2R})} - ikm \frac{\bar{u}_d\cdot\bar{r}_R}{d+r_{2R}}} \int_{S_{ud}} e^{-ik' \frac{\bar{u}\cdot\bar{s}}{r_2}}$$

$$\times e^{ik\delta - ikm^2 r_{2R} \frac{|\bar{a}|^2 - 2\bar{u}_d\cdot\bar{a}}{2d(d+r_{2R})} - ikm \frac{(\bar{u}-\bar{a})\cdot\bar{r}_R}{d+r_{2R}} - ikm^2 r_{2R} \frac{\bar{u}\cdot(\bar{u}_d-\bar{a})}{d(d+r_{2R})}}$$

$$\times \tilde{D}^* \left(km \frac{\bar{u}+\bar{u}_d-\bar{a}}{d}\right) d\bar{u}. \tag{36}$$

Again consider the case in which the errors δ and $\bar{\Delta}$, are zero.

Then

$$\Psi_{I_{32}}(\bar{\omega}) = 2\pi F_3\, e^{-i k m^2 \frac{|\bar{u}_d|^2 \bar{r}_{3R}}{2\lambda(\lambda+\bar{r}_{3R})} - i k m \frac{\bar{u}_d \cdot \bar{r}_R}{\lambda+\bar{r}_{3R}}} \int_{S_{Hd}} e^{-i\bar{u}\cdot\left(\frac{k'\bar{\omega}}{z_2} + \frac{k m \bar{r}_R}{\lambda+\bar{r}_{3R}}\right)}$$

$$\times e^{-i\bar{u}\cdot k m^2 \frac{\bar{r}_{3R}\bar{u}_d}{\lambda(\lambda+\bar{r}_{3R})}} \tilde{D}^*\left(k m \frac{\bar{u}+\bar{u}_d}{\lambda}\right) d\bar{u}$$

Letting $$\bar{w} = k m \frac{\bar{u}+\bar{u}_d}{\lambda},$$

$$\Psi_{I_{32}}(\bar{\omega}) = 2\pi F_3\, e^{-i k m^2 \frac{|\bar{u}_d|^2 \bar{r}_{3R}}{2\lambda(\lambda+\bar{r}_{3R})} - i k m \frac{\bar{u}_d\cdot\bar{r}_R}{\lambda+\bar{r}_{3R}}}$$

$$\times \frac{\lambda^2}{k^2 m^2} \int_{S_{Hd}} e^{-i\left(\frac{\lambda\bar{w}}{km} - \bar{u}_d\right)\cdot\left(\frac{k'\bar{\omega}}{z_2} + \frac{km\bar{r}_R}{\lambda+\bar{r}_{3R}} + k m^2 \frac{\bar{r}_{3R}\bar{u}_d}{\lambda(\lambda+\bar{r}_{3R})}\right)} \tilde{D}^*(\bar{w})\, d\bar{w}.$$

So

$$\Psi_{I_{32}}(\bar{\omega}) = 2\pi F_3\, e^{-i k m^2 \frac{|\bar{u}_d|^2 \bar{r}_{3R}}{2\lambda(\lambda+\bar{r}_{3R})} - i k m \frac{\bar{u}_d\cdot\bar{r}_R}{\lambda+\bar{r}_{3R}} + i\bar{u}_d\cdot\left(\frac{k'\bar{\omega}}{z_2} + \frac{km\bar{r}_R}{\lambda+\bar{r}_{3R}} + k m^2 \frac{\bar{r}_{3R}\bar{u}_d}{\lambda(\lambda+\bar{r}_{3R})}\right)}$$

$$\times \frac{\lambda^2}{k^2 m^2} \int_{S_{Hd}} e^{-i\bar{w}\frac{\lambda}{km}\left(\frac{k'\bar{\omega}}{z_2} + \frac{km\bar{r}_R}{\lambda+\bar{r}_{3R}} + k m^2 \frac{\bar{r}_{3R}\bar{u}_d}{\lambda(\lambda+\bar{r}_{3R})}\right)} \tilde{D}^*(\bar{w})\, d\bar{w}.$$

$$= 4\pi^2 F_3\, e^{-i k m^2 \frac{|\bar{u}_d|^2 \bar{r}_{3R}}{2\lambda(\lambda+\bar{r}_{3R})} - i k m \frac{\bar{u}_d\cdot\bar{r}_R}{\lambda+\bar{r}_{3R}} + i\bar{u}_d\cdot\left(\frac{k'\bar{\omega}}{z_2} + \frac{km\bar{r}_R}{\lambda+\bar{r}_{3R}} + k m^2 \frac{\bar{r}_{3R}\bar{u}_d}{\lambda(\lambda+\bar{r}_{3R})}\right)}$$

$$\times D^*\left(\frac{\lambda k'\bar{\omega}}{m z_2} + \frac{\lambda\bar{r}_R}{\lambda+\bar{r}_{3R}} + \frac{m\bar{r}_{3R}\bar{u}_d}{\lambda+\bar{r}_{3R}}\right).$$

Letting the coefficient of D^* be F_3' ,

$$\psi_{I_{S3}}(\bar{\alpha}) = F_3' D^* \left(\frac{\lambda k' \bar{\alpha}}{m k t_2} + \frac{\lambda \bar{r}_R}{\lambda + r_{3R}} + \frac{m r_{3R} \bar{u}_d}{\lambda + r_{3R}} \right). \tag{37}$$

Thus a real or virtual image, depending on whether $z_2 > 0$ or < 0 , respectively, of the complex conjugate of the disturbance in the plane S_o is formed in the plane of the value of z_2 satisfying the focusing condition C_3 .

Finally, obtain the component of the reproduction corresponding to the term I_4 in Equation (14) .

(d) Contribution from I_4 . Let

$$\psi_{I_{S4}}(\bar{\alpha}) = \frac{-A i k' B B^* C f}{2\pi z_1 z_2 (\lambda + r_{3R})^2} e^{i k' \left(z_1 + z_2 + f + \frac{|\bar{\alpha}|^2}{2 z_1} \right)} \int_{S_{od}} e^{i k' \frac{|\bar{u}|^2}{2} \left(\frac{1}{z_1} + \frac{1}{z_2} \right) - i k' \frac{\bar{\alpha} \cdot \bar{u}}{z_1}} d\bar{u}.$$

The focusing condition is the same as it was in the treatment of $\psi_{I_{S1}}(\bar{\alpha})$; i.e.,

$$C_1: \qquad \frac{1}{z_1} + \frac{1}{z_2} = 0. \tag{38}$$

Applying this condition,

$$\psi_{I_{S4}}(\bar{\alpha}) = \frac{-A i k' B B^* C f}{2\pi z_1 z_2 (1+\xi_{3R})^2} e^{ik'\left(z_1+z_2+f+\frac{|\bar{\alpha}|^2}{2z_2}\right)} \int_{S_H} e^{-ik'\frac{\bar{\alpha}\cdot\bar{u}}{z_2}} d\bar{u} .$$

That is,

$$\psi_{I_{S4}}(\bar{\alpha}) = \frac{-A i k' B B^* C f}{2\pi z_1 z_2 (1+\xi_{3R})^2} e^{ik'\left(z_1+z_2+f+\frac{|\bar{\alpha}|^2}{2z_2}\right)} 4\pi^2 \delta\left(\frac{k'\bar{\alpha}}{z_2}\right) \quad (39)$$

so that in the z-plane in which z_2 satisfies the focusing condition, $\psi_{I_{S4}}(\bar{\alpha})$ is a delta-function.

In the foregoing, the plane S_H, on (or near) which the hologram is formed has been assumed to be infinite in extent. This necessitates the violation of the assumption made in going from Equation (1) to Equation (2), that

$$\frac{\hat{\lambda}_3 \cdot \bar{r}}{r} \approx 1.$$

In practice, of course, the hologram is of finite extent. The finite size of the hologram may be taken into account in the foregoing mathematics by multiplying the right side of Equation (9), and hence the right sides of Equations (11), (12), (13), and (14), by

$$\text{Rect}\left(\frac{X}{X}\right)\text{Rect}\left(\frac{Y}{Y}\right),$$

where the function Rect (x) is defined to have the value unity for $-1<x\leq 1$, and zero otherwise, and X_1 and X_2 are constants. This factor will ride through the entire analysis, with suitable substitution for x_1 and x_2 in terms of u_1 and u_2, and, in the end, expressions for $\psi_{I_{S1}}$, $\psi_{I_{S2}}$, $\psi_{I_{S3}}$, and $\psi_{I_{S4}}$ will be obtained that are convolutions of the expressions that have been obtained above for these quantities with the Fourier transforms of the multiplying Rect functions. The Fourier transform of the Rect function is a sinx/x function that approaches a delta-function as X_1 and X_2 tend to infinity. Thus for large but finite values of X_1 and X_2, the effect of the finite size of the hologram is to smear the images that have been predicted in the above treatment, with the resulting resolution being determined in the usual way by the ratio of X_1 and X_2 to the operating wavelength.

SOME PARAMETERS DESCRIBING THE HOLOGRAPHIC PROCESS

Magnification

From either Equation (31) or Equation (37) describing the images corresponding to the quantities I_2 and I_3 from Equations (12) and (13), respectively, it is apparent that in the case that a real image is formed, a unit length in the object plane S_o corresponds to a length $mkz_2/\ell k'$ in the image plane S_I. Accordingly, the magnification of the holographically produced image will be defined as

$$m_{\parallel} = \frac{m k z_2}{l k'} \quad . \tag{40}$$

The subscript $\parallel$ on $m_{\parallel}$ stands for parallel, as a reminder of the fact that the magnification corresponding to directions lying in the plane S_o is different from that corresponding to the direction perpendicular to that plane. To obtain the magnification, $m_{\perp}$, corresponding to the direction perpendicular to S_o, consider, for example, the focusing condition C_2:

$$G = k'\left(\frac{1}{z_1} + \frac{1}{z_2}\right) + \frac{k m^2 \xi_{3R}}{l(l + \xi_{3R})} = 0.$$

The magnification $m_{\perp}$ is found by inquiring what change in z_2 is required to bring into focus an object at $l + \delta l$, assuming the height above S_H of the reference, $l + \xi_{3R}$, to remain constant. Letting $l_R = l + \xi_{3R}$, G may be rewritten as

$$G = k'\left(\frac{1}{z_1} + \frac{1}{z_2}\right) + \frac{k' m^2 (l_R - l)}{l l_R} \quad . \tag{41}$$

Setting $dG = 0$ for simultaneous variation of z_2 and l, there results

$$dG = -\frac{k'}{z_2^2} dz_2 - \frac{k m^2}{l^2} dl = 0.$$

Hence,

$$m_\perp = \left| \frac{dz_2}{d\lambda} \right| = \frac{k m^2}{k'} \frac{z_1^2}{\lambda^2}, \tag{42}$$

and

$$\frac{m_\perp}{m_\parallel} = \frac{m z_2}{\lambda} \tag{43}$$

Resolution

The resolution capability of a holographic system depends on whether the two points to be resolved lie in a plane parallel to the array aperture or on a line perpendicular to that aperture. These two resolution capabilities will be termed parallel and perpendicular resolution, respectively.

Parallel Resolution

As described near the end of the preceding section of this Appendix, the use of a holographic recording plane of finite extent leads to expressions for images that are convolutions of the expressions that have been obtained for an infinite aperture with the Fourier transform of the actual finite aperture shape. In the case of a square aperture, the function with which the true image is convolved is a two-dimensional sinx/x function. Consider the result for the case of a point source in the object plane; i.e., $D(\bar{\xi})$ is a δ-function. By Equation (17), setting $\hat{D}(\bar{\xi}) = (2\pi)^{-1}$,

$$\Psi_{I,2}(\bar{x}) = F_2 \int_{-\frac{L}{m}}^{\frac{L}{m}} \int_{-\frac{L}{m}}^{\frac{L}{m}} e^{-i\bar{u}\cdot\left(\frac{k'\bar{x}}{z_1} - \frac{k m \bar{r}_1}{\lambda + z_{21}}\right)} d\bar{u}, \tag{44}$$

where the aperture in the hologram plane, S_H, is taken to be a square of length 2L on a side. Let

$$\bar{v} = \frac{k'\bar{\alpha}}{z_2} - \frac{k\bar{m}\bar{r}_R}{\lambda + r_{3R}}$$

Carrying out the integration,

$$\psi_{I_{S2}}(\bar{\alpha}) = \frac{4L^2}{m^2} F_2 \frac{\sin\frac{Lv_1}{m}}{\frac{Lv_1}{m}} \frac{\sin\frac{Lv_2}{m}}{\frac{Lv_2}{m}}, \qquad (45)$$

in which v_1 and v_2 are the components of $\bar{v}$ along the α_1 and α_2 axes, respectively. If two point sources are present, they will be said to be resolved when the first zero of the function $\psi_{IS2}(\bar{\alpha})$ for one source occurs at the peak of the $\psi_{IS2}(\bar{\alpha})$ function for the other source. If the sources are displaced along the α_1 direction, this corresponds to a variation in the v_1 variable of v_{1d} such that

$$\frac{Lv_{1d}}{m} = \pi$$

$$v_{1d} = \frac{\pi m}{L}.$$

This corresponds to a variation in α_1 of α_{1d}, where

$$\alpha_{1d} = \frac{z_2 m \pi}{k' L},$$

which, in turn, corresponds to a displacement L_d in the object plane. Using Equation (40)

$$L_d = \frac{\ell k'}{m k z_2} \alpha_{1d} = \frac{\lambda \ell}{2L} . \tag{46}$$

(Strictly speaking, this result would be modified by a factor of $\sqrt{2}$ if the displacement of the two point sources had been in any of the directions $\pm(u_1 \pm u_2)$. This change will be ignored, inasmuch as the definition of resolution is somewhat arbitrary anyway.)

Perpendicular Resolution

The perpendicular resolution can be determined by inspection of Equation (27) or Equation (34). Consider Equation (27) and assume $\bar{u}_d = 0$ and $\bar{\Delta} = \delta = 0$. Assume that a point source lies at $\bar{\xi} = 0$ in the object plane, S_o. Then $D(km\bar{u}/\ell) = (2\pi)^{-1}$, and

$$\psi_{I_{S2}} = F_2 \int_{S_{Hd}} e^{i \frac{|\bar{u}|^2 G}{2} - i \bar{u} \cdot \bar{v}} d\bar{u}. \tag{47}$$

For $G = 0$, the behavior of $\psi_{I_{S2}}$ has been investigated in the above determination of the parallel resolution. Now assume that $\bar{v} = 0$ and investigate $\psi_{I_{S2}}$ as a function of z_2. That is, now investigate the (possibly virtual) reconstructed field along an axis perpendicular to the focal plane of the image and passing through the center of the image in that plane.

Equation (47) becomes

$$\Psi_{I_{S1}} = F_2 \int_{-\frac{L}{m}}^{\frac{L}{m}} \int_{-\frac{L}{m}}^{\frac{L}{m}} e^{-i\frac{G}{2}(u_1^2+u_2^2)}\, du_1\, du_2$$

$$= 4F_2 \left(\int_0^{\frac{L}{m}} e^{-i\frac{Gu_1^2}{2}}\, du_1 \right)^2 \qquad (48)$$

Note that if $G = 0$,

$$|\Psi_{I_{S2}}|^2 = |\Psi_{I_{S1}}|_0^2 = \frac{16|F_2|^2 L^4}{m^4}.$$

Equation (48) may be rewritten as

$$\Psi_{I_{S2}} = \frac{4\pi F_2}{G} \left[\int_0^{\frac{L}{m}\sqrt{\frac{G}{\pi}}} e^{-i\frac{\pi}{2}t^2}\, dt \right]^2,$$

where the (Fresnel) integral in the above equation is tabulated [12]. Taking the magnitude of $\psi_{I_{S2}}$,

$$|\Psi_{I_{S2}}|^2 = \frac{16\pi^2|F_2|^2}{G^2}\left[C^2\left(\frac{L}{m}\sqrt{\frac{G}{\pi}}\right) + S^2\left(\frac{L}{m}\sqrt{\frac{G}{\pi}}\right)\right]^2 \qquad (49)$$

The functions C and S are tabulated in Reference 12. The function of G, $\left|\psi_{I_{S2}}\right|^2$, has no zeroes. At G = 0, $\left|\psi_{I_{S2}}\right|^2$ has the value $\left|\psi_{I_{S2}}\right|_0^2$. As G becomes larger, the quantity in brackets in Equation (49) grows to a value of the order of unity, then decreases to a value of the order of 0.05, after which it increases again and oscillates with decreasing amplitude about its asymptotic value of 0.25. As a resolution criterion, it will be considered that a second point source will produce an image that can be resolved from that of the first, if the center of the second image falls at a value of z_2 such that $\left|\psi_{I_2}\right|^2 / \left|\psi_{I_2}\right|_0^2$ is 0.1. That is,

$$0.1 = \frac{\pi^2 m^4}{G^2 L^4}\left[C^2\left(\frac{L}{m}\sqrt{\frac{G}{\pi}}\right) + S^2\left(\frac{L}{m}\sqrt{\frac{G}{\pi}}\right)\right]^2$$

This condition is satisfied when

$$\frac{L}{m}\sqrt{\frac{G}{\pi}} \sim 1.5,$$

or

$$G \sim \frac{2.25\,\pi\, m^2}{L^2}.$$

From Equation (41)

$$\delta G \approx \left.\frac{\partial G}{\partial z_2}\right|_{G=0} \delta z_2 = -\frac{R'}{z_2^2}\,\delta z_2,$$

so

$$|\delta z_\perp| \sim \frac{1.12\, m^2 z_\perp^2 \lambda'}{L^2} \sim \frac{m^2 z_\perp^2 \lambda'}{L^2}.$$

This displacement in image space corresponds to a displacement ℓ_d in object space, where

$$\ell_d = \frac{|\delta z_\perp|}{m_\perp} = \frac{\lambda \ell^2}{L^2} = L_d \frac{2\ell}{L}. \tag{50}$$

Thus the perpendicular resolution is usually much poorer than the parallel resolution.

APPENDIX 2

WAVEFRONT RECONSTRUCTION FROM SAMPLED DATA

In performing microwave imaging, whether by a holographic technique or by a method analogous to optical image formation with a lens, the scattered field is distributed over such a large region that it is generally impractical to record the field on a continuum basis. Consequently, it is necessary to resort to sampling the scattered field and to some method of reproducing an image from such sampled data. If, in the case of holographic imaging, an actual reference signal were present, it would be desirable to measure directly the amplitude of the resultant of the reference field and the field scattered from the target, because by so doing the requirement on knowledge of station location would be minimized. However, because no actual reference signal of controlled location is available in any of the microwave imaging techniques that have yet been devised for use in this investigation, all methods for microwave imaging considered as yet in this study assume that the amplitude and phase of the scattered signal from the target are recorded at each station. If, then, it is desired to reconstruct the wavefront at optical frequencies from a hologram, the amplitude and phase that a reference signal from a source at a given location would have at each of the observing stations can be computed (assuming station location is known with sufficient accuracy--see Section IV), and the computed reference signal can be combined with the measured scattered signal to find the resultant field amplitude that would have been observed at each station, if an actual reference signal had been present. This measured amplitude (or, more precisely, the square of this amplitude) furnishes samples corresponding to those of a hologram measured at the various stations.

In the two techniques of wavefront reconstruction described in the following under Methods 1 and 2, the abovementioned hologram samples are used to form a "discrete" hologram, scaled down suitably for optical reproduction (see Example) that consists of a set of square holes in an opaque screen, one square for each sampling station, with each square having constant light transmission over its area. Methods 1 and 2 are alternate methods of reconstructing a wavefront from a sampled hologram, assuming the initial sampling is done at intervals over the earth's surface suitable for recording data from a target of some specified maximum size. Of these two methods, the first is considered superior because of simplicity and reduced sampling requirements.

In addition to Methods 1 and 2, the following presents still another wavefront reconstruction technique, Method 3, not making use of a hologram at all, but reconstructing the wavefront directly from the sampled values of scattered field amplitude and phase. The requirement on the spatial interval at which the scattered field is sampled is the same in Methods 1 and 3. Methods 1 and 2 require that the hologram be illuminated by a coherent plane wave and that the amplitude of the illumination passing through each square of the hologram be controlled by varying the transmission of the squares. Method 3 requires that both amplitude and relative phase be controlled of each of a number of beams (the number being equal to the number of sampling stations). Methods 1 and 2, of course, each require the synthesis of a reference signal, which, in turn, requires a knowledge of sampling station location. Method 3 does not make use of a reference signal, but places equally stringent requirements on knowledge of station location in order to determine the appropriate phases of the beams used in the direct wavefront reconstruction. Method 1 is preferred over Method 3 as well as over Method 2, because it appears to be the simplest. Because Method 1 is currently, at least, the

preferred technique for reconstruction, it will be presented in some detail, while Methods 2 and 3 will be dealt with more briefly.

METHOD 1: DIRECT RECONSTRUCTION FROM CHECKERBOARD HOLOGRAM

In the following, the hologram will still be considered of infinite extent (the effect of using a finite hologram may be determined by the procedure described near the end of the preceding Appendix), but it will be assumed that the value of the function I of Equation (9) of Appendix 1 is known only at the points x_{1j} , x_{2n} of a square grid. The points x_{1j} and x_{2n} map into the points u_{1j} , u_{2n} in the S_{Hd} plane by Equation (15) of Appendix 1. In the following, the error functions, δ and $\bar{\Delta}$, will be taken to be zero, inasmuch as it is the effect of using a sampled hologram that is to be investigated. Further, for the present purpose, only one of the terms, I_2 , of the four terms in Equation (10) of Appendix 1 will be considered. The displacement $\bar{u}_d$ will be taken to be zero, for simplicity.

An obvious way in which to attempt to reconstruct an image from the sample values of the hologram specified above is to make a hologram having its transmission constant over square cells of length 2b' on a side, where 2b' is yet to be specified, with the cells centered in the scaled hologram at the points corresponding to the location of the receiving stations in the original hologram plane. The constant transmission over each cell is that value determined by the measurement at the corresponding receiving station. Reconstruction of an image from such a discrete hologram will now be considered.

Making use of Equation (12) of Appendix 1, setting $\delta = 0$, the second term in the discrete hologram may be written

$$A\, I_{s2}(\bar{x}) = A \sum_{j,m} \mathrm{Rect}\left(\frac{x_1 - x_{1j}}{b'}\right) \mathrm{Rect}\left(\frac{x_2 - x_{2m}}{b'}\right) I_2(x_{1j}, x_{2m})$$

where $x_{1j} = 2jb$ and $x_{2n} = 2nb$. If this hologram is mapped into the $\bar{u}$-plane, using Equation (15) of Appendix 1, with $\bar{u}_d$ and $\bar{\Delta}$ both zero, the hologram in the $\bar{u}$-plane is

$$A\, I_{s2}'(\bar{u}) = A\, I_{s2}(m\bar{u}) \tag{1}$$

Using Equation (16) of Appendix 1 for the reconstruction,

$$\Psi_{I_{s2}}(\bar{\alpha}) = -\frac{A i k' C f}{2\pi z_1 z_2} e^{i k'\left(e_1 + z_2 + f + \frac{|\bar{\alpha}|^2}{2z_2}\right)} \int\!\!\int_{S_{uA}} \sum_{i,m} \mathrm{Rect}\left[\frac{m(u_1 - u_{1j})}{b'}\right] \mathrm{Rect}\left[\frac{m(u_2 - u_{2m})}{b'}\right]$$

$$\times\, I_2(m u_{1j}, m u_{2m})\, e^{i k'\left(\frac{|\bar{u}|^2}{2z_1} + \frac{|\bar{u}|^2}{2z_2} - \frac{\bar{\alpha}\cdot\bar{u}}{z_2}\right)} d\bar{u} \tag{2}$$

Here $mu_{1j} = x_{1j}$ and $mu_{2n} = x_{2n}$. Let

$$g = \frac{1}{z_1} + \frac{1}{z_2} \tag{3}$$

Consider now the integral over $\bar{u}$. The following integrations are involved

$$\int \mathrm{Rect}\left[\frac{m(u_1-u_{1j})}{b'}\right] e^{ik'\frac{u_1^2 g}{2} - ik'\frac{\alpha_1 u_1}{z_2}} du_1 \int \mathrm{Rect}\left[\frac{m(u_2-u_{2n})}{b'}\right] e^{ik'\frac{u_2^2 g}{2} - ik'\frac{\alpha_2 u_2}{z_2}} du_2$$

It will now be assumed that the distance b' is sufficiently small so that for all u_1 and u_2 such that $|u_1 - u_{1j}| < \frac{b'}{m}$ and $|u_2 - u_{2n}| < \frac{b'}{m}$,

$$\frac{k'|u_1^2 - u_{1j}^2| g}{2} \ll 1 \tag{4}$$

and

$$\frac{k'|u_2^2 - u_{2n}^2| g}{2} \ll 1 \tag{5}$$

for all j and n. In the above integrals, the quadratic phase factors may then be considered constant. The result of the integrations over u_1 and u_2 is then

$$\frac{2z_2}{\alpha_1 k'} \frac{2z_2}{\alpha_2 k'} e^{ik'\frac{u_{1j}^2 + u_{2n}^2}{2} g - ik'\frac{\bar{\alpha}\cdot\bar{u}_{j,n}}{z_2}} \sin\frac{k'\alpha_1 b'}{m z_2} \sin\frac{k\alpha_2 b'}{m z_2}$$

where

$$\bar{u}_{j,n} = \hat{i}_1 u_{1j} + \hat{i}_2 u_{2n}$$

Substituting the result of the $\bar{u}$ integration into Equation (2),

$$\Psi_{I_{s_2}}(\bar{\alpha}) = -i\frac{A2k'cf}{\pi z_1 z_2}\frac{b'^2}{m^2}\frac{\sin\frac{k'\alpha_1 b'}{m z_2}}{\frac{k'\alpha_1 b'}{m z_2}}\frac{\sin\frac{k'\alpha_2 b'}{m z_2}}{\frac{k'\alpha_2 b'}{m z_2}} e^{ik'\left(z_1+z_2+f+\frac{|\bar{\alpha}|^2}{2z_1}\right)}$$

$$\times \sum_{j,m} e^{ik'g\frac{|\bar{u}_{j,m}|^2}{2} - ik'\frac{\bar{\alpha}\cdot\bar{u}_{j,m}}{z_2}} I_2(m u_{j,}, m u_{j,m}). \qquad (6)$$

Now consider only the summation in Equation (6), and substitute from Equation (12) of Appendix 1, with $\delta = 0$, and as usual assume

$$\frac{k|\bar{\xi}|^2}{2\ell} \ll 1,$$

$$\frac{k|x_3||\bar{x}-\bar{\xi}|^2}{2\ell^2} \ll 1,$$

$$\frac{k|x_3||\bar{x}-\bar{\xi}_\ell|^2}{2(\ell+\xi_{3\ell})^2} \ll 1.$$

The summation becomes

$$-i\frac{kB^*}{2\pi\ell(\ell+\xi_{3\ell})} e^{-ik\xi_{3\ell} - ik\frac{|\bar{\xi}_\ell|^2}{2(\ell+\xi_{3\ell})}} \sum_{j,m} e^{ikg\frac{|\bar{u}_{j,m}|^2}{2} - ik'\frac{\bar{\alpha}\cdot\bar{u}_{j,m}}{z_1}}$$

$$\times e^{ik\frac{m^2|\bar{u}_{j,m}|^2\xi_{3\ell}}{2\ell(\ell+\xi_{3\ell})} + ikm\frac{\bar{u}_{j,m}\cdot\bar{\xi}_\ell}{\ell+\xi_{3\ell}}} \int_{S_0} D(\bar{\xi}) e^{-ikm\frac{\bar{u}_{j,m}\cdot\bar{\xi}}{\ell}} d\bar{\xi}. \qquad (7)$$

Now let it be assumed that $D(\bar{\xi})$ is zero except possibly over the square region in the plane S_o,

$$-L_D \leq \xi_1 \leq L_D$$
$$-L_D \leq \xi_2 \leq L_D$$

in this case $D(\bar{\xi})$ may be considered to be repeated periodically over the plane S_o, and, in the square interval specified above, may be represented by a Fourier series as follows,

$$D(\bar{\xi}) = \sum_{j,m} a_{j,m} e^{i \frac{\pi}{L_D} (\xi_1 j + \xi_2 m)} \tag{8}$$

Here

$$a_{j,m} = \frac{1}{4L_D^2} \int_{-L_D}^{L_D} \int_{-L_D}^{L_D} D(\bar{\xi}) e^{-i \frac{\pi}{L_D} (\xi_1 j + \xi_2 m)} d\xi_1 d\xi_2 \tag{9}$$

$$= \frac{\pi}{2L_D^2} \tilde{D}\left(\frac{\pi j}{L_D}, \frac{\pi m}{L_D} \right) \tag{10}$$

and the last step follows from the vanishing of $D(\bar{\xi})$ outside of the square region. Thus

$$D(\bar{\xi}) = \frac{\pi}{2L_D^2} \sum_{j,m} \tilde{D}\left(\frac{\pi j}{L_D}, \frac{\pi m}{L_D} \right) e^{i \frac{\pi}{L_D} (\xi_1 j + \xi_2 m)} \tag{11}$$

Now insert in Equation (7) the focusing condition

$$C_2: \quad kg + \frac{km^2 \bar{s}_{3R}}{\ell(\ell + \bar{s}_{3R})} = 0 \tag{12}$$

to obtain

$$-i \frac{k B^*}{2\pi \ell (\ell + \bar{s}_{3R})} e^{-ik\bar{s}_{3R} - ik\frac{|\bar{s}_R|^2}{2(\ell+\bar{s}_{3R})}}$$

$$\times \sum_{j,n} e^{-i\bar{u}_{j,n}\cdot\left(\frac{k'\bar{\alpha}}{z_2} - \frac{km\bar{s}_R}{\ell+\bar{s}_{3R}}\right)} 2\pi\tilde{D}\left(\frac{km\bar{u}_{j,n}}{\ell}\right) \tag{13}$$

Note that

$$\frac{km\bar{u}_{j,n}}{\ell} = \hat{i}_1 \frac{km u_{1j}}{\ell} + \hat{i}_2 \frac{km u_{2n}}{\ell}$$

$$= \hat{i}_1 \frac{kzjb}{\ell} + \hat{i}_2 \frac{kzmb}{\ell}$$

and let b be such that

$$\frac{\pi}{L_D} = \frac{2kb}{\ell} \tag{14}$$

Then, using Equations (11) and (14), Equation (13) may be written

$$-i\frac{kB^*}{\ell(\ell+\zeta_{3R})}\,e^{-ik\zeta_{3R}-ik\frac{|\bar{\zeta}_R|^2}{2(\ell+\zeta_{3R})}}\,\frac{2L_b^2}{\pi}\,D\left[-\frac{2L_3b}{m\pi}\left(\frac{k\bar{\alpha}}{z_1}-\frac{km\bar{\zeta}_R}{\ell+\zeta_{3R}}\right)\right] \tag{15}$$

or, again using Equation (14),

$$-i\frac{2kB^*}{\pi\lambda(\ell+\zeta_{3R})}\,e^{-ik\zeta_{3R}-ik\frac{|\bar{\zeta}_R|^2}{2(\ell+\zeta_{3R})}}\,\frac{\pi^2\ell^2}{4k^2b^2}\,D\left(-\frac{\ell k'\bar{\alpha}}{mkz_1}+\frac{\ell\bar{\zeta}_R}{\ell+\zeta_{3R}}\right) \tag{16}$$

Now substitute from Equation (16) for the summation in Equation (6).

$$\psi_{I_{S2}}(\bar{\alpha}) = -\frac{Ak'kB^*Cf}{z_1z_2\ell(\ell+\zeta_{3R})}\,\frac{\ell^2}{k^2m^2b^2}\,\frac{\sin\frac{k'\alpha_1b'}{mz_1}}{\frac{k'\alpha_1b'}{mz_1}}\,\frac{\sin\frac{k'\alpha_2b'}{mz_2}}{\frac{k'\alpha_2b'}{mz_2}}$$

$$\times e^{ik'\left(z_1+z_2+f+\frac{|\bar{\alpha}|^2}{2z_2}\right)-ik\zeta_{3R}-ik\frac{|\bar{\zeta}_R|^2}{2(\ell+\zeta_{3R})}}$$

$$\times(b')^2D\left(-\frac{\ell k'\bar{\alpha}}{mkz_1}+\frac{\ell\bar{\zeta}_R}{\ell+\zeta_{3R}}\right). \tag{17}$$

Thus, if sampling of the hologram is done at a spacing of 2b, where b is not larger than the distance determined by Equation (14), and if b'

satisfies the inequalities (Equations 4 and 5), which are necessary to permit focusing, Equation (17) indicates that an image of the distribution $D(\bar{\xi})$ can be produced from a sampled hologram.

In Equation (17) there are two sinx/x functions multiplying the desired image function. To minimize degradation by this intensity modulation, the desired image should be placed between zeroes of the modulation. This can be done easily. Another source of image degradation lies in the periodicity of the reconstruction described by Equation (13). That is, the image described by Equation (16) is repeated periodically in the $\bar{\alpha}$-plane, with period $m_{\|} 2L_D$, where $m_{\|}$ is the previously defined parallel magnification. To prevent serious interference with the desired image from the periodically repeated reconstruction fields due to the hologram terms I_1, I_3, and I_4, the system should be operated with $|\xi_{3R}|$ sufficiently different from zero so that the desired reconstructed image (i.e., that due to either I_2 or I_3) can be isolated by focusing. Because of the focusing condition the value of ξ_{3R} that is used sets an upper limit on b' through Equations 4 and 5. This upper limit is not a source of difficulty in system design, however.

METHOD 2

In this method, the sampled hologram data is used to form a continuous, scaled down, reconstruction of the original hologram, which, in turn, is used to reconstruct an image.

Let $I_s(\bar{u}) = I(m\bar{u})$, and assume $I_s(\bar{u})$ to be known at the points (u_{1j}, u_{2n}) of a square grid, where u_{1j} and u_{2n} have been previously defined. As before, the function $I(\bar{x})$ is that given by Equation (9) of Appendix 1. It is assumed here (in distinction to the case in Method 1) that the spacing of the points at which $I_s(\bar{u})$ is given is such that $I_s(\bar{u})$ could

be reproduced exactly by use of the sampling theorem, if the square grid were of infinite extent. This assumption introduces additional questions inasmuch as the hologram contains a quadratic phase term, the frequency corresponding to which increases indefinitely as the size of the hologram is increased. However, it may be assumed that the hologram is continued beyond the region in which it is known in some manner other than that in which it actually continues. With this assumption, there arise questions of what sort of continuation (perhaps periodic) might be assumed in order to improve the representation of the actual hologram by sampling functions, artificially extending the hologram beyond the region in which it is known. These questions will not be considered here, however. Instead, it is simply assumed that a function is given over the entire $\bar{u}$-plane that coincides with the hologram over the known region of the hologram, and that is reproduced exactly by the sampling theorem (at least over the known region of the hologram). An estimate of the required sampling interval will be given later.

Let the "discrete" hologram,

$$I_{sc}(\bar{u}) = \sum_{n,j} I(\bar{u}_{n,j}) \, \mathrm{Rect}\left[\frac{m(u_1 - u_{1m})}{b'}\right] \mathrm{Rect}\left[\frac{m(u_2 - u_{2j})}{b'}\right], \tag{18}$$

be formed from the measured values, $I_s(\bar{u}_{n,j}) = I(\bar{x}_{n,j})$, with $\bar{x}_{n,j} = m\bar{u}_{n,j}$. Let the Fourier transform of the central square, i.e., that corresponding to $\bar{u}_{o,o}$ be taken optically, using a lens "f to f." The resulting disturbance in the back focal plane of the lens is

$$\psi'(\bar{w}) = -i\frac{k'}{f} e^{i2k'f} \tilde{I}_{oo}\left(\frac{k'\bar{w}}{f}\right), \tag{19}$$

where $\tilde{I}_{0,0}(\bar{x})$ is defined to be

$$\tilde{I}_{0,0}(\bar{x}) = \frac{1}{2\pi} \int_{\bar{u}\text{-plane}} I_s(\bar{u}_{0,0}) \, \mathrm{Rect}\left[\frac{m u_1}{b'}\right] \mathrm{Rect}\left[\frac{m u_2}{b'}\right] e^{-i \bar{x} \cdot \bar{u}} \, d\bar{u}, \tag{20}$$

or

$$\tilde{I}_{0,0}(\bar{x}) = \frac{2 b'^2}{\pi m^2} \, I_s(\bar{u}_{0,0}) \, \frac{\sin \frac{x_1 b'}{m}}{\frac{x_1 b'}{m}} \, \frac{\sin \frac{x_2 b'}{m}}{\frac{x_2 b'}{m}} . \tag{21}$$

Inserting Equation (21) into Equation (19),

$$\psi'_{0,0}(\bar{w}) = -\frac{i k'}{f} \, e^{i 2 k' f} \, \frac{2 b'^2}{\pi m^2} \, I_s(\bar{u}_{0,0}) \, \frac{\sin \frac{k' w_1 b'}{f m}}{\frac{k' w_1 b'}{f m}} \, \frac{\sin \frac{k' w_2 b'}{f m}}{\frac{k' w_2 b'}{f m}} . \tag{22}$$

If the same processing is performed for the square with center at $\bar{u}_{n,j}$, with the axis of the lens moved to the location $\bar{u}_{n,j}$, the disturbance in the $\bar{w}$-plane will be

$$\psi'_{n,j}(\bar{w}) = -\frac{i k'}{f} \, e^{i 2 k' f} \, \frac{2 b'^2}{\pi m^2} \, I_s(\bar{u}_{n,j}) \, \frac{\sin \frac{k' b'}{f m}(w_1 - u_{1,n})}{\frac{k' b'}{f m}(w_1 - u_{1,n})} \, \frac{\sin \frac{k' b'}{f m}(w_2 - u_{1,j})}{\frac{k' b'}{f m}(w_2 - u_{1,j})} \tag{23}$$

The sum of such disturbances over n and j is then

$$\sum_{n,j} \psi'_{n,j}(\bar{w}) = -\frac{2ik'b'^2}{\pi f m^2} e^{i2k'f} \sum_{n,j} I_s(\bar{u}_{n,j}) \frac{\sin \frac{k'b'}{fm}(w_1-u_{1,m})}{\frac{k'b'}{fm}(w_1-u_m)} \frac{\sin \frac{k'b'}{fm}(w_2-u_{2,j})}{\frac{k'b'}{fm}(w_2-u_{2,j})} \quad (24)$$

Let the focal length, f, of the lenses used in this processing be such that the zeroes of the sin x/x function appearing in the summation fall at the sample points $\bar{w}_{n,j}$ $(=\bar{u}_{n,j})$, spaced by 2b/m.

Thus it is required that

$$\frac{2k'bb'}{fm^2} = \pi,$$

or

$$f = \frac{4bb'}{\lambda' m^2} \quad (25)$$

where $\lambda' = 2\pi/k'$. Using this value of f, the summation on the right of Equation (24) is $I_s(\bar{w})$, by the sampling theorem. The total disturbance in the back focal plane of the lens system is

$$\psi'_T(\bar{w}) = -i e^{i2k'f} I_s(\bar{w}), \quad (26)$$

where Equation (25) has been used in Equation (24). Thus, except for a constant phase factor, the unsampled, continuous hologram has been recreated in the $\bar{w}$-plane. This hologram may now be utilized in reconstructing an image of the disturbance that gave rise to the original hologram $I(\bar{x})$.

Sampling Requirements

As stated earlier, it is the object of the present reconstruction method to reproduce first from the sampled hologram a continuous, scaled down reproduction of the original hologram, from which the actual reconstruction can be made. Hence, it is necessary to sample the original hologram at a rate sufficient to reproduce the highest spatial frequencies occurring therein. Inspection of Equations (11), (12), (13), and (14) in Appendix 1 reveals that the spatial frequency spectrum of the original hologram may be represented schematically by the following diagram.

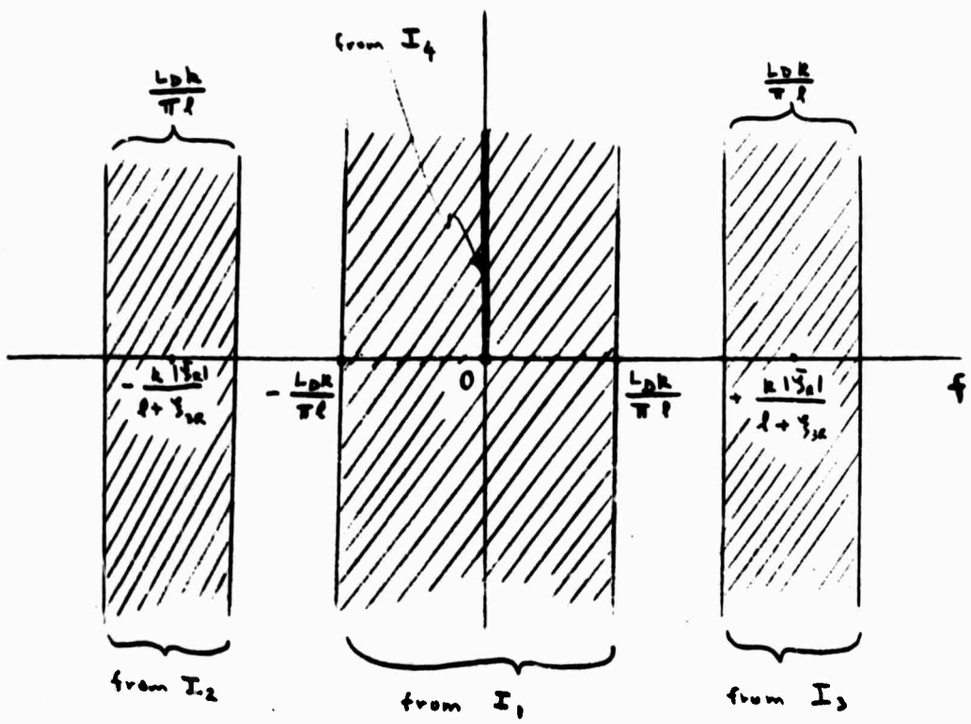

Figure 1

In order to obtain spatial separation of the desired image from interference terms in the reconstruction, $|\bar{\xi}_R|$ should be chosen at least large enough so that the frequency ranges shown in Figure 1 do not overlap. With $|\bar{\xi}_R|$ chosen as small as possible without overlap occurring, the spectral content of the hologram is seen to occupy the range $\left(-\frac{2L_D k}{\pi \ell}, \frac{2L_D k}{\pi \ell}\right)$ requiring a sampling rate of $\frac{4L_D k}{\pi \ell}$, or a sampling interval of

$$2b = \frac{\pi \ell}{4L_D k} = \frac{\lambda \ell}{8L_D}. \tag{27}$$

This is one-fourth of the interval required by Method 1, and results in sixteen times as many sampling stations as that method This is not to say that it might not be possible to form a reconstructed hologram (not image) as in Method 2, using thinner sampling, and then to separate the desired image in the reconstruction by use of focusing. However, this has not yet been investigated.

METHOD 3: DIRECT WAVEFRONT RECONSTRUCTION

R. W. Roig of the MITRE Corporation has proposed a wavefront reconstruction technique that does not require the use of a hologram at all. A hologram, of course, serves as one method of preserving phase information concerning an incident wavefront. In the microwave case, both amplitude and phase would be recorded at each receiving station in any imaging method not using an actual reference beam. The phase information about the received wave is then already recorded, and Roig has pointed out that it is not necessary to use a hologram at all in order to reconstruct, at another frequency, a scaled approximation to the original wavefront.

One significant disadvantage of the Roig reconstruction method is that it requires not only control of the amplitude of a discrete set of coherent sources of optical illumination, but control of their relative phases as well. Another disadvantage is that the reconstructed wavefront, at a particular surface, S_2, in Figure 2, is a reproduction of the original incident wavefront at the earth's surface only in the case that that wavefront originated from scatterers at a particular distance, depending on the location of S_2 from the earth's surface. Observe that this is a different situation from that that exists in the reconstruction of an image, in which case, in a given focal plane, an image is produced corresponding only to objects at given distance. The difference in the two situations is that in the present case, it is not an image of the scattering object that is being produced, but rather a reproduction of the as yet unfocused fields produced by scattering objects.

In Figure 2, there is one modulator in the modulator array for each point at which the original field was sampled. Beams of coherent light of equal amplitude and phase are incident upon the inputs of the modulators. Each modulator controls the amplitude and phase of the light incident upon it in accordance with the measured values of these quantities at the receiving station to which the modulator corresponds. The modulator outputs pass through the lens system, L_1, L_2, and produce on the surface S_2 an optical wavelength approximation to the microwave field that was originally incident upon the earth's surface. This field can then be viewed by eye, just as the virtual image produced by reconstruction from a hologram may be viewed. Alternatively, if it is desired, an optical system could produce from the reconstructed field a real image, which could be recorded on a photographic plate. The spatial locations of the beams exiting from the modulators and the phases of the beams must be controlled to an accuracy corresponding to a small fraction of a wavelength of the optical reconstruction radiation.

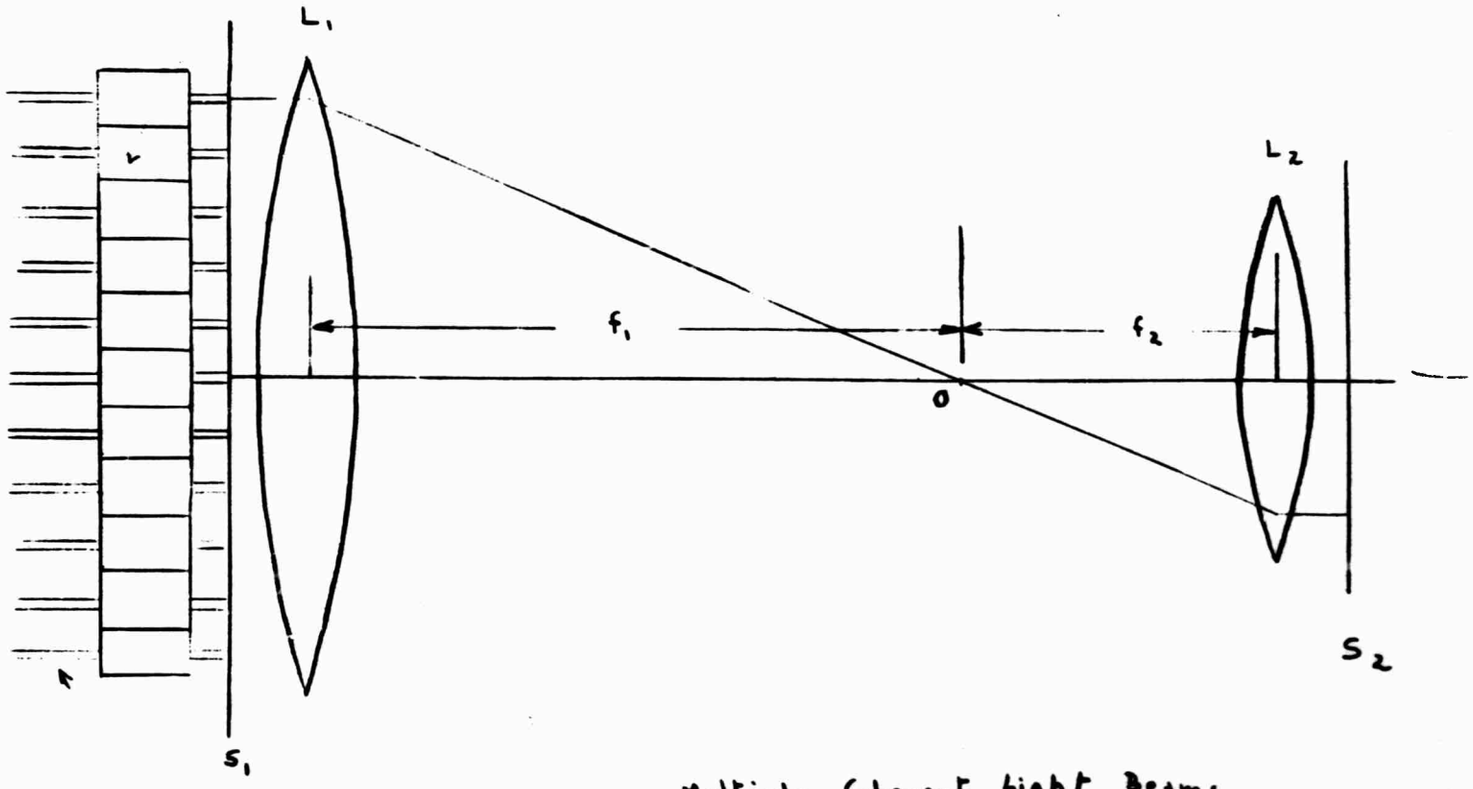
Modulator Array
L1
L2
f1
f2
0
S1
S2
Multiple Coherent Light Beams

Figure 2

It follows from a spatial form of the sin x/x sampling theorem that the interval between stations sampling the field at the earth's surface must be less than or equal to $\ell\lambda/2L_D$, which is the same result as was obtained by a somewhat different method in the preceding section. The relation between array aperture size and resolution remains the same as in Appendix 1.

Because it appears that the present method of wavefront reconstruction is more demanding (in that it requires controlled variation of the phases of the reconstructing beams) than is the reconstruction scheme of Method 1 (or Method 2, for that matter), the direct wavefront reconstruction method will not be discussed further here.

APPENDIX 3

SIGNAL-TO-NOISE RATIO ANALYSIS

In considering the feasibility of performing holographic imaging at microwave frequencies using the outputs of a large coherent array of radar sensors, a critical problem area is that of the influence of thermal noise in the individual sensors on the signal-to-noise ratio (SNR) of the reconstructed image. This ratio, for given receiver noise characteristics and a given array, will depend on the nature of the object being imaged. This dependence is complex and the effect of the scattering object on SNR cannot be described solely in terms of a backscattering cross section. It is not possible to specify the SNR that will obtain in an image produced by a coherent array by any single number; instead, the performance of the array must be determined for a range of target characteristics sufficiently broad to include those of the majority of targets of interest. As a first study of the SNRs resulting when holographic imaging is carried out with such a large aperture radar array, approximate expressions are developed in the present analysis for the SNRs obtained when the array is used to image a point (i.e., unresolved) target, and a target consisting of a flat conducting plate that is assumed to be resolved. The method of analysis is readily applicable to other targets. Results are expressed in terms of various system parameters, among which are radar wavelength, transmitter power, transmitting and receiving antenna gains, coherent integration time, array dimensions, number of stations, and receiver noise temperature (assumed common to all receivers.)

PROBLEM STATEMENT

For the sake of definiteness, a system will be assumed consisting of a single transmitting station illuminating a target, and a square array of dimensions $2L$ on a side of receivers separated from one another by

distance 2b. It is assumed that the real and virtual images are separated in space from one another and from the other two interference terms arising in the holographic process. Also, the process described in Appendix 2 as Method 1 for reconstructing a continuous image from a sampled hologram will be assumed.

In order to obtain, with as little delay as possible, an estimate of the seriousness of the SNR problem, and of the requirements that must be placed on system parameters in order to obtain an acceptable SNR, a number of approximations have been used. These will be pointed out as they are introduced. In the future, a more exact analysis of the problems considered here will be conducted, insofar as such treatment seems required.

NOISE ANALYSIS

Coherent Integration-Equivalence of Receiver Noise to an Incident Field

It is assumed that each receiving station is arranged to receive a scattered field of the same polarization. If E_i is the complex field intensity (of the polarization component of interest) incident on a receiving antenna, the power flux per unit area carried by the wave is $|E_i|^2/2\eta$, where η is the impedance of free space. If the gain of the receiving antenna is G_R, the power absorbed by a matched load attached to the antenna is

$$P_a = \frac{|E_i|^2}{2\eta} \frac{G_R \lambda^2}{4\pi} \qquad (1)$$

If the antenna and load are represented by the circuit of Figure 1,

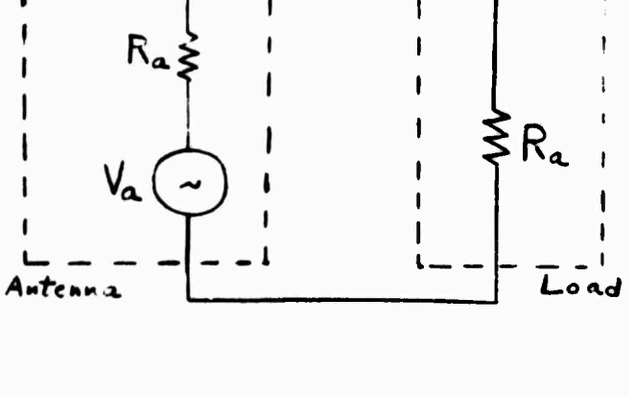

Figure 1

where R_a is the radiation resistance of the antenna, P_a may be written

$$P_a = \frac{|V_a|^2}{8 R_a} \tag{2}$$

where V_a is understood to be a peak value. Thus

$$|V_a| = 2\sqrt{2 P_a R_a} ,$$

and

$$|E_i| = \sqrt{\frac{8\pi\eta P_a}{G_R \lambda^2}} \tag{3}$$

$$|E_i| = |V_a| \sqrt{\frac{\pi \eta}{G_R \lambda^2 R_a}} \quad . \tag{4}$$

If a sequence of N pulses is received from a given target and added coherently, the magnitude of the resultant voltage will be $N|V_a|$, if $|V_a|$ is that corresponding to a single pulse. Further, by Equation (4) the field intensity that would lead to the voltage $N|V_a|$ is just

$$E_{iI} = NE_i \tag{5}$$

Now consider the noise. Assume that the background noise picked up from the sky by the receiver is characterized by a temperature T_B, the noise due to antenna losses by temperature T_A, and the noise introduced by the input stages of the receiver by temperature T_R. The total noise temperature is then $T = T_B + T_A + T_R$. If the bandwidth of the receiver, Δf, is assumed to be small compared with the center frequency, f, the resulting noise may be pictured as a carrier wave of frequency f of amplitude A_N and phase φ_N, where A_N and φ_N are functions of time that cannot vary substantially in time intervals of duration less than $1/\Delta f$. Assuming that the receiver bandwidth is approximately that corresponding to a received pulse of duration τ_P (i.e., $\Delta f \sim 1/\tau_P$), the effect of the noise is to add a voltage vectorially to the vector voltage of each single pulse. Thus, if for the jth pulse the received voltage is v_{rj}, and if the complex noise voltage during the interval of that pulse is n_j (where n_j can be considered constant over the duration of a single pulse), the total voltage recorded by the receiver for the jth pulse is

$$v_j = v_{rj} + n_j \tag{6}$$

where the magnitude of n_j is that of the (substantially constant) envelope of the noise during the time of the jth pulse, and the phase of n_j is the (substantially constant) phase of the noise during that pulse. The sum of N such pulses is

$$v_N = \sum_{j=1}^{N} (v_{rj} + n_j) = N v_r + \sum_{j=1}^{N} n_j$$

where it is assumed that v_{rj} is constant with value v_r (that is, it is assumed that the successive received pulses are phase shifted so that they may be added in phase). Then,

$$\overline{|v_N|^2} = \overline{(N v_r + \sum_{j=1}^{N} n_j)(N v_r^* + \sum_{k=1}^{N} n_k^*)}$$

$$= N^2 |v_r|^2 + N \overline{|n|^2}$$

where $\overline{|n|^2} = \overline{n_j n_j^*}$, a quantity independent of j . The bar indicates an ensemble average.

According to Equation (4), a voltage at the input of the receiver of mean* square magnitude $N\overline{|n|^2}$ would be produced by a single incident pulse having electric field of mean square magnitude

$$\overline{|E_N|^2} = \frac{\pi \eta}{G_R \lambda^2 R_a} N \overline{|n^2|}$$

However, the mean square noise amplitude, for the case of narrow band noise is (this is twice the mean square noise voltage**),

$$\overline{|n|^2} = 8 \tilde{k} T R_a \Delta f \tag{7}$$

so

$$\overline{|E_N|^2} = \frac{8 \pi \eta N \tilde{k} T \Delta f}{G_R \lambda^2} \tag{8}$$

The noise amplitude and phase to be added to a given pulse at a particular station is considered to be independent of those quantities for all pulses, including the corresponding pulse, at all other stations (this may not be true for the noise due to the sky background), and to be independent of those

*The word "mean" will be used consistently to refer to an ensemble average.

**The noise voltage is assumed to be Gaussian with zero mean. Under this assumption, the envelope of narrow band noise is governed by a Rayleigh distribution,[13] and it is straightforward to show that the mean square value of this envelope is twice the mean square instantaneous noise voltage.

quantities for all other pulses at the given station. The pulse amplitudes will be Rayleigh distributed for the narrow band noise case, and the phases distributed uniformly over $(0, 2\pi)$. It is assumed that at each station the interval between pulses is long compared to $1/\Delta f$. Thus, the noise voltage that is present at each station after the coherent integration of a train of N pulses may be represented by

$$E_N e^{i\phi}, \tag{9}$$

where $|E_N|^2$ is given above, φ is uniformly distributed over $(0, 2\pi)$, and E_N is Rayleigh distributed. The quantities E_N and φ are independent at the different stations, and are independent of each other at a given station. (As indicated above, E_N and φ at different stations may not be independent, if the predominant noise component arises from the sky background.)

Noise Terms in Hologram

If the reference signal used in forming the hologram is $E_R(\bar{x})$, where $\bar{x}$ is a two-dimensional vector describing a point on the hologram surface, the total field falling on the hologram plane is

$$E_T(\bar{x}) = E_D(\bar{x}) + E_R(\bar{x}) + E_N(\bar{x}). \tag{10}$$

Here $E_D(\bar{x})$ is the field scattered by the object to be imaged, and $E_N(\bar{x})$ is the fictitious noise field described in the preceding section. The power flux falling on the hologram plane is then $|E_T|^2/2\eta$. The squared term, $|E_T|^2$, may be written in full as

$$|E_T|^2 = |E_D|^2 + |E_R|^2 + |E_N|^2 + E_D E_R^* + E_R E_D^* + E_D E_N^* + E_R E_N^* + E_N E_D^* + E_N E_R^* . \quad (11)$$

If the signal, E_T, is used to form a hologram (either continuous or sampled), and an image is reconstructed from the hologram by Method 1 of Appendix 2, the terms $|E_D|^2$, $|E_R|^2$, $E_D E_R$ and $E_R E_D^*$ lead to results in the reconstruction process that are described in Appendices 1 and 2. In particular, the terms $E_D E_R^*$ and $E_R E_D^*$ lead to the production of images, and the terms $|E_D|^2$ and $|E_R|^2$ to undesired components. By suitable placement of the reference signal, it can be arranged that the fields produced in the reconstruction by the terms $|E_D|^2$, $|E_R|^2$, and $E_R E_D^*$, are not brought to a focus in the same plane as the field due to $E_D E_R^*$. Experience gained in optical, on-axis, Fraunhofer holography indicates that weak, out-of-focus fields do not seriously degrade the desired image. The effects of the terms,

$$I_N(\bar{x}) = |E_N|^2 + E_D E_N^* + E_R E_N^* + E_N E_D^* + E_N E_R^* , \quad (12)$$

involving the thermal noise, will now be investigated.

Effect of Noise Terms in Reconstruction

According to Equation (6) in Appendix 2, the noise terms of Equation (12) will give rise to the following sum, S, which must be evaluated in order to determine the effect of these terms on the reconstructed image of the target object.

$$S = \sum_{j,m} e^{ik'g\frac{|\bar{u}_{j,m}|^2}{2} - ik'\frac{\bar{\alpha}\cdot\bar{u}_{j,m}}{z_2}} I_N(m\bar{u}_{j,m}). \qquad (13)$$

The various symbols appearing in Equation (13) have been defined in the preceding Appendices. The mean squared magnitude of S is

$$\overline{SS^*} = \sum_{\substack{j,m \\ j',m'}} e^{\frac{ik'g}{2}(|\bar{u}_{j,m}|^2 - |\bar{u}_{j',m'}|^2) - \frac{ik'\bar{\alpha}}{z_2}\cdot(\bar{u}_{j,m} - \bar{u}_{j',m'})} \times \overline{I_N(m\bar{u}_{j,m})\, I_N(m\bar{u}_{j',m'})} \,. \qquad (14)$$

Note that $I_N(\bar{x})$ is real. This has been used in Equation (14). In order to evaluate $\overline{S\,S^*}$, write

$$I_{N_{j,m}} = |E_{N_{j,m}}|^2 + (E^*_{D_{j,m}} + E^*_{R_{j,m}})E_{N_{j,m}} + (E_{D_{j,m}} + E_{R_{j,m}})E^*_{N_{j,m}} \,. \qquad (15)$$

Here the subscripts j, n indicate the evaluation of a quantity at $\bar{x} = m\bar{u}_{j,n}$. Let $a_{j,n} = E_{Dj,n} + E_{Rj,n}$. Then Equation (15) becomes

$$I_{N_{j,m}} = |E_{N_{j,m}}|^2 + a^*_{j,m} E_{N_{j,m}} + a_{j,m} E^*_{N_{j,m}} \,. \qquad (16)$$

Now observe that

$$\overline{(I_{N_{j,m}} - \bar{I}_{N_{j,m}})(I_{N_{j',m'}} - \bar{I}_{N_{j',m'}})} = \overline{I_{N_{j,m}} I_{N_{j',m'}}} - \bar{I}_{N_{j,m}} \bar{I}_{N_{j',m'}} \qquad (17)$$

because the amplitude and the phase of $E_{Nj,n}$ are independent, and the phase is uniformly distributed over $(0, 2\pi)$, $\overline{E_{Nj,n}} = 0$. Using this, and observing that $a_{j,n}$ is not random, it is seen that

$$\overline{I_{Nj,m}} = \overline{|E_{Nj,m}|^2} \tag{18}$$

Substituting Equations (16) and (18) into Equation (17) and rearranging, there results

$$\begin{aligned}\overline{I_{Nj,m} I_{Nj',m'}} = {} & \overline{\left(|E_{Nj,m}|^2 - \overline{|E_{Nj,m}|^2} + a^*_{j,m} E_{Nj,m} + a_{j,m} E^*_{Nj,m}\right)} \\ & \times \overline{\left(|E_{Nj',m'}|^2 - \overline{|E_{Nj',m'}|^2} + a^*_{j',m'} E_{Nj',m'} + a_{j',m'} E^*_{Nj',m'}\right)} \\ & + \overline{|E_{Nj,m}|^2}^2 \end{aligned} \tag{19}$$

Here the noise $E_{Nj,n}$ is assumed statistically homogeneous, so that, for example, $\overline{|E_{Nj,n}|^2} = \overline{|E_{Nj',n'}|^2}$. The independence of the noise at the different receiving stations, i.e., for different pairs j, n, is now used to simplify Equation (19)

$$\begin{aligned}\overline{I_{Nj,m} I_{Nj',m'}} = {} & \Big[\overline{|E_{Nj,m}|^4} - \overline{|E_{Nj,m}|^2}^2 + 2 a^*_{j,m} \overline{|E_{Nj,m}|^2 E_{Nj,m}} \\ & + 2 a_{j,m} \overline{|E_{Nj,m}|^2 E^*_{Nj,m}} + a^{*2}_{j,m} \overline{E^2_{Nj,m}} \\ & + 2 |a_{j,m}|^2 \overline{|E_{Nj,m}|^2} + a^2_{j,m} \overline{E^{*2}_{Nj,m}} \Big] \delta_{jm,j'm'} \\ & + \overline{|E_{Nj,m}|^2}^2 \end{aligned}$$

However, again using the independence of amplitude and phase of $E_{Nj,n}$ and the uniformity of phase distribution over $(0, 2\pi)$,

$$\overline{|E_{Nj,m}|^2 E_{Nj,m}} = \overline{|E_{Nj,m}|^2 E^*_{Nj,m}} = 0$$

and

$$\overline{E^2_{Nj,m}} = \overline{E^*_{Nj,m}} = 0$$

Hence

$$\overline{I_{Nj,m} I_{Nj',m'}} = \left(\overline{|E_{Nj,m}|^4} - \overline{|E_{Nj,m}|^2}^2 + 2|a_{j,m}|^2 \overline{|E_{Nj,m}|^2}\right)\delta_{j,m,j',m'} + \overline{|E_{Nj,m}|^2}^2 \tag{20}$$

Equation (20) can be simplified somewhat further by using the fact that $|E_{Nj,n}|$ is governed by a Rayleigh distribution to write

$$\overline{|E_{Nj,m}|^4} = 2\overline{|E_{Nj,m}|^2}^2$$

Using statistical homogeneity to drop the subscripts j,n from E_N, Equation (20) becomes

$$\overline{I_{Nj,m} I_{Nj',m'}} = \overline{|E_N|^2}\left(\overline{|E_N|^2} + 2|a_{j,m}|^2\right)\delta_{j,m,j',m'} + \overline{|E_N|^2}^2 \tag{21}$$

Now substitute Equation (21) into Equation (14) and sum on j', n' to obtain

$$\overline{SS^*} = \sum_{j,m} \overline{|E_N|^2} \left(\overline{|E_N|^2} + 2|a_{j,m}|^2 \right)$$

$$+ \overline{|E_N|^2}^2 \left| \sum_{j,m} e^{i \frac{k'g}{2} |\bar{u}_{j,m}|^2 - i \frac{k'\bar{\alpha}}{z_2} \cdot \bar{u}_{j,m}} \right|^2$$

$$= M \overline{|E_N|^2}^2 + 2 \overline{|E_N|^2} \sum_{j,m} |a_{j,m}|^2 + \overline{|E_N|^2}^2 P \tag{22}$$

where M is the total number of stations, and

$$P = \left| \sum_{j,m} e^{i \frac{k'g}{2} |\bar{u}_{j,m}|^2 - i \frac{k'\bar{\alpha}}{z_2} \cdot \bar{u}_{j,m}} \right|^2 \tag{23}$$

In order that the reconstructed fields corresponding to the terms $|E_D|^2$, $|E_R|^2$, and $E_R E_D^*$, will not be in focus in the same plane as that in which the field due to $E_D E_R^*$ is in focus, it is desirable that the phase $k'g\,|\bar{u}_{j,n}|^2/2$ vary over the aperture (i.e., over j, n) by an amount at least equal to 2π, and perhaps by considerably more. Considering also the phase change over the range of j, n due to the term $k' \bar{\alpha} \cdot \bar{u}_{j,n} / z_2$, it appears that the magnitude of the sum in Equation (23) can be estimated by considering the sum to represent a random walk in the complex plane, each step being of unit length. Thus, as a crude estimate, $P \sim M$. This estimate will be refined in future work. For the present, however, estimate P by M and substitute in Equation (22) to obtain

$$\overline{SS^*} = 2\,\overline{|E_N|^2}\left(M\,\overline{|E_N|^2} + \sum_{j,m}|a_{j,m}|^2\right) \tag{24}$$

Equation (24) involves, in the quantity $a_{j,n}$, the strengths and the distributions over the hologram plane of the field E_D scattered from the target and the reference field E_R. Using the definition of $a_{j,n}$,

$$\sum_{j,m}|a_{j,m}|^2 = \sum_{j,m}|E_{Dj,m}+E_{Rj,m}|^2$$

$$= \sum\left(|E_{Dj,m}|^2 + E^*_{Dj,m}E_{Rj,m} + E_{Dj,m}E^*_{Rj,m} + |E_{Rj,m}|^2\right).$$

A careful evaluation of this summation would be tedious; however, for present purposes, it is probably sufficiently accurate to assume that the contribution to the summation of the middle two terms in the above expression is small, because of the variation in phase of those terms in the summation over j and n. If this assumption is made, the above expression becomes

$$\sum_{j,m}|a_{j,m}|^2 \approx M\left(E^2_{DA} + E^2_{RA}\right) \tag{25}$$

in which

$$E^2_{DA} = \frac{1}{M}\sum_{j,m}|E_{Dj,m}|^2 \tag{26}$$

and

$$E_{RA}^2 = \frac{1}{M} \sum_{j,m} |E_{Rj,m}|^2. \tag{27}$$

Thus, E_{DA}^2 and E_{RA}^2 are the average values of $|E_{Dj,n}|^2$ and $|E_{Rj,n}|^2$, respectively, over the various receiving stations. These averages, in turn, are approximately equal to averages taken over the entire area of the hologram. Using Equation (25), Equation (24) becomes

$$\overline{SS^*} = 2M \overline{|E_N|^2} \left(\overline{|E_N|^2} + E_{DA}^2 + E_{RA}^2 \right). \tag{28}$$

Consider now the averages E_{DA}^2 and E_{RA}^2. Two cases will be studied: a point target (i.e., an unresolved target), and a flat plate (assumed to be resolved).

Case i – Point Target

From the first term of Equation (7) of Appendix 1, the signal field from a point source located at $\bar{\xi}_S$ is [taking $D(\bar{\xi}) = A' \delta(\bar{\xi} - \bar{\xi}_S)$, with A' constant],

$$\frac{-ikA'}{2\pi l} e^{ik\left(l + \frac{|\bar{x}|^2}{2l} - \frac{\bar{x} \cdot \bar{\xi}_s}{l} + \frac{|\bar{\xi}_s|^2}{2l}\right)} \tag{29}$$

Here the quantity x_3, appearing in Appendix 1, is taken to be zero. The constant A' will be evaluated by equating the energy flow at $\bar{x} = 0$ predicted by Equation (29) to that that would exist at the location if there were a point

radar reflector at $\bar{\xi}_S$ scattering energy from some illuminating signal toward the point $\bar{x} = 0$ in the hologram plane. Let σ be the scattering cross-section describing this process. Then

$$\frac{k^2 A'^2}{8\pi^2 \ell^2 \eta} = \frac{P_T G_T \sigma}{(4\pi)^2 \ell_T^2 \ell^2}$$

and

$$A' = \frac{\sqrt{P_T G_T \sigma \eta}}{\sqrt{2}\, k \ell_T} \tag{30}$$

where P_T is the transmitter power (during each individual pulse), G_T is the transmitter antenna gain, and ℓ_T is the range from the transmitter to the scatterer ($\ell_T \approx \ell$). Substituting Equation (30) into Equation (29), and multiplying by N to account for coherent integration of N pulses,

$$E_D(\bar{x}) = -\frac{i\sqrt{P_T G_T \sigma \eta}\; N}{2\sqrt{2}\,\pi \ell \ell_T}\, e^{ik\left(\ell + \frac{|\bar{x}|^2}{2\ell} - \frac{\bar{x}\cdot\bar{\xi}_s}{\ell} + \frac{|\bar{\xi}_s|^2}{2\ell}\right)} \tag{31}$$

The reference signal is obtained from the second term of Equation (7) of Appendix 1 by setting $\delta = x_3 = 0$. Thus,

$$E_R(\bar{x}) = \frac{B}{\ell + \bar{\xi}_{3R}}\, e^{ik\left[\ell + \bar{\xi}_{3R} + \frac{|\bar{x}|^2}{2(\ell+\bar{\xi}_{3R})} - \frac{\bar{x}\cdot\bar{\xi}_R}{\ell+\bar{\xi}_{3R}} + \frac{|\bar{\xi}_R|^2}{2(\ell+\bar{\xi}_{3R})}\right]} \tag{32}$$

in which B is a constant, and the other terms are defined in Appendix 1.

To evaluate E_{DA}^2 and E_{RA}^2 of Equations (26) and (27), inasmuch as a point scatterer cannot give rise to fine structure in its scattering pattern, it is probably adequate to assume that both $|E_{Dj,n}|^2$ and $|E_{Rj,n}|^2$ are constant over the receiving array. In this case, using Equations (31) and (32),

$$E_{DA}^2 = \frac{P_T G_T \sigma \eta N^2}{8\pi^2 \ell^2 \ell_T^2}, \tag{33}$$

and

$$E_{RA}^2 = \frac{|B|^2}{(\ell + \bar{s}_{BR})^2}. \tag{34}$$

Now, turning to Equation (6) of Appendix 2, observing the definition of the sum S in Equation (13), it is apparent that the mean squared magnitude of the contribution to the reconstructed field of the noise terms in the hologram may be written

$$\overline{|E_{REC}|^2} = \frac{4A^2 k'^2 C^2 f^2}{\pi^2 z_1^2 z_2^2} \frac{k^4}{m^4} \overline{SS^*} = K \overline{SS^*} \tag{35}$$

where C , f , z_1 , z_2 , and m , are constants.

In obtaining Equation (35) from Equation (6) of Appendix 2, the sinx/x factors in Equation (6) have been ignored, because any constant multiplication factor arising from these factors would also appear in the expression that will be obtained in the following work for the squared field intensity of the image of the target. Thus, when the ratio of the squared signal field to the mean squared noise field is taken, the factors will cancel. It should also be observed that, although Equation (6) is written with particular reference to

reconstruction of an image from the hologram term I_2, the expression of Equation (6) is equally applicable to the calculation of the field appearing in the reconstruction arising from any other term in the hologram.

Case ii – Flat Plat Target

The first term of Equation (7) of Appendix 1 gives for the field at the hologram surface due to the target

$$-\frac{ik}{2\pi l}\int D(\bar{\xi})\, e^{ik\left(l+\frac{|\bar{x}|^2}{2l}-\frac{\bar{x}\cdot\bar{\xi}}{l}+\frac{|\bar{\xi}|^2}{2l}\right)} d\bar{\xi}, \qquad (36)$$

where, as before, x_3 has been taken as zero. Assume the disturbance $D(\bar{\xi})$ giving rise to the field to be of the form

$$D(\bar{\xi}) = B' \,\mathrm{Rect}\left(\frac{\bar{\xi}}{a}\right),$$

in which B' is a constant (assumed real) and, if $\bar{\xi} = \hat{i}_1\xi_1 + \hat{i}_2\xi_2$, where $\hat{i}_1$ and $\hat{i}_2$ are orthogonal unit vectors parallel to the image plane,

$$\mathrm{Rect}\left(\frac{\bar{\xi}}{a}\right) = \begin{cases} 1, & \text{if } -a \le \xi_1 \le a \text{ and } -a \le \xi_2 \le a \\ 0, & \text{otherwise.} \end{cases}$$

Assuming the hologram surface to be in the Fraunhofer region, the term $k|\bar{\xi}|^2/2l$ in the exponent in Equation (36) will be neglected. Substituting for $D(\bar{\xi})$ in Equation (36) and integrating yields,

$$-\frac{ikB'a^2}{2\pi l}\, e^{ik\left(l+\frac{|\bar{x}|^2}{2l}\right)} \frac{4l^2}{k^2a^2x_1x_2} \sin\frac{kax_1}{l} \sin\frac{kax_2}{l}, \qquad (37)$$

in which $\bar{x} = \hat{i}_1 x_1 + \hat{i}_2 x_2$. The constant B' may be expressed in terms of radar parameters and parameters describing a familiar target by observing that, if the radar wavelength is much less than 2a, the backscattering cross section of a perfectly conducting, square, flat plate of sides 2a is

$$\sigma_P = \frac{64\pi a^4}{\lambda^2}. \tag{38}$$

Hence at $\bar{x} = 0$, equating the power flow that Equation (37) predicts will strike the hologram plane to that that would strike the plane in the case of scattering from a flat plate with backscattering cross section σ_P,

$$\frac{2k^2 B'^2 a^4}{\pi^2 \ell^2 \eta} = \frac{P_T G_T}{(4\pi)^2 \ell_T^2 \ell^2} \frac{64\pi a^4}{\lambda^2}$$

$$B' = \sqrt{\frac{P_T G_T \eta}{2\pi \ell_T^2}}. \tag{39}$$

Substituting Equation (39) into Equation (37) and multiplying by N to account for coherent integration of N pulses, there is obtained

$$E_D(\bar{x}) = -\frac{2ika^2 N}{\pi \ell \ell_T} \sqrt{\frac{P_T G_T \eta}{2\pi}}\, e^{ik\left(\ell + \frac{|\bar{x}|^2}{2\ell}\right)} \times \frac{\ell^2}{k^2 a^2 x_1 x_2} \sin\frac{kax_1}{\ell} \sin\frac{kax_2}{\ell}. \tag{40}$$

The average E_{DA}^2 can be approximated by a continuous average of $|E_D(\bar{x})|^2$ over the region of the hologram, i.e., over $-L \leq x_1 \leq L$ and $-L \leq x_2 \leq L$. The result is

$$E_{DA}^2 \sim \frac{N^2 P_T G_T \eta a^2}{2\pi \ell_T^2 L^2} \tag{41}$$

The expression for E_{RA}^2 is given by Equation (34). Equation (35) again gives the mean squared value of the noise field in the reconstructed image, provided that the expression for E_{DA}^2 given in Equation (41) is used in evaluating SS^* in Equation (35).

INTENSITY OF RECONSTRUCTED SIGNAL**

A point target and a flat plate target are again considered separately.

Point Target

In this case, in the reconstructed image the target is not resolved. There will be the diffraction pattern of the hologram aperture where the point image should appear. The squared field value at the center of this pattern will be evaluated and compared with the mean squared noise field, in order to determine the SNR. The actual diffraction pattern resulting by reconstruction from a sampled hologram will differ somewhat from that obtained by reconstruction from a continuous hologram, but for present purposes this difference will be neglected.* In the case of a continuous

* The result obtained by this assumption (i.e., Equation (46)) is the same as that that would be obtained by considering in detail the reconstruction from a sampled hologram, provided that the number of receiving stations is large compared to unity.

** See addendum, p. 161.

hologram, from Appendix 1,

$$E_{rec} = F_2 \int_{\text{hologram}} e^{-i\bar{u}\cdot\left(\frac{k'\bar{\rho}}{z_2} - \frac{km\bar{r}_R}{l + r_{2R}}\right)} d\bar{\rho} \qquad (42)$$

In obtaining Equation (42) from Appendix 1, the displacement vector $\bar{u}_d$ has been set equal to zero, and, for the function $\bar{D}$, the constant value $(2\pi)^{-1}$ has been substituted in accordance with Equation (19) of Appendix 1 (i.e., a point scatterer has been assumed). The quantity F_2 is a constant. If the original hologram was square, of length 2L on a side, and if the hologram was scaled down by a factor m before optical reconstruction, the above integral should be taken over a square region centered at the origin and length 2L/m on a side.

The result of the integration is*

$$E_{rec} = \frac{4F_2L^2}{m^2} \cdot \frac{\sin\frac{L}{m}\left(\frac{k'u_1}{z_2} - \frac{km\,r_{1R}}{l + r_{2R}}\right)}{\frac{L}{m}\left(\frac{k'u_1}{z_2} - \frac{km\,r_{1R}}{l + r_{2R}}\right)} \cdot \frac{\sin\frac{L}{m}\left(\frac{k'u_2}{z_2} - \frac{km\,r_{2R}}{l + r_{2R}}\right)}{\frac{L}{m}\left(\frac{k'u_2}{z_2} - \frac{km\,r_{2R}}{l + r_{2R}}\right)} \qquad (43)$$

Thus, in the case in which the source term $D(\bar{\xi})$ in Equation (36) is of the form $\delta(\bar{\xi})$, in the reconstruction the squared field at the point at which the image of the target should appear is

$$|E_{rec}|^2 = \frac{16|F_2|^2L^4}{m^4}. \qquad (44)$$

*See addendum, p. 161.

The constant $|F_2|^2$ is, from Appendix 1,

$$|F_2|^2 = \frac{A'^2 k'^2 |B|^2 R'^2 C^2 f^2}{16\pi^4 z_1^2 z_2^2 \lambda^2 (\lambda + r_{SR})^2} \tag{45}$$

In the present instance, the magnitude of the δ-function representing the point scatterer is NA', where A' is defined in Equation (30). Then, using Equations (44), (45), and (30), the squared field magnitude at the center of the reconstructed image of a point scatterer is

$$|E_{rec}|^2_{point} = \frac{A^2 L^4 |B|^2 k'^2 C^2 f^2 N^2 P_T G_T \bar{\tau} \eta b'^4}{2\pi^4 \lambda_T^2 m^4 z_1^2 z_2^2 \lambda^2 (\lambda + r_{SR})^2 b^4}. \tag{46}$$

Flat Plate Target

In this case, the squared field magnitude at any point within the image of the target is readily obtained from Equation (17) of Appendix 2. As before, the effect of the sinx/x terms in Equation (59) is neglected. The result is, multiplying by N^2 for coherent integration,

$$|E_{rec}|^2_{plate} = \frac{A^2 k'^2 |B|^2 C^2 f^2 N^2}{z_1^2 z_2^2 (\lambda + r_{SR})^2} \frac{\lambda^2 g'^2 b'^4}{k^2 m^4 b^4},$$

or, substituting from Equation (39) for B'

$$|E_{rec}|^2_{plate} = \frac{A^2 k'^2 |B|^2 C^2 f^2 \lambda^2 P_T G_T \eta N^2 b'^4}{2\pi z_1^2 z_2^2 (\lambda + r_{SR})^2 k^2 m^4 \lambda_T^2 b^4} \tag{47}$$

SIGNAL TO NOISE RATIO

General Result

Using the foregoing results, it is possible at once to obtain the ratio of the squared magnitude of the signal component of the image field to the mean squared magnitude of the noise component.

Point Target

Dividing Equation (46) by Equation (35), and substituting from Equations (8), (28), (33), and (34), there is obtained, after some simplification,

$$\frac{|E_{rec}|^2_{point}}{|E_{rec}|^2_{noise}} = \frac{L^4 |B|^2 N P_T G_T \sigma G_R}{32\pi k^2 \lambda_T^2 \lambda^2 (\lambda + s_{3R})^2 b^4 M \tilde{k}_T \Delta f}$$

$$\times \left[\frac{8\pi \eta N \tilde{k}_T \Delta f}{G_R \lambda^2} + \left(\frac{P_T G_T \sigma \eta N^2}{8\pi^2 \lambda^2 \lambda_T^2} + \frac{|B|^2}{(\lambda + s_{3R})^2} \right) \right] \tag{48}$$

Some implications of Equation (47), and some simplification of that equation to special cases will be considered later. First, however, the flat plate target will be treated.

Flat Plate Target

Divide Equation (47) by Equation (35), and substitute from Equations (8), (28), (34), and (41) to obtain, after simplifying

$$\frac{|E_{rec}|^2_{plate}}{|E_{rec}|^2_{noise}} = \frac{\pi^2 |B|^2 \lambda^2 P_T G_T G_R N}{32(1+\bar{\xi}_{3R})^2 k^4 \lambda_T^2 b^4 M \tilde{K} T \Delta f}$$

$$\times \left[\frac{2\pi \eta N \tilde{K} T \Delta f}{G_R \lambda^2} + \left(\frac{P_T b_T a^2 \eta W^2}{2\pi L_T^2 L^2} \right) + \frac{|B|^2}{(1+\bar{\xi}_{3R})^2} \right]^{-1} \qquad (49)$$

Simplification and Numerical Results

For brevity, let

$$R_o^2 = \frac{|E_{rec}|^2_{point}}{|E_{rec}|^2_{noise}}$$

and

$$R_L^2 = \frac{|E_{rec}|^2_{plate}}{|E_{rec}|^2_{noise}} .$$

Equations (48) and (49) indicate that R_o^2 and R_L^2 start at zero for $|B|^2$ equal to zero, and increase monotonically, asymptotically approaching constant values, as $|B|^2$ becomes larger. The value of $|B|^2$ that is required to bring R_o^2 or R_L^2 to a value that is one-half of its asymptotic maximum is that value of $|B|^2$ for which the quantity $2|B|^2/(1 + \bar{\xi}_{3R})^2$ is equal to the sum of the other terms in the factor in brackets in the expression in question, i.e., a value of reference signal power roughly equal to the sum of the power of the target signal and the noise. Increasing $|B|^2$ beyond this

value brings R_o^2 or R_L^2 still closer to the maximum, with a value of R_o^2 or R_L^2 of 0.9 of the maximum occurring when $|B|^2$ is nine times the abovementioned value.

The asymptotic maximum SNR is found from Equation (48) or Equation (49) by letting $|B|^2$ approach infinity. The result is:

$$R_{o\,max}^2 = \frac{L^4 N P_T G_T G_R \sigma}{32\pi k^2 l_T^2 l^2 b^4 M \bar{R} T \Delta f} = \frac{L^4 \lambda^2 N P_T G_T G_R \sigma}{2(4\pi)^3 l_T^2 l^2 b^4 M \bar{R} T \Delta f} \qquad (50)$$

$$R_{L\,max}^2 = \frac{\pi^2 l^2 P_T G_T G_R N}{32 k^4 l_T^2 b^4 M \bar{R} T \Delta f} = \frac{\lambda^4 l^2 N P_T G_T G_R}{32(4\pi)^2 l_T^2 b^4 M \bar{R} T \Delta f} \qquad (51)$$

If the bandwidth of the receiver is matched to the pulse bandwidth, the pulse duration, τ_p, and the bandwidth, Δf, appearing in Equations (50) and (51), are related by $\tau_p \sim 1/\Delta f$.

Defining the dimensionless "radar parameter"

$$F_R = \frac{P_T G_T G_R N}{(4\pi)^2 \bar{R} T \Delta f}, \qquad (52)$$

Equations (50) and (51) may be written

$$R_{o\,max}^2 = \frac{L^4 \lambda^2 \sigma F_R}{8\pi \ell_T^2 \ell^2 b^4 M}, \tag{53}$$

and

$$R_{L\,max}^2 = \frac{\lambda^4 \ell^2 F_R}{32 \ell_T^2 b^4 M} \tag{54}$$

Note also that, by Equations (46) and (47), the magnitude of the reconstructed field at the center of the diffraction spot for a point target will equal the magnitude of the reconstructed field in the interior of the image of a plate, if the scattering cross section of the point target is

$$\sigma_1 = \frac{\pi \lambda^2 \ell^4}{4 L^4}. \tag{55}$$

This value of of σ also corresponds to equality of $R_{o\,max}^2$ and $R_{L\,max}^2$.

As a numerical example , consider the case in which the various parameters have the following values:

$P_T = 10^6$ watts,

$G_T = 5 \times 10^5$ (~57db) ~ 90 foot dish at S-band,

$N = 1$,

$G_R = 10$,

λ = 0.1m (S-band)

$\ell_T = \ell = 3 \times 10^5$m,

$T = 300^{\circ}$K,

$\tau_P = 1/\Delta f = 10^{-6}$ sec,

$L = 1.5 \times 10^4$m,

$M = 121$,

$\sigma = 10^{-2}$m^2,

$b = 1.50 \times 10^3$m,

and $\tilde{k}$ = Boltzmann's constant = 1.38×10^{-23} joule/$^{\circ}$K.

The radar parameter is

$$F_R = 7.82 \times 10^{24},$$

$$R_o^2{}_{max} = 0.32 \text{ or } -4.9 \text{ db},$$

$$R_L^2 max = 4.0 \times 10^4 \text{ or } 46 \text{ db},$$

and

$$\sigma_1 = 1260\text{m}^2 \text{ or } 31 \text{ dbsm}.$$

The above SNR for the plate is quite large, but the ratio is low for the point source. If it were desired to increase the SNR by, say, 20db, so that point sources of low cross section would be more clearly visible, it would probably be necessary to use coherent integration. Thus, in the above case, if N had been 100, the result would have been

$$N = 100$$

$$R_{o\ max}^{2} = 15 \text{ db}$$

$$R_{2\ max}^{2} = 66 \text{ db} .$$

The great difference in SNR for the point source and the plate may indicate that some form of amplitude compression would be advisable.

If new holograms were required of the target complex at a rate, f_b, of 100 per second, for example, the average power required of the transmitter would be

$$P_a = P_T \tau_P N f_b$$

$$= 10^4 \text{ watts, for } N = 100.$$

Regarding the coherent integration time, τ_I, note that this interval must be sufficiently short so that in the time, τ_I, no two parts of the target complex that have significant cross-section can move more than, for example, a tenth of the operating wavelength relative to one another. If 10 meters/sec is taken as a reasonable upper limit to the relative velocities of such scatterers, the maximum permissible value for τ_I is 10^{-3} sec. If the pulse duration is 10^{-6} sec, and $N = 100$, it is seen that the total transmitting time required for producing a single hologram is 10^{-4} sec. The 100 pulses required for a single hologram may be easily fitted within the maximum permissible time interval of 10^{-3} sec. It is understood that in performing the coherent integration, compensation is made for the rather uniform phase change that is occurring from pulse to pulse due to the translational motion of the target complex. The use of an individual pulse duration of

10^{-6} sec prevents significant phase change from occurring due to target translational motion during a single pulse. Of course, rather than a sequence of discrete one-microsecond pulses, a single long pulse could be used, making appropriate compensation for phase change due to translation. (The effect on the results of the present analysis of the use of a single long pulse will be investigated. Some changes in the results may occur, because it has been assumed that the noise on successive pulses is independent.)

In the numerical example presented above, the requirements on the receiver stations, aside from that of coherent integration, have been made fairly modest; i.e., an antenna gain of 10 and a noise temperature of 300^{o}K. That the individual receiving station be as simple as possible is dictated by the required number of such stations (121 in the example). On the other hand, only one (or at most a few) transmitter is needed, so that the requirement of a 90 foot dish at the transmitter is not unreasonable.

In the future, continuing attention will be given to the problem of SNR. In particular, the effect of reconstructing the sampled hologram by methods other than the one that has been assumed here will be investigated.

ADDENDUM

On pages 151 and 152 of M68-2, in obtaining the intensity at the center of the diffraction spot resulting from the reconstruction of the image of a point target of unit strength (i.e., a δ-function,) there was used for simplicity the expression that had been obtained for reconstruction of a continuous hologram. In the event that $b' = b$ (i.e., the holes in the scaled down sampled hologram are so large that they abut,) such a procedure is legitimate; however, when $b' \neq b$, it is necessary to use the reconstruction expression for a sampled hologram. If this is done, using Equations (6) and (7) of Appendix 2, and assuming the focusing condition C_2,

$$E_{rec}(\bar{\alpha}') = \frac{4F_2L^2}{m^2}\frac{b'^2}{b^2}\,\mathrm{sinc}\,\frac{k'\alpha_1'b'}{mz_2}\,\mathrm{sinc}\,\frac{k'\alpha_2'b'}{mz_2} \quad ,$$

where

$$\bar{\alpha}' = \frac{mkz_2\bar{\xi}_R}{k'(\ell + \xi_{3R})} \quad ,$$

the location of the center of the diffraction spot. The above expression for $E_{rec}(\bar{\alpha}')$ replaces Equation (43) of Appendix 3 of M68-2. Neglecting sinc function, as explained on page 148. Equation (44) of Appendix 3 is replaced by

$$\left|E_{rec}\right|^2 = \frac{16\left|F_2\right|^2L^4}{m^4}\,\frac{b'^4}{b^4} \quad ,$$

Equations (45) and (46) of that Appendix, were, in fact, derived using the correct expression for $E_{rec}(\bar{\alpha}')$. They remain unchanged.

REFERENCES

1. P. L. Bender, IEEE Proceedings, 55, 6 (1967) 1039-1045.

2. E. Bergstrand, J. Geophys. Res., 65, (February 1960) 404-409.

3. M. T. Prelinen, Tr. Tsentr. Nauchno Issled.Inst. Geodezii, Aerosemski i Kartograffii, No. 114.

4. P. L. Bender and J. C. Owens, J. Geophys. Res., 70, (May 1965) 2461-2462.

5. K. E. Erickson, J. Opt. Soc. Am., 52, (July 1962) 777-780.

6. J. C. Owens, Appl. Opt., 6, (January 1967) 51-59.

7. C. Bare et al., Science, 157, (1967) 189-191.

8. T. Gold, Science, 157, (1967) 302-304.

9. J. B. Keller, Opt. Soc. Am. 52, (1962) 116-129.

10. E. L. O'Neill, Introduction to Statistical Optics, Addison-Wesley Publishing Co., Inc., Reading,Mass., 1963, Section 8 - 2.

11. ibid., Section 5 - 2.

12. E. Jahnke, F. Emde, Tables of Functions, 4th Edition, Dover Publications, New York, 1945.

13. W. B. Davenport, Jr., W. L. Root, An Introduction to the Theory of Random Signals and Noise, McGraw-Hill Book Co., Inc., New York, 1958, Chapter 8.

Security Classification

DOCUMENT CONTROL DATA - R & D

(Security classification of title, body of abstract and indexing annotation must be entered when the overall report is classified)

1. ORIGINATING ACTIVITY *(Corporate author)*
The MITRE Corporation
Bedford, Massachusetts

2a. REPORT SECURITY CLASSIFICATION
Unclassified

2b. GROUP

3. REPORT TITLE
Radar-Optics Imaging -- A Feasibility Study - Interim Report

4. DESCRIPTIVE NOTES *(Type of report and inclusive dates)*
N/A

5. AUTHOR(S) *(First name, middle initial, last name)*
Kent R. Johnson, Joseph F. A. Ormsby, Nicholas M. Tomljanovich

6. REPORT DATE
January, 1969

7a. TOTAL NO. OF PAGES
166

7b. NO. OF REFS
13

8a. CONTRACT OR GRANT NO
AF19(628)-5165

b. PROJECT NO.
8051

c.

d.

9a. ORIGINATOR'S REPORT NUMBER(S)
M68-2

9b. OTHER REPORT NO(S) *(Any other numbers that may be assigned this report)*

10. DISTRIBUTION STATEMENT
This report has been approved by the Directorate for Security Review, Office of the Secretary of Defense, for public dissemination.

11. SUPPLEMENTARY NOTES
N/A

12. SPONSORING MILITARY ACTIVITY
Advanced Research Projects Agency

13. ABSTRACT

An investigation and evaluation is given on the possible application of radar-optics imaging methods. The discussion concentrates largely on microwave holography. Problem areas and alternatives are treated, including a brief discussion on thinned array techniques.

The analytical work centers on array imaging, sampled reconstruction, and sensitivity-noise effects. In addition to other system considerations, an example is given comparing microwave and optical setups. Finally, an examination is made of experimental back-up in terms of requirements, advantages, frequency selection, and appropriate optical simulation.

DD FORM 1 NOV 65 1473

Security Classification

14 KEY WORDS	LINK A		LINK B		LINK C	
	ROLE	WT	ROLE	WT	ROLE	WT
Microwave Holograph						
Real Time Images						
Array Spacing and Location Accuracy						
Sampling and Reconstruction						
Thermal Noise and Sensitivity						